UNIVERSITEIT VAN PRETORIA
UNIVERSITY OF PRETORIA
YUNIBESITHI YA PRETORIA

A Raman- and XRD study of the crystal chemistry of cobalt blue

by

Ellen Mwenesongole

Submitted in partial fulfillment of the requirements for the degree

Master of Science (Chemistry)

In the Faculty of Natural and Agricultural Sciences
University of Pretoria
Pretoria

December 2008

UNIVERSITEIT VAN PRETORIA
UNIVERSITY OF PRETORIA
YUNIBESITHI YA PRETORIA

DECLARATION

I declare that the thesis/dissertation that I hereby submit for the degree in Master of Science (Chemistry) at the University of Pretoria has not previously been submitted by me for degree purposes at any other university.

SIGNATURE: …….. DATE: ……..…

Ellen Musili Mwenesongole

ACKNOWLEDGEMENTS

I would like to thank the following people who have supported and assisted me during the completion of this degree:

- My supervisor, Prof. Peet van Rooyen and co-supervisor Prof. Sylvia Paul for taking on the project 'out of the blue' and their support and dedication in ensuring the written work was eligible for submission.
- David Kok and Werner Barnard for showing me the ropes on the theoretical and practical aspects of Raman and Infra-red spectroscopy. I would not have understood the instrumentation and grasped the concepts of vibrational spectroscopy as quickly as I did without your help.
- Ljiliana Popovic for your invaluable input and support during the final stages of the write-up. I am glad you were 'close enough' to offer such assistance.
- Dr Sabine Verryn for recording all the XRD, even at short notice, and for helping me understand the results.
- A.N. Hall and A.J. Botha for your assistance with recording SEM/EDS and TEM.
- Dr. Danita De Waal, for suggesting such an interesting project and for her initial support.
- The National Research Foundation (NRF) for financial assistance.
- My family for their moral, spiritual and financial support.

"The greatest thing in the world is to know how to be oneself."

Montaigne

ABSTRACT

A Raman- and XRD study of the crystal chemistry of cobalt blue

by

Ellen Mwenesongole

Supervisor: Prof. P.H. van Rooyen

Co-supervisor: Prof. S.O. Paul

Submitted in partial fulfillment of the requirements for the degree Master of Science

Department of Chemistry, University of Pretoria, Pretoria

The aim of this research project was to synthesise both the normal and inverse cobalt aluminate spinels by various methods and characterise them mainly by Raman spectroscopy with the support of X-ray powder diffraction (XRD), Fourier transform infra-red spectroscopy (FT-IR), energy disperse spectroscopy (EDS), and scanning electron microscopy (SEM). Four different synthesis methods (glycine-gel, citrate-gel, polyol and solid-state) were used to synthesise the cobalt aluminate powders with the general formula $Co^{II}Co^{III}_{x}Al_{2-x}O_4$ (where x = 0-2). The gel or powder precursors were annealed at various temperatures ranging from 350 ºC - 1000 ºC. The properties of the intermediate and final products, influenced by the synthesis method, processing temperature, processing time and particle size, were compared. Raman spectra and XRD patterns indicating the presence of both normal and inverse cobalt aluminate spinel were observed. The inverse spinel was identified both as a transitional phase as well as a final phase, depending on the synthesis method and annealing temperature used.

The various synthesis methods were also used to gain further insight into the crystal chemistry of cobalt aluminate. The solid-state method is the more traditional synthesis method. Solution techniques (glycine-gel, citrate-gel and polyol) were used in an attempt to synthesise blue cobalt aluminate at relatively low temperatures and processing times in order to obtain homogeneous, nanosized crystals with broad

applicability. The polyol method was found to be most favourable for the synthesis of blue cobalt aluminate with regard to processing temperature and processing time.

The various characterisation methods used, show that the intensity of the colour of the powders produced are strongly related to the degree of material crystallinity as well as Al/Co ratio. Inverse (Co_2AlO_4) and Co_3O_4 spinels are formed at lower temperatures or when the Co/Al ratio is greater than 0.5. The normal spinel ($CoAl_2O_4$) is produced at higher temperatures or when the Co/Al ratio is 0.5. The XRD patterns of $CoAl_2O_4$, Co_2AlO_4 and Co_3O_4, are very similar because they share the same spinel cubic structure (space group *Fd3m*) differing only slightly in the lattice size. It has been demonstrated that Raman and XRD can be used to distinguish between inverse and normal spinels while FT-IR and EDS are useful for assessing the purity of the powders produced. As predicted by group theory, five Raman and four IR active vibrations were evident in the results.

TABLE OF CONTENTS

LIST OF FIGURES

LIST OF TABLES

Page

LIST OF EQUATIONS

ACRONYMS

BET	Brunauer-Emmett-Teller
CG	Citrate-Gel Preparation Method
DTA	Differential Thermal Analysis
EDS	Energy Dispersive Spectroscopy
EXAFS	Extended X-Ray Absorption Fine Structure
FT-IR	Fourier Transform Infra-Red Spectroscopy
FWHM	Full Width at Half Maximum
GG	Glycine-Gel Preparation Method.
HRTEM	High-Resolution Transmission Electron Microscopy
P	Polyol Preparation Method
SEM	Scanning Electron Microscopy
SS	Solid-state Preparation Method
TGA	Thermogravimetric Analysis
XANES	X-Ray Absorption Near-Edge Structure
XRD	X-Ray Powder Diffraction

SYNONYMS

The following words are used interchangeably throughout the dissertation:

1. Raman effect / Raman scattering / Raman spectroscopy
2. Cobalt blue / Cobalt aluminate
3. Zinc cobalt oxide / Cobalt green
4. Lattice plane / Diffraction plane / Lattice peak
5. Oxide particles / Crystalline powders
6. Light beam / Radiation / Monochromatic light
7. Annealing / Calcination

Chapter 1

Literature Review

Various research groups have synthesised spinel oxides using diverse methods such as solid-state, polyol, sol-gel, co-precipitation, hydrothermal, alkoxide hydrolysis, thermal decomposition of organic precursors, and polymerized complex methods.[1,2,3,4,5,6,7] The solid-state method, in which corresponding metal salts in powder form are mixed and calcined, is considered to be a more traditional method which has advantages of producing highly crystalline products but is limited by the use of high temperatures (1000 - 1400 ºC) and long processing times ranging from several hours to days. This results in coarse, heterogeneous crystals with a large surface area and limited applicability.[5,8]

Various solution techniques have been developed in the past 10 years in an attempt to produce spinel oxides in shorter processing times and at lower temperatures.[1,2,3,5,9] The outcome has been highly crystalline homogeneous powders with low surface areas that have broader applicability. In order to determine the crystal chemistry of the resultant powders, characterisation methods have mainly used X-ray powder diffraction (XRD),[1,3,5,8,10] Fourier transform infra-red spectroscopy (FT-IR),[3,5,11] scanning electron microscopy (SEM)[3,5,12] and transmission electron microscopy (TEM).[1,2,5]

In this research, cobalt aluminate ($CoAl_2O_4$) and zinc cobalt oxide ($ZnCo_2O_4$) spinels were prepared and characterised by using various methods. Both are spinels which exhibit a cubic crystal system with space group *Fd*3*m* (O^7_h). Their difference in cationic distribution allows for a comparison in structural properties to be made. However, very little has been published with respect to their characterisation using the techniques of Raman scattering and IR spectroscopy. The few publications that give them any credence have mainly concentrated on characterisation by XRD, TEM and SEM.[1,3,5,13,14]

Cho and Kakihana[1] used the polymerzed complex technique method (referred to as the citrate-gel method in this research) to synthesise $CoAl_2O_4$ nanocrystals, by heating the polymeric precursor in air at 350 °C - 1000 °C for 2 h. Characterisation was based on XRD, high-resolution transmission electron microscopy (HRTEM) and energy dispersive spectroscopy (EDS). Based on the results, the process of the formation of $CoAl_2O_4$ crystals from the amorphous polymeric precursor was postulated. Well-defined $CoAl_2O_4$ crystals were formed at 500 °C and characteristic XRD patterns of cubic cobalt blue were observed. Crystal growth and grain growth were observed by HRTEM.

Poul et al.[2] synthesised $CoAl_2O_4$ by the polyol method with the aim of determining the effect the hydrolysis ratio, reaction temperature and anion in the precursor have on the formation of $CoAl_2O_4$. Characterisation was by X-ray absorption near-edge structure (XANES), extended X-ray absorption fine structure (EXAFS), TEM and SEM. Acetates, as opposed to chlorides and sulfates, were found to give the best results. A comparison to the sol-gel alkoxide method is also made with the polyol having advantages over the sol-gel method with regard to the use of common ionic salts rather than alkoxide, wide temperature range resulting in good crystallinity, and the possibility of controlling the morphological characteristics for specific applications.

In terms of comparing synthesis methods for the preparation of $CoAl_2O_4$, Zayat and Levy[3] have done this with the sol-gel and citrate-gel methods. The formation process and characterisation of the powder was done using XRD, FTIR, UV-VIS, SEM and thermogravimetric analysis/ differential thermal analysis (TGA/DTA). They found that the structure, colour, particle size and formation temperature of $CoAl_2O_4$ were dependant on the precursors used, method used, and calcination temperature. The processing time and temperature of formation of the desired compounds was significantly lower in comparison to the solid-state reaction method. In addition, more homogeneous gels were formed due to these being solution techniques. The characteristics of the final product can be predetermined by the choice of precursors and preparation conditions.

Feldman[4,6,12] discusses the preparation of various oxides and inorganic pigments by the polyol method. Appropriately chosen metal salts and water are heated in diethyleneglycol to obtain the desired oxides. The adjustment of experimental conditions such as temperature, processing time, concentration of metal precursor and water, produces particles of different sizes. The polyol method has the advantages of broad applicability and the use of relatively low temperatures to produce homogeneous nanoscale (30-200nm) and crystalline oxides. Characterisation was mainly by XRD, SEM, atomic force microscopy (AFM), and DTA/TGA. The surface areas were measured using the Brunauer-Emmett-Teller (BET) method.

A solution technique similar to the citrate-gel method, and referred to as the glycine-gel method in this research, has been used by Wang et al.[5] However, in this method, the Co:Al ratio of the final powder could be determined from the onset by carefully weighing the precursors. Nanocrystalline $Co^{II}Co^{III}_{x}Al_{2-x}O_4$ spinels (where x = 0, 0.5, 0.8, 1, 1.5 and 2) were obtained by the thermal decomposition of gel precursors derived from metal salts and glycine. The gel precursors containing different Co and Al ratios exhibited different thermal behaviour, crystal development, powder morphology and particle size. Due to this, the inverse and normal oxide spinels could be distinguished from each other. Although the desired oxides were obtained at temperatures of 1000 ºC as per the solid-state method, the processing time was significantly less at 2 h compared to 24 h for the solid-state method. Characterisation was based on XRD, FT-IR, DTA/TGA, SEM, HRTEM and BET analyses.

Understanding the properties of spinels would not be complete without understanding their general and crystallographic properties. These have been discussed in various publications.[3,15,16] The classification of ceramics and pigments into idiochromatic and allochromatic pigments as well as the origins of their various colours is explained in Mimani et al.[8] The general chemistry of cobalt as well as its simple and complex compounds are well explained by Bate et al.[17] The structure and symmetry of spinels as well as the prediction of the number of Raman and IR active vibrations by means of

group theory is covered in such publications as those by Stanojevic et al.[15], Julien et al.[16], Kringe et al.[18] and Eastaugh et al.[19]

A comparison of the properties of $CoAl_2O_4$ spinel with other types of mixed oxide spinels reaffirms its structure and symmetry.[15,16,18,20] From these, the expected position and number of Raman and IR vibrational modes can be obtained and assignments for each band made. More specifically, $ZnCo_2O_4$, an oxide spinel, was prepared by the polyol method and characterised for comparison purposes with $CoAl_2O_4$.[12,13,14]

A comparison of the experimentally obtained spectra and Raman and IR vibrational modes of $CoAl_2O_4$ spinels can be made with those found in the publications that used Raman spectroscopy to characterise cobalt aluminate and/or cobalt oxide.[21,22,23,24,25,26] The results indicate that similar products are made, with a few exceptions due to experimental conditions. Comparisons with published XRD and IR spectra are also made inferring that the intended products are synthesised.[1,3, 5,7, 8,10,11]

The advantages of Raman spectroscopy over other techniques, have been provided in publications that have used Raman spectroscopy for characterising $CoAl_2O_4$ pigments and artefacts of historical importance.[26,27,28] These include depth-profiling, minimal sample preparation and minimal to no damage to samples. In addition,only a relatively small quantity or area of the sample needs to be analysed. The theory behind Raman spectroscopy and IR has also been covered in various publications.[29,30,31]

The references mentioned above, spanning the last 8 years, are just examples of some of the references used in understanding the crystal chemistry of cobalt blue, which exists either as a normal ($CoAl_2O_4$) or an inverse spinel (Co_2AlO_4). While various methods have been used to synthesise cobalt blue, mainly XRD has been used for characterisation. Other spectroscopic techniques such as Raman have not been used to their full potential. In addition, very few publications compare synthesis methods in order to determine the most suitable method for cobalt blue of particular

characteristics. To address this, four different methods for the synthesis of cobalt blue were identified: glycine-gel, citrate-gel, solid-state and polyol. Raman spectroscopy has been identified as the main characterisation technique in comparison to XRD, FT-IR and SEM/TEM, to monitor the influence of synthesis method on the structure, crystallinity, colour and morphology of the intermediate and final products.

1.1 References

1. Woo-Seok Cho, M. Kakihana, *J. Alloys Compd.,* 1999, **287**, 87-90.
2. L. Poul, S. Ammar, N. Jouini. And F. Fievet, F. Villain, *J. Sol-gel Sci. Techn,* 2003, **26**, 261-265.
3. M. Zayat, D. Levy, *Chem. Mater.* 2000, **12**, 2763-2769.
4. C. Feldmann, Hans-Otto Jungk, *Angew. Chem. Int. Ed.,* 2001, **40**, 359-362.
5. C. Wang, S. Liu, L. Liu, X. Bai, *Mater. Chem. Phys.,* 2006, **96**, 361-370.
6. C. Feldman, *Adv. Funct. Mater.*, 2003, **13**, 101-107.
7. N. Ouahdi, S. Guillemet, J.J. Demai, B. Durand, L. Er Rakho, R. Moussa, A. Samdi, *Mater. Lett.,* 2005, **59**, 334-340.
8. T. Mimani, S.Ghosh, *Curr. Sci.*, 2000, **78**, 892-896.
9. G. Carta, M. Casarin, N. El Habra, M. Natali, G. Rossetto, C. Sada, E. Tondello, P. Zanella, *Electrochim. Acta,* 2005, **50**, 4592–4599.
10. W.M. Shaheen, M.M. Selim, *Int. J. Inorg. Mater.,* 2001, **3**, 417–425.
11. G. Busca, V. Lorenzelli, V. Bolis, *Materials Chemistry and Physics,* 1992, **31**, 221-228.
12. C. Feldmann, *Adv. Mater.*, 2001, **13**, 1301-1303.
13. X. Wei, D. Chen, W. Tang, *Mater. Chem. Phys.,* 2007, **103**, 54-58.
14. Xinshu Niu, Weiping Du, Weimin Du, *Sensor Actuat. B-Chem,* 2004, **99**, 405–409.
15. Z.V. Marinković Stanojević, N. Romčević, B. Stojanović, *J. Eur. Ceram. Soc.*, 2007, **27**, 903–907.

16. C.M. Julien, F. Gendron, A. Amdouni, M. Massot, *Mat. Sci. Eng. B-Solid,* 2006, **130**, 41-48.
17. L. C. Bate and G. W. Leddicotte, *The Radiochemistry of Cobalt*, National Academy of Sciences- National Research Council, Nuclear Science Series (NAS-NS 3041), 1-96, September 1961, http://library.lanl.gov/cgi-bin/getfile?rc000054.pdf (accessed March 12, 2009)].
18. C. Kringe, B. Oft, V. Schellenschlägar, H.D. Lutz, *J. Mol. Struct,* 2001, **596**, 25-32.
19. Eastaugh, Nicholas, *The Pigment Compendium; Optical Microscopy of Historical Pigments*, Elsevier, London.
20. T. Shimada, T. Tachibana, T. Nakagawa, T.A. Yamamoto, *J. Alloys Compd,* 2004, **379**, 122-126.
21. G. Busca, V. Lorenzelli, V. Sanchez Escribano, R. Guidetti, *J. Catal.,* 1991,**131**, 167-177.
22. D. de Waal, *Asian Chem. Lett.*, 2004, **8**, 57-63.
23. B. Jongsomjit, J. Panpranot, J. G. Goodwin, *J. Catal.,* 2001, **204**, 98-109.
24. D. de Waal, *J. Raman Spectrosc.* 2004, **35**, 646–649.
25. L. D. Kock, D. De Waal, *J. Raman Spectrosc.* 2007, **38**, 1480–1487.
26. D. de Waal, *J. Raman Spectrosc.,* 2007, **38**, 956–957.
27. L. Bellot-Gurlet, S. Pagés-Camagna, C. Coupry, *J. Raman Spectrosc., 2006, **37**, 962–965.*
28. P. F. Bernath, *Spectra of Atoms and Molecules*, Oxford University Press, New York, 1995.
29. I. R. Lewis (Ed), *Handbook of Raman spectroscopy; from the research laboratory to the process line*, Marcel Dekker, New York, 2001.
30. J G. Grasselli (Ed), *Analytical Raman Spectroscopy*, John Wiley & Sons, USA, 1991.
31. J.C.D. Brand, *Applications of spectroscopy to organic chemistry*, Oldbourne Book Co. Ltd, London, 1965.

CHAPTER 2

General Introduction

2.1 Nanoscale Materials

The preparation, characterisation and application of nanoscale materials, i.e. particles with a mean particle diameter of 30 to 300 nm, is an area of great interest in the scientific and industrial fields. Traditionally, they have been applied in the production of catalysts, ceramics, fillers, coatings, and passive electronic components.[1,2] Their use in coatings involves the selective surface modification of various substrates, and they also play a role in the development of new ideas of technical applications, such as quantum-confined materials which include photonic crystals or new types of transparent solar cells.[1,2] A low degree of agglomeration, uniform particle size distribution, specific particle diameter shape or pore structure are some of the qualities required by nanoscale materials in order to fulfil these applications. The challenge is then to find the appropriate synthesis method to suit a particular application.

2.2 Inorganic Pigments

Inorganic pigments are of great importance in conventional applications such as in paints, building materials, plastics, enamel, and ceramics, as well as non-conventional applications such as in archeological samples and documentation.[3] Examples of widely used pigments include $CoAl_2O_4$ (blue), Cr_2O_3 (dark green), $ZnCo_2O_4$ (green), $(Ti_{0.85}Ni_{0.05}Nb_{0.10})O_2$ (yellow), and α-Fe_2O_3 (red). For most purposes, pigment materials prepared at temperatures greater than 500 ºC and with particle sizes greater than 500 nm are adequate. More specialized applications such as colouring and UV-stabilization of plastics, inks, transparent thin films on glass, and coatings on luminescent materials, require nano-sized particles of less than 500 nm.[3] The intensity of the colour of the nanoscale pigments mentioned above is strongly related to the degree of material crystallinity, but their preparation is complicated by the unfavorable

surface-to-volume ratio of the particles. In order to limit the particle growth, low temperatures are required during the synthesis.[3]

Pigments can be further classified into idiochromatic and allochromatic pigments. Idiochromatic pigments are those in which transition metal ions are an important part of the crystal structure and contribute to the colour of the pigment. They determine which wavelengths are absorbed and which are reflected. Examples include chrome green (Cr_2O_3) and cobalt blue ($CoAl_2O_4$). Allochromatic pigments are those in which transition or lanthanide metal ions do not form an integral part of the crystal lattice but are present as 'foreign' particles in trace amounts or as impurities. Examples include the mineral ruby, in which the pink colour is due to trace amounts of chromium present in α-Al_2O_3. The ability of pigments to absorb and scatter light depends on the wavelength of irradiating light, particle size, particle shape and refractive index. In order for pigments to impart maximum colour to a substrate, their particle size should lie between 1 and 10 μm and they should have a high refractive index.[4] Oxide materials such as aluminates, silicates, borates, and zircons mixed with transition metal or rare earth ions meet these requirements of colourants. Of these, the cobalt pigments are known to occur in a wide range of colours, have high tinting strength and excellent stability under chemical, thermal and reducing conditions.[4] It is no wonder that they have found widespread use in various applications, especially ceramics.

2.3 Cobalt Blue

Nano-sized transition metal-oxide spinels have further potential for application in such diverse fields as electrochemical, magnetism, and catalysis. [4,5,6,7] Their attractive qualities include high thermal resistance and excellent electronic and optical properties. An example of a metal-oxide spinel investigated in this research is cobalt aluminate ($CoAl_2O_4$), also known as Thénard's blue and cobalt blue. [4,5,6,7] Its unique properties include its intense blue colour, thermal, chemical, solar and atmospheric stability, excellent optical properties and its transparency effect together with colour generation when dispersed in a matrix.[6,7] These properties enable cobalt aluminate to

have widespread use in ceramics, plastics, glass, rubber, the paint industry, and colour TV tubes.

The properties of $CoAl_2O_4$ are mainly due to its crystal structure, which is a normal spinel structure in which Co^{2+} ions are accommodated in tetrahedral positions while Al^{3+} ions are in octahedral positions.[3] This has been expounded in section 3.3.

2.4 Crystalline Substances

Most pigments tend to be crystalline in form. Crystalline substances have an ordered, repeating and regular internal molecular structure. This ordered arrangement of atoms occurs throughout the whole material and if crystallisation occurred under ideal conditions, this would result in compounds with perfect crystal shapes. This is not always the case, resulting in crystalline compounds with defects in their crystal faces or lattices.[8]

Crystalline materials are classified into seven crystallographic groups according to the symmetry of the crystalline forms; triclinic, monoclinic, orthorhombic, tetragonal, cubic, trigonal and hexagonal. The repeating unit in a crystal lattice is a 3-D unit cell characterised by the relative lengths of the three axes, *a, b* and *c* and the angles between these axes, α, β and γ. Of interest in this research is the cubic crystallographic system in which $a = b = c$ and $\alpha = \beta = \gamma = 90°$. Environmental conditions such as temperature and pressure as well as inclusion of trace or major elements into the crystalline lattice have been known to alter the crystalline form of a compound.[8] Solid substances that do not have a crystalline structure are referred to as amorphous.

The observed colour of a pigment is as a result of the absorption of certain wavelengths of light and the transmission of others. Colour of pigments is therefore determined by crystal structure and chemical composition.[8]

The size of particles may be described in relative or absolute terms. Examples of the former would be 'fine, medium or coarse' and an example of the latter would be '5 µm'. It should be noted that since particle size distribution is not always uniform, a range of sizes should be given in such instances.

Particles in pigments have diverse origins and are prepared in a variety of ways including the grinding of larger particles and aggregates, as precipitates, or sieving naturally occurring substances. This can lead to a wide array of particle shapes which can be helpful in the characterisation of the composition of the pigment as well as preparation method. Although crystals tend to adopt the shape defined by their crystallographic system, some are capable of displaying shapes characteristic of other crystallographic systems, or often occur in irregular shapes.

2.5 History and Chemistry of Cobalt

Cobalt was discovered in 1739 by Georg Brandt, a Swedish chemist, while attempting to prove that an unknown element, and not bismuth, was responsible for the ability to colour glass blue.[9] Therefore, cobalt compounds have historically been used as a dye in porcelain, glass, pottery, tile, enamel and currency.

Due to its ability to resist oxidation, metallic cobalt is used in electroplating and in alloys. Cobalt containing alloys have been used in magnets, jet engines, gas turbines, magnetic steels and certain stainless steels.[9]

Medically, cobalt derivatives have been used to treat certain forms of cancer, as a medical tracer and as an important part of vitamin B_{12}.[9]

2.5.1 Metallic Cobalt

Crude metallic cobalt is normally obtained as a result of smelting ores such as smaltite ($CoAs_2$), linnaeite (Co_3S_4), cobaltite (CoAsS) and erythrite [$Co_3(AsO_4)_2$], with the main ore being cobaltite (CoAsS).[9] Cobalt is also recovered as a by-product of mining and refining nickel, silver, lead, copper and iron.

The physical properties of metallic cobalt are noted as, silvery white with a faint tinge of pink, density of 8.9 gcm^{-3}, melting point of 1480 ºC, boiling point of 2900 ºC and an atomic mass of 58.94 amu.[10] At temperatures below 300 ºC, cobalt is not easily oxidized by air or water in compact form. Above 300 ºC, it is readily oxidized in air. When heated or in its molten state, cobalt readily forms complexes with most metalloids as well as other metals such as aluminum, chromium, zinc, nickel, and iron.

2.5.2 Co-ordination Compounds of Cobalt

Co-ordination compounds of cobalt are known to produce a wide variety of colours as summarized by Mimani and Ghosh[4]. Generally, cobalt compounds range in colour from blue or green to pink depending upon the host lattice and coordination site and coordination number of the cobalt ion.[4]

Compounds in which cobalt is in the octahedral position tend to be pink to violet in colour while those in which cobalt is in the tetrahedral position tend to be blue. For instance the cobalt aquo-complex, $[Co(H_20)_6]^{2+}$ is pink while the cobalt halo-complex, $(CoX_4)^{2-}$ is blue.[10] The pink colour changes to blue upon heating, dehydration or in the presence of concentrated acids.[10]

2.5.3 Chemical Properties of Cobalt

Since cobalt is positioned between iron and nickel in the periodic table, it can be assumed that its chemical properties may be a combination of those of iron and nickel. Cobalt compounds have different degrees of solubility in water and in other aqueous media.[10] It mainly forms compounds in which it has an oxidation of +2 or +3 but it has also been known to form a few compounds in which it has an oxidation state of +1 and +4. The most stable oxidation state of cobalt in simple compounds is +2. The cobaltous ion, Co^{2+}, is basic and is quite stable in aqueous solutions. Complex compounds of Co^{2+}, on the other hand, are very unstable and can be readily oxidized to the Co^{3+} form. In contrast, simple Co^{3+} compounds are unstable in aqueous

solutions due to the strong oxidizing abilities of Co^{3+} e.g. CoF_3. However, Co^{3+} forms one of the largest groups of complex compounds known, which also tend to be stable in aqueous solutions e.g. cobalt nitrates. These observed differences can be attributed to the fact that Co^{3+} has a coordination number of six, leading to most Co^{3+} complexes being stable. Co^{2+}, on the other hand, has a coordination number of either 4 or 6, leading to the complex Co^{2+} compounds being susceptible to oxidation.

Although cobalt reacts less readily than iron with weak acids, it is easily dissolved by weak sulfuric, hydrochloric and nitric acids whereas ammonium hydroxide and sodium hydroxide attack it very slowly.[10]

2.6 Aim

Cobalt blue, which exists either as a normal ($CoAl_2O_4$) or an inverse spinel (Co_2AlO_4), is a widely used pigment in such applications as ceramics, plastics, paints, building materials and items of historical importance. While various methods have been used to synthesise cobalt blue, XRD has mainly been the characterisation technique of choice. Other techniques such as Raman spectroscopy have not been explored to a greater extent. In addition, very few publications exist which compare synthesis methods with the aim of determining the most appropriate method based on the desired properties of cobalt blue.

Therefore, this research seeks to address the following gaps identified from the literature reviewed:

- the exploration and comparison of various synthesis methods with the aim of determining under which experimental conditions the different spinels exist,
- the isolation and characterisation of intermediate and final products, in order to track compositional, structural and morphological changes as the reaction goes to completion,
- more in-depth exploration of the potential of Raman spectroscopy, capitalising on its advantages and,

- identifying the most suitable holistic technique for characterising cobalt blue.

In order to answer the above, four different methods for the synthesis of cobalt blue were identified based on their ease of applicability: glycine-gel, citrate-gel, solid-state and polyol. Raman spectroscopy has been identified as the main characterisation technique in comparison with XRD, FT-IR and SEM/TEM to monitor the influence of synthesis method on the structure, crystallinity, colour and morphology of the intermediate and final products.

A short background summary of the theory behind Raman and infra-red spectroscopy is included in this project as these techniques have not routinely and extensively been applied in the analysis of oxide spinels, in particular, cobalt aluminate. However, as XRD and SEM/TEM are more mature techniques often routinely used for the characterisation of oxide spinels, no further background to the theory is summarized. References that provide a good background to the theory and applications of XRD, including for the analysis of oxide spinels, include Mimani and Ghosh[4], Zayat and Levy[5], Wang et al.[6], Azaroff[11], Dinnebier and Billinge[12], Cho and Kakihana[13], Shaheen and Selim[14], Ji et al.[15], Sampanther and Zeng[16], Jongsomjit et al.[17], and Taniguchi[18].

2.7 References

1. C. Feldmann, Hans-Otto Jungk, *Angew. Chem. Int. Ed.,* 2001, **40**, 359-362.
2. C. Feldman, *Adv. Funct. Mater.*, 2003, **13**, 101-107.
3. C. Feldmann, *Adv. Mater.,* 2001, **13**, 1301-1303.
4. T. Mimani, S.Ghosh, *Curr. Sci.*, 2000, **78**, 892-896.
5. M. Zayat, D. Levy, *Chem. Mater.* 2000, **12**, 2763-2769.
6. C. Wang, S. Liu, L. Liu, X. Bai, *Mater. Chem. Phys.,* 2006, **96**, 361-370.
7. G. Carta, M. Casarin, N. El Habra, M. Natali, G. Rossetto, C. Sada, E. Tondello, P. Zanella, *Electrochim. Acta,* 2005, **50**, 4592–4599.

8. Eastaugh, Nicholas, *The Pigment Compendium; Optical Microscopy of Historical Pigments*, Elsevier, London, 2000.
9. Jefferson Lab, http://education.jlab.org/itselemental/ele027.html (accessed November 07, 2008) Thomas Jefferson National Accelerator Facility - Office of Science Education.
10. L. C. Bate and G. W. Leddicotte, *The Radiochemistry of Cobalt*, National Academy of Sciences- National Research Council, Nuclear Science Series (NAS-NS 3041), 1-96, September 1961, http://library.lanl.gov/cgi-bin/getfile?rc000054.pdf (accessed March 12, 2009)].
11. Azaroff, L.V, *Elements of X-ray Crystallography*, McCraw-Hill Book Company, New York, 1968.
12. R.V. Dinnebier (Ed), S.J.L. Billinge (Ed), Powder *Diffraction, Theory and Practice*, Royal Society of Chemistry, Cambridge, UK, 2008.
13. Woo-Seok Cho, M. Kakihana, *J. Alloys Compd.,* 1999, **287**, 87-90.
14. W.M. Shaheen, M.M. Selim, *Int. J. Inorg. Mater.,* 2001, **3**, 417–425.
15. L. Ji, J. Lin, H.C. Zeng, *J. Phys. Chem. B*, 2000, **104**, 1783-1790.
16. J.T. Sampanthar, H.C. Zeng, *Chem. Mater.,* 2001, **13**, 4722-4730.
17. B. Jongsomjit, J. Panpranot, J.G. Goodwin, *J. Catal.,* 2001, **204**, 98-109.
18. I. Taniguchi, *Mater. Chem. Phys.,* 2005, **92**, 172-179.

CHAPTER 3

Background to Spinels

3.1 General

Spinel pigments are derived from the naturally occurring colourless mineral spinel $MgAl_2O_4$. By replacing Mg or Al with Co^{2+}, Cr^{3+}, Cu^{2+}, Ni^{2+}, and Fe^{3+} cations, various colours of powders can be obtained. Spinel pigments are known to be stable to photodegradation and high temperatures. They are insoluble in water and most solvents, are generally non-toxic, and are resistant to acidic and alkaline media.

3.2 Vibrational Spectroscopy for Spinels

Solid-state chemistry has benefited from vibrational spectroscopy techniques, especially Raman and infrared (IR) spectroscopy, for the characterisation of crystalline solids and spinels in particular. According to lattice vibration theory, there is a strong relationship between the crystal structure and the associated lattice vibrations. Raman and IR spectroscopic techniques therefore complement each other with regard to providing a means for obtaining structural information of spinel-type oxides such as $CoAl_2O_4$. This is enhanced by the ability of spinel-type oxides to show distinct changes in the recorded spectra with a change in the composition, i.e. cation content (e.g. Cobalt or Zinc cations), cation substitution etc.[1,2,3]

3.3 Crystal Structure and Symmetry of Spinels

Spinel oxides of the general formula AB_2O_4 exhibit a cubic structure with space group *Fd*3*m* (O^7_h) containing eight AB_2O_4 units per unit cell (Z = 8). ‘A’ represents divalent cations in tetrahedral sites and ‘B’ represents trivalent cations in octahedral sites e.g. $CoAl_2O_4$. In this structure, the oxygen anions form a cubic close-packed (ccp) sub-

lattice surrounded by tetrahedral and octahedral sites occupied by cations. The cations occupy only ⅛ of the tetrahedral sites and ½ of the octahedral sites.[1,2,4]

Spinel oxides can be further sub-divided into normal and inverse spinels. This can be further explained using $CoAl_2O_4$ as an example. When one type of metal cation individually occupies the tetrahedral (e.g. Co^{2+}) and octahedral (e.g Al^{3+}) sites, the result is a normal spinel. On the other hand, with inverse spinels, two different types of metal cations (e.g. Co^{3+} and Al^{3+}) occupy the octahedral site with only one type of cation (e.g. Co^{2+}) present at the tetrahedral site. [14,17] In general, the normal spinel forms when the ratio of A/B is equal to 0.5 and the inverse spinel forms when the ratio of A/B is greater than 0.5, due to possible inversion between A and B leading to the A cation occupying the octahedral sites in addition to the B cation.

3.4 Group Theory for Spinels

Group theory has made it possible to determine the number of Raman and IR active vibrations allowed for a particular crystal structure. This is useful in determining 'abnormalities' in the crystal structure based on recorded spectra. According to the group theory for spinels, normal and inverse spinels, both in the cubic space group *Fd*3*m,* should exhibit the following normal vibrational modes: [1,2]

$$\Gamma(AB_2O_4)= A_{1g}(R) + E_g(R) + F_{1g}(in) + 3F_{2g}(R) + 2A_{2u}(in) +2E_u(in) + 4F_{1u}(\mathbf{IR}) + 2F_{2u}(in) \quad ....(3\text{-}1)$$

where (R), (IR) and (in) denote Raman- and IR-active vibrations and inactive modes, respectively. In a 'perfect' $CoAl_2O_4$ spinel, it is expected that that there should be five Raman-active and four IR-active normal vibrational modes.

Table 3-1 lists the theoretically allowed vibrational modes for spinel lattices[2], where *a, d* and *e* are Wyckoff crystal sites (denotes where atoms are positioned within a crystal).

Table 3-1: Vibrational modes for the cubic *Fd*3*m* (z=8) (O^7_h) phase.

Phase	*Fd*3*m* (Z=8) (O^7_h)
Atom Occupancy	1(Co): 8*a*; 1(Al): 16*d*; 1(O): 32*e*
Vibrational Modes	A_{1g}(R)
	E_g(R)
	F_{1g}(in)
	$3F_{2g}$(R)
	$2A_{2u}$(in)
	$2E_u$(in)
	$4F_{1u}$(IR)
	$2F_{2u}$(in)

3.5 Raman Active Modes of Spinels

Transition-metal normal spinel oxides of the general formula AB_2O_4 tend to exhibit Raman vibrational modes in the 100 – 800 cm^{-1} spectral region. Generally, strong bands are observed around the 200 cm^{-1}, and the 500 – 700 cm^{-1} regions. Bands of weaker intensity tend to be in the 200 – 400 cm^{-1} and 700 – 800 cm^{-1} regions. Raman bands in the 600 – 700 cm^{-1} region are normally attributed to the stretching vibrations of oxygen atoms inside the octahedral unit BO_6. The high-wave number bands are assigned to the A_{1g} species in the O^7_h spectroscopic symmetry. Raman bands around 580 cm^{-1} are due to the vibration of Al-O bonding and assigned to the first F_{2g} symmetry species. The bands around 483/516 cm^{-1} are assigned to the second F_{2g} symmetry species, the band around 490 cm^{-1} has the E_g symmetry and the band around 195 cm^{-1} is assigned to the third F_{2g} symmetry species.[1,2]

3.6 IR Active Modes of Spinels

As mentioned in section 3.4, transition-metal normal spinel oxides of the general formula AB_2O_4 are expected to exhibit four IR-active bands. For $CoAl_2O_4$, these vibrations generally occur in the v_1 (680 - 650 cm^{-1}), v_2 (580 - 540 cm^{-1}), v_3 (520 - 490 cm^{-1}), and v_4 (240 - 200 cm^{-1}) spectral regions. A general rule of thumb for spinels is that the IR band with the highest wavenumber is assigned to vibrational modes of the coordinated cation with the highest valency. In the case of the normal spinel $CoAl_2O_4$, this corresponds to the band at 660 cm^{-1} which is typical for octahedrally coordinated Al^{3+}. Therefore, the high-frequency v_1 and v_2 IR bands tend to be assigned to the Al-O stretching vibrations of the BO_6 (i.e. AlO_6) octahedral groups i.e. displacement of oxide anions relative to the aluminium cations along the direction of the octahedral chains. The equivalent for $ZnCo_2O_4$ is the Co-O vibration. The low-frequency v_3 and v_4 bands are due to vibrations of both cations in tetrahedral and octahedral sites, i.e. displacement of all ions in the lattice but mainly due to combined vibrations of Al and Co ions, respectively.[1,2,4,5] The equivalent for $ZnCo_2O_4$ would be vibrations related to Co and Zn.

According to group theory, the inverse spinel should also exhibit five Raman-active and four IR-active vibrational modes. However, a breakdown in the Raman and IR selection rules can occur due to various factors, including ordering of the cations on tetrahedral and octahedral sites, the presence of vacancies, interstitial cations, and general defects within the crystal structure which can affect the crystal symmetry. This can subsequently lead to an increase in the number of IR- and Raman-active modes.[1,2,4]

3.7 References

1. Z.V. Marinković Stanojević, N. Romčević, B. Stojanović, *J. Eur. Ceram. Soc.*, 2007, **27**, 903–907.
2. C.M. Julien, F. Gendron, A. Amdouni, M. Massot, *Mater. Sci. Eng. B-Solid,*

2006, **130**, 41-48.

3. T. Shimada, T. Tachibana, T. Nakagawa, T.A. Yamamoto, *J. Alloys Compd.,* 2004, **379**, 122-126.
4. C. Kringe, B. Oft, V. Schellenschlägar, H.D. Lutz, *J. Mol. Struct.,* 2001, **596**, 25-32.
5. G. Busca, V. Lorenzelli, V. Sanchez Escribano, R. Guidetti, *J. Catal.,* 1991,**131**, 167-177.

CHAPTER 4

Background of Infrared and Raman Spectroscopy

4.1 Molecular Energy

The energy of a molecule can be considered to be made up of translational, rotational, vibrational, and electronic energy. Electronic energy transitions normally give rise to absorption or emission in the ultraviolet (UV) and visible regions of the electromagnetic spectrum. Rotational energy transitions give rise to absorption in the microwave or the far infrared (IR) regions. Vibrational energy transitions give rise to absorption bands throughout most of the infrared region.[1] In this work, the emphasis will be on molecular vibrations in the IR and visible regions of the spectrum.

4.2 The Electromagnetic Spectrum

Electromagnetic waves are comprised of a range of wavelengths that are subdivided into 8 regions of the electromagnetic spectrum. These regions are referred to by different names; radio frequency, microwave, infrared (IR), visible, ultraviolet (UV), X-rays, γ-rays and cosmic rays.[1,2,3] In this work, only the region ranging from infrared to ultraviolet will be considered. Table 4-1 depicts the regions of interest in more detail.

Rather than absorbing radiation over the whole range of the electromagnetic spectrum, molecules tend to absorb radiation over the relatively narrow spectral regions as shown in table 4-1.[3]

Table 4-1: Selected regions of the electromagnetic spectrum with respective wavenumbers ($\bar{\nu}$) and wavelengths (λ).

REGION	$\bar{\nu}$ (cm^{-1})	λ (nm)
Far UV	1,000,000 to 50,000	10 to 200
Near UV	50,000 to 26,300	200 to 380
Visible	26,300 to 12,800	380 to 780
Near IR	12,800 to 4000	780 to 3000
Mid IR	4000 to 400	3000 to 30,000
Far IR	400 to 40	30,000 to 300,000

4.3 Molecules and Radiation

A wave of electromagnetic radiation consists of a fluctuating electric component and a fluctuating magnetic component which lie at right angles to each other. The electric field strength (*E*) at a given time (*t*) is expressed by:

$$E = E_o \cos 2\pi\nu t \quad \ldots.(4.1)$$

where E_o is the amplitude and ν is the frequency of radiation.

The distance between two equivalent points on the wave is called the wavelength, λ.

The frequency, ν, is the number of waves per unit time (Hz or cycles/s), i.e. time required for the wave to travel a distance, *s*. The frequency and wavelength are related by:

$$\nu = c/\lambda \qquad \text{....(4.2)}$$

where c is the velocity of light in a vacuum (3×10^{10} cm/sec) and λ is in cm.

The wavenumber $\bar{\nu}$ is the number of waves per unit length, and is defined by;

$$\bar{\nu} = \nu/c \qquad \text{....(4.3)}$$

Therefore the wavenumber, generally applied in units of cm^{-1}, is related to the other parameters by;

$$\bar{\nu} = 1/\lambda \ (cm^{-1}) \ \text{ and } \ \nu = c/\lambda = c\bar{\nu} \qquad \text{....(4.4)}$$

A light wave can thus be described by its frequency or wavelength. [1,3]

4.4 Absorption of Radiation by Matter

A monochromatic beam consists of photons with equal energies, $h\nu$. When a molecule comes in contact with an electromagnetic field (light beam), a transfer of energy (photons) from the field to the molecule can occur. That is, a molecule exposed to radiation either absorbs or emits a photon of energy or it remains unchanged. This is represented by the following equation:

$$\Delta E = h\nu = h(c/\lambda) = hc\bar{\nu} \qquad \text{....(4.5)}$$

where ΔE is the difference in energy between two energy states, h is Planck's constant (6.62 X 10^{-34} joules/sec) and c is the velocity of light. Thus the wavenumber, $\bar{\nu}$, is directly proportional to the energy of transition.

If $\Delta E = E_1 - E_0$ ….(4.6)

where,

E_0 = energy of the ground state

E_1 = energy of the excited state

then the molecule absorbs ΔE when it is excited from $E_0 - E_1$ and emits ΔE when it reverts from $E_1 - E_0$.

The value of ΔE depends on whether the transition of energy is from a lower or higher energy state. According to the Maxwell-Boltzmann distribution law, the population ratio of the $\nu = 1$ and $\nu = 0$ states is given by;

$$\frac{P_{v=1}}{P_{v=0}} = e^{-\Delta E/kT} \quad \text{….(4.7)}$$

Where,

k = Boltzmann's constant (1.3807 X 10^{-16} erg/degree)

T = absolute temperature

Since $\Delta E = hc\bar{\nu}$, the ratio becomes smaller as $\bar{\nu}$ becomes larger.

While the energy, $h\nu$, represents the energy of the individual photons in a beam of light, the intensity of the energy is represented by the actual number of photons present in the same beam. Hence, when a beam comes into contact with an absorbing substance, some of the photons get absorbed resulting in transmitted light

of a lower intensity than the incident radiation. It is worth mentioning that any energy absorbed by a molecule is retained for only a short period of time (i.e. 10^{-3} - 10^{-8} s in UV and IR regions) before it is dissipated by various processes such as fluorescence, photochemical decomposition, heat etc. Absorption spectra are therefore a result of absorption by molecules in their most stable, ground states only.[3]

4.5 Origin of IR and Raman Spectra

Incident radiation interacts with molecular energy levels in different ways depending on the region of the electromagnetic spectrum. IR absorption and Raman scattering techniques can be used to obtain information about the structure and properties of molecules based on their vibrational transitions, thereby aiding in their identification. In IR absorption, there is a direct interaction between the frequency of the IR radiation and the vibrational frequency of a particular mode of vibration in a molecule brought on as a result of the change in the dipole moment of the molecule during the vibration. When an IR photon interacts with a molecule, the photon is consumed and the molecule gains vibrational energy of an amount equal to the energy of the photon. IR absorption can therefore be considered as a one-photon event. [3,4,5]

Fig 4-1 depicts the change in dipole moment. If the charges, δ+ and δ-, are on atoms of masses M_1 and M_2, then the dipole moment is represented by the charge multiplied by the distance between charges (bond length). [3,4,5]

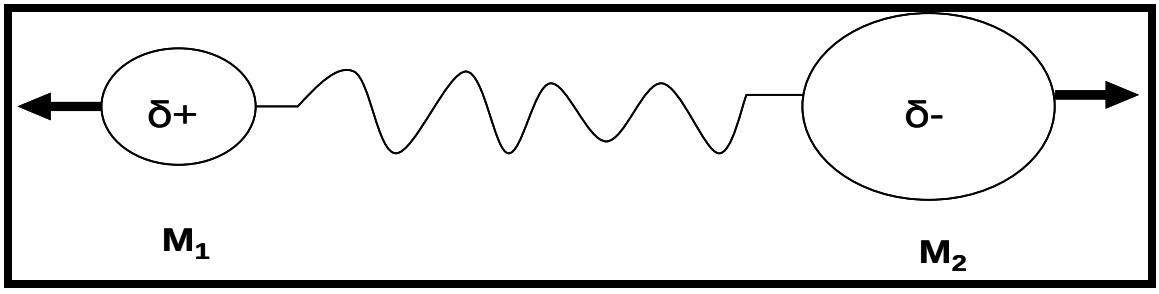

Figure 4-1: Schematic representation of the vibration of a diatomic molecule.

Usually in IR transmittance the IR radiation absorbed by a sample, is plotted as a percentage of the light intensity transmitted, T(%), at a given wavenumber ($\bar{\nu}$ cm^{-1}). Alternatively, a graph of absorption intensity against wavenumber can also be made. This is known as an absorption spectrum.[3] In this work, percentage transmittance was plotted against wavenumber.

$$T(\%) = I/I_o \text{ X } 100 \qquad \ldots.(4.8)$$

The intensity of IR absorption is governed by the Beer-Lambert law:

$$I = I_o e^{-\varepsilon cd} \qquad \ldots.(4.9)$$

where I and I_o represent the intensities of the incident and transmitted beams respectively, ε is the molecular absorption coefficient, c and d are the concentration of the sample and the sample path length respectively.[3]

Raman scattering, on the other hand, can be considered a two-photon event. Raman spectroscopy involves the indirect interaction of incident radiation with an induced dipole moment brought about by a change in the polarisability of the molecule during the vibration.[4]

When a molecule is irradiated by a light beam, it succumbs to the fluctuating electric field of the radiation, which induces a dipole moment. The observed Raman effect is as a result of scattering by the induced dipole moment. The magnitude of the induced dipole is proportional to the electric field intensity of the radiation, as shown by equation 4.10 below;

$$\mu = \alpha E \qquad \ldots.(4.10)$$

where $E = E_o \cos 2\pi\nu_o t$ (as already depicted in equation 4.1).

E_o is the fluctuating electric field intensity, brought on by a light wave of frequency ν_o. The proportionality constant, α, is referred to as polarisability. The induced dipole moment ranges from + αE_o to – αE_o with the frequency ν_o. The induced dipole subsequently emits the frequency ν_o resulting in Rayleigh scattering (scattering of the same frequency as during incident radiation). Raman scattering will only occur when the molecular vibration produces a change in polarisability.[3]

4.6 The Raman Effect

As mentioned in section 4.5, the Raman Effect is a light scattering effect. When a monochromatic beam of light of frequency ν_o, usually from a laser, interacts with a molecule, most of the incident radiation is transmitted, refracted, reflected and scattered at the same frequency. Light scattered at the same frequency as that of the incident beam is referred to as Rayleigh scattering. Scattered light can also be at different frequencies from that of the incident beam by the vibrational energy that is gained or lost in the molecule, $\nu_s = \nu_o \pm \nu_T$. This is referred to as Raman scattering. The observed change in frequency,ν_T, is as a result of the interaction between the incident beam and rotational, vibrational, or electronic energy levels of molecules. The Raman Effect is mostly concerned with vibrational transitions. Radiation that is scattered at lower frequencies than the incident beam ($\nu_s = \nu_o - \nu_T$) is referred to as Stokes scattering while the light scattered at higher frequencies than the incident beam ($\nu_s = \nu_o + \nu_T$) is referred to as anti-Stokes scattering. The difference in frequency between the incident beam and the Stokes or the anti-Stokes line is referred to as the Raman shift, $\Delta\nu = \nu_o \pm \nu_T$.[2,4,5]

Raman scattering is less intense than Rayleigh scattering and is directly proportional to the intensity of the incident beam and the concentration of the sample. According to the Maxwell-Boltzmann distribution law, the population of any excited level is always less than that of the ground state, therefore Stokes scattering is more intense than anti-Stokes. Since both Stokes and anti-Stokes scattering provide similar

information, normally only the Stokes side of the spectrum is used for interpretation.[2,4,5]

The Raman Effect is observed when incident and Raman scattered radiation, are in the near UV, visible and near IR region of the electromagnetic spectrum, depending on the laser used. Raman spectra are normally plotted on a graph as intensity against the Raman shift ($\Delta v = \nu_o \pm \nu_T$) in cm^{-1}.[5]

Fig 4-2 depicts the Raman Effect and IR absorption. When the initial state is regarded as the ground vibrational state and final state is regarded as the 1st vibrational level, then IR changes energy states in one step (one-photon event) while Raman scattering changes energy states in two steps (two-photon event) that involves photon energies that are higher than that of the IR photon or energy of the vibrational transition.[4]

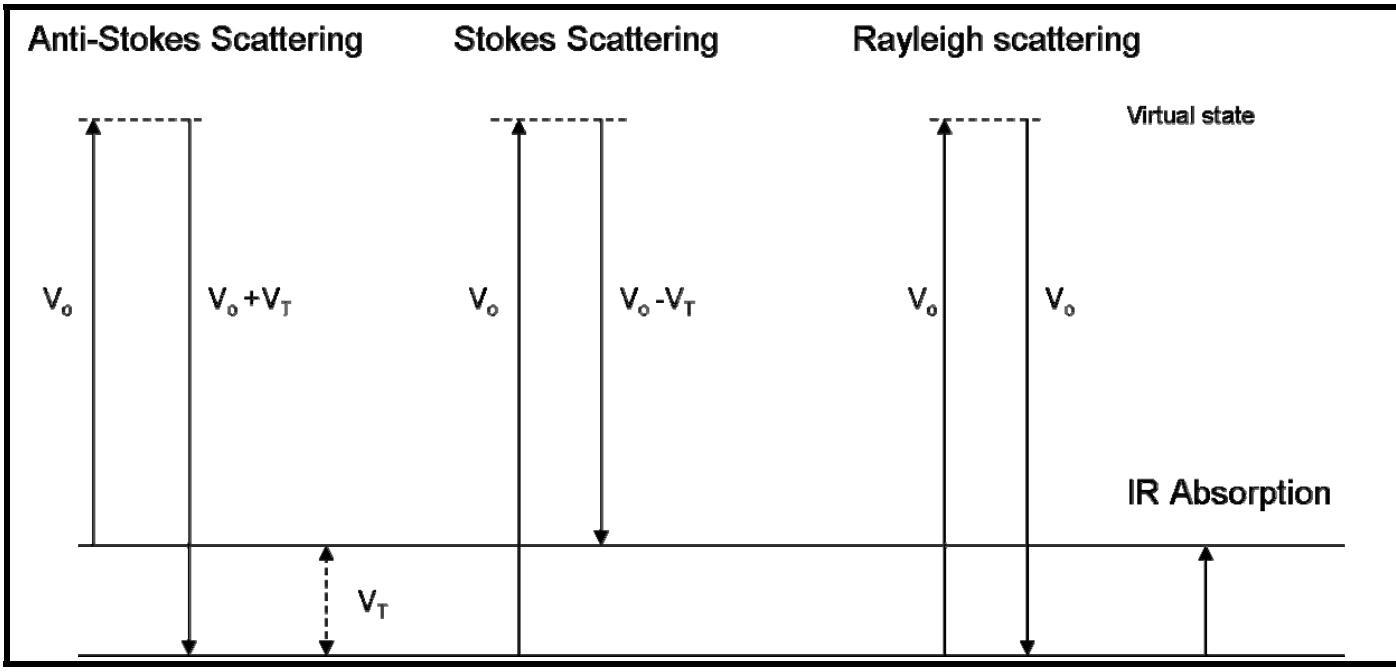

Figure 4-2: Schematic representation of the Raman effect and IR absorption.

4.7 Advantages of Raman Spectroscopy

Both Raman and IR are used in the study of vibrational and rotational frequencies of molecules. Although similar types of information can be obtained from the two techniques, they are not exact duplicates and each has its advantages. Generally, a vibration is either Raman active or IR active or active in both. Some vibrations are weak in IR and strong in Raman or vice versa. Generally, vibrations are strong in Raman if the bond is covalent and strong in IR if the bond is ionic. Some advantages of Raman spectroscopy in relation to IR spectroscopy are discussed below:

- There is minimal sample preparation for recording of Raman spectra, while IR normally requires some sort of sample preparation, depending on the nature of the specimen.

- With Raman spectroscopy, changes in structure can be tracked more accurately due to sharper peak definition and resolution, where IR bands would be broad or non-existant.

- Since the diameter of the laser beam used in Raman spectroscopy is normally 1 - 2 mm, only a small sample area is needed to obtain Raman spectra. Therefore, Raman spectra can be obtained from micro-sized samples (1 - 2 μm), single crystals, single grains of powder, individual filaments from synthetic or natural polymers and even liquid samples with no or minimal sample preparation. This is useful especially when only a small sample is available.

- For fluorescent coatings, trace impurities, coatings on polymers, additives etc., IR has traditionally been the preferred method of investigation due to intense fluorescence that potentially masks major components on Raman spectra under visible excitation. However, the use of UV excitation and the advent of Fourier Transform Raman spectroscopy with near-IR excitation has also enabled the study of naturally fluorescent biological materials.

- Water and hydroxyl groups exhibit strong absorption in the IR but only weak scattering intensity in the Raman Effect. Therefore, Raman spectroscopy is the preferred method for characterisation of hydrated biological materials as well as samples in aqueous solutions due to minimal interference from water vibrations. In addition, Raman spectra of hygroscopic and/or air sensitive compounds can be obtained by placing samples in a sealed glass container which would pose a problem in IR since glass absorbs IR and would be a source of interference.

- With Raman spectroscopy, the entire vibrational spectrum i.e. from 50 - 4000 cm^{-1} can be observed with a single recording and instrumentation. Inorganic and mineral pigments used in paintings, manuscripts, documents and currency, show strong absorption bands in low-wavenumber regions of the vibrational spectrum (i.e. < 400 cm^{-1}). Their characterisation therefore requires ease of accessibility to this region of which Raman spectroscopy fulfils this role. With IR, changes to instrumentation would need to be made to cover the region below 400 cm^{-1}.

- As most historical and archeological samples cannot be subjected to mechanical or chemical pre-treatment such as scraping, drilling etc., the shape and reflectivity of surfaces play an important role in their analysis. Curved surfaces are not ideal for IR analysis and flattening and crushing of samples would be required. With Raman spectroscopy, there is minimal or no damage to samples. Damage is usually as a result of the high laser powers necessary for sample illumination which can heat, burn or melt the sample. Although probes can be used for collecting IR and Raman data, spectra obtained in this way need to be carefully interpreted. However, the advent of portable Raman or IR instruments is increasing the applicability of these techniques for in situ examination of artefacts in e.g. in museums.

- Depth-profiling can be performed on suitable specimen such as protective varnish coatings, using Raman spectroscopy, due to advances in confocal microscopy using visible excitation and a CCD detector.. [2,5]

4.8 Applications of Raman Spectroscopy

As a non-destructive analytical technique, Raman spectroscopy is increasingly being used by art historians, archaeological scientists, museum conservators and forensic scientists in trying to decipher and identify the composition of their specimen.

Examples of applications of Raman spectroscopic techniques in different fields include:

- The differentiation between genuine and counterfeit specimen e.g. currency, ivory.

- The spectroscopic analysis of dyes, pigments and resins used in various specimen is of use in mapping of archaeological and historical trade routes. Pigments are found on a variety of objects such as paintings, frescoes, manuscripts, currency and china. Normally the pigment will only be located on a small section of the specimen and may additionally have been subjected to environmental deterioration. Resins are normally encountered during archaeological excavations and identification of these resins can provide further essential information about ancient trade routes and cultures.

- The identification of biological materials used in carved artwork (e.g. horn, hoof) to provide a better understanding of bio-deterioration processes, which could therefore assist with their proper restoration and conservation.

In addition, Raman spectroscopy is also finding use in determining the historical period as well as ancient technologies and methods used in the creation of specimen.[2]

4.9 References

1. N.B. Colthup, *Introduction to Infrared and Raman spectroscopy*, 3rd Edition, Academic Press Inc, USA, 1990.
2. P. F. Bernath, *Spectra of Atoms and Molecules*, Oxford University Press, New York, 1995.
3. J.C.D. Brand, *Applications of spectroscopy to organic chemistry*, Oldbourne book Co. Ltd, London, 1965
4. I. R. Lewis (Ed), *Handbook of Raman spectroscopy; from the research laboratory to the process line*, Marcel Dekker, New York, 2001.
5. J G. Grasselli (Ed), *Analytical Raman Spectroscopy*, John Wiley & Sons, USA, 1991.

CHAPTER 5

Experimental

5.1 General Synthesis of $CoAl_2O_4$

Various methods have been used to synthesise nanoscale oxide materials including cobalt aluminate ($Co^{2+}Al_2O_4$). These have ranged from solid-state to solution techniques such as chemical vapor deposition, laser ablation, and microemulsion techniques.[1] In addition, attempts to synthesize homogeneous fine powders at low temperatures have been carried out by various solution techniques, such as sol-gel, co-precipitation, hydrothermal, alkoxide hydrolysis, thermal decomposition of organic precursors, and polymerized complex methods.[1,2,3] The thermal decomposition of metal organic precursors is of major interest due to its numerous advantages, including a homogeneous metal ion distribution on the atomic level.[3]

As the various synthesis methods can lead to diverse oxide properties, the desired properties of the final material normally determines the preparation method used.[2]

Four types of synthesis techniques were employed in this research in order to prepare and characterise both the normal ($Co^{2+}Al_2O_4$) and inverse ($Co^{2+}Co^{3+}AlO_4$) spinels with the aim of understanding the development of the characteristic 485 cm^{-1} and 519 cm^{-1} Raman peaks. The synthesis techniques used were based on published methods with only a few minor changes and are mentioned in more detail below. In addition different batches of samples that were made on different days resulted in reproducible spectra (Raman, FT-IR and XRD) upon characterization.

All chemicals used in this research are listed in Appendix A.

5.2 Citrate-Gel / Glycine-Gel Synthesis Methods (Polymerized Complex Techniques)

Polymerized complex techniques are based on the polymerization of a solution of ethylene glycol, citric acid or glycine and metal ions. This gives rise to intermediate polymeric precursor-gels (i.e. citrate-gel and glycine-gel) which, upon pyrolysis, results in highly dispersed, homogeneous mixed oxides.[2,4] The stable metal-chelating complexes (gels) which are produced are then pyrolyzed at relatively low temperatures and short processing times in order to burn off the organic material and produce the appropriate oxide compositions.[3]

5.2.1 Glycine-Gel Synthesis Method

The glycine-gel synthesis is an example of a solution technique which allows for the preparation of highly purified, nanosized crystalline powders in a relatively shorter time period. The glycine-gel synthesis method allows for the preparation of $Co^{2+}Co^{3+}_{x}Al_{2-x}O_4$ (x = 0 - 2) crystalline spinels derived from Co-Al-glycine complexes, which are referred to as precursor gels.[3] The Co/Al ratio in the final powder was determined by modifying the mass of precursors used. In this regard, the normal ($Co^{2+}Al_2O_4$) and inverse ($Co^{2+}Co^{3+}AlO_4$) spinels were determined at precursor stage. Glycine was chosen as the complexing agent due to its ability to form strong complexes with Co and Al metal-ions.[3]

The precursor gels with different Co/Al ratios were heat treated under similar conditions to produce different $Co^{2+}Co^{3+}_{x}Al_{2-x}O_4$ (x = 0 - 2) crystalline spinels.

The glycine-gel synthesis method used in this research was based on the method of Wang et al.[3] The different masses of precursors used to prepare the $Co^{2+}Co^{3+}_{x}Al_{2-x}O_4$ (x = 0 - 2) crystalline spinels are shown in Table 5-1. The mass of aluminium (III) nitrate nonahydrate was kept constant, while the masses of cobalt (II) nitrate hexahydrate and glycine were varied. Cobalt (II) nitrate hexahydrate,

aluminium (III) nitrate nonahydrate and glycine, were added to 36 mL distilled water, under stirring, in a beaker. Glycine acted as a chelating agent. The purple solution was heated on a hotplate until the excess water had evaporated. The resulting thick, sticky gel-like, purple substance (precursor gel) was dried in an oven overnight at 100 ºC. Samples were then placed in an Al_2O_3 crucible in a furnace at room temperature and heated progressively to 1000 ºC (at a rate of 2 °C/min) which was maintained for 2 h, before being allowed to cool to room temperature in the same furnace and at the same rate.

Since no observed precipitation occurred during the concentration process, it can be assumed that the resulting gels contained a homogeneous mixture of the two metal ions (Co^{2+} and Al^{3+}). All six precursor gels (GG-1 to GG-6) shared the same precursors and reaction media with the exception of GG-6 which does not contain aluminium. In addition, GG-5 is an exception to the equation $Co^{2+}Co^{3+}_{x}Al_{2-x}O_4$.

In the method of Wang et al.[3], the precursor gels were calcined in a furnace under a gas stream of air at a specified flow-rate. For this research, the precursor gels were calcined in a furnace without a stream of air being applied.

Table 5-1 also shows the resultant colours of final powders based on treatment temperature. The brightest blue colouration was obtained for x = 0 (i.e. GG-1).

Table 5-1: Precursors, annealing temperatures and resultant colours for various $Co^{2+}Co^{3+}_{x}Al_{2-x}O_4$ powders, prepared by the glycine-gel method (where x = 0 - 2).

Sample	Co/Al (molar ratio*)	Glycine g (mol)	$Co(NO_3)_2.6H_2O$ g (mol)	$Al(NO_3)_3.9H_2O$ g (mol)	Colour
GG-1 ($Co^{2+}Al_2O_4$)	0.5	3.4 (0.045)	2.2 (0.0075)	5.6 (0.015)	Blue
GG-2 ($Co^{2+}Co^{3+}_{0.5}Al_{1.5}O_4$)	1.0	4.5 (0.060)	4.4 (0.0150)	5.6 (0.015)	Green
GG-3 ($Co^{2+}Co^{3+}_{0.8}Al_{1.2}O_4$)	1.5	5.6 (0.075)	6.6 (0.0225)	5.6 (0.015)	Green
GG-4 ($Co^{2+}Co^{3+}AlO_4$)	2.0	6.8 (0.090)	8.7 (0.0300)	5.6 (0.015)	Green/ Black
GG-5 ($Co^{2+}Co^{3+}_{1.5}AlO_4$)	2.5	7.9 (0.105)	10.9 (0.0375)	5.6 (0.015)	Black
GG-6 ($Co^{2+}Co^{3+}_{2}O_4$)	∞	7.9 (0.105)	15.3 (0.0525)	0	Black

GG = Glycine gel.

*Based on Wang et al.[3]

5.2.2 Citrate-Gel Synthesis Method

Another example of a solution technique is the citrate-gel synthesis method which is based on the method of Cho et al.[2] Unlike the glycine-gel synthesis where different masses of precursors were used to prepare $Co^{2+}Co^{3+}_{x}Al_{2-x}O_4$ (x = 0 - 2) crystalline spinels, the same mass of precursors were used. The normal ($Co^{2+}Al_2O_4$) and inverse ($Co^{2+}Co^{3+}AlO_4$) spinels were obtained by treating the gel precursor at different temperatures and time periods. Ethylene glycol (EG, 68 mL, 1.2 mol) was placed in a beaker and pre-heated to 50 ºC in a silicone oil bath under stirring. Cobalt (II) nitrate hexahydrate (6 g, 0.02 mol), was added and stirred

until dissolved. The solution turned magenta in colour. Citric acid monohydrate (63 g, 0.3 mol) was then added to this solution and stirred until completely dissolved. Aluminium (III) nitrate nonahydrate (15 g, 0.04 mol) was then added to the mixture under stirring and the temperature raised to 80 ºC. Upon complete dissolution, the temperature was then increased to 130 ºC to promote polymerization and to remove excess solvents. The temperature was further increased to 250 ºC and heated until the mixture became thick, sticky and gel-like with a dark-brown colouration. This precursor gel was dried in an oven overnight at 250 ºC resulting in a sponge-like structure which had a 'crumbly' texture. Samples were then placed in Al_2O_3 crucible in a cold oven, and then heated progressively to the desired temperature (350 - 1000 ºC) which was maintained for 2 h before cooling to room temperature and removing from the furnace.[2]

The observations made during preparation differed somewhat from those of Cho et al.,[2] in that the solution never became transparent after addition of aluminium (III) nitrate nonahydrate and it never solidified into a black solid mass which needed to be ground. Instead, the solution turned from a magenta colour (after addition of cobalt (II) nitrate hexahydrate) to a brown colour which eventually solidified into a brown gel-like substance that resembled soft breadcrumbs after drying overnight in the oven. In addition, only a fifth of the quantities given by Cho et al.[2] were used.

Table 5-2 shows the various precursors used in the citrate-gel synthesis of $Co^{2+}Co^{3+}_xAl_{2-x}O_4$ (x = 0 - 2), as well as the resultant colours of powders based on treatment temperature.

Table 5-2: Precursors, annealing temperatures and resultant colours for various $Co^{2+}Co^{3+}_{x}Al_{2-x}O_4$ (x = 0 – 2) powders prepared by the citrate-gel method.

Precursors: 6 g cobalt(II)nitrate hexahydrate, 15 g aluminium(III)nitrate nonahydrate, 63 g citric acid monohydrate, 68 mL ethylene glycol		
Sample	**Temperature (annealed for 2 h)**	**Colour**
CG-350 ºC	at 350 ºC	Ash-black (green)
CG-400 ºC	at 400 ºC	Green
CG-500 ºC	at 500 ºC	Green
CG-600 ºC	at 600 ºC	Green-black
CG-700 ºC	at 700 ºC	Green (blue-green)
CG-800 ºC	at 800 ºC	Blue
CG-900 ºC	at 900 ºC	Blue
CG-1000 ºC	at 1000 ºC	Blue

CG = citrate-gel.

5.3 Polyol Synthesis Method

The polyol method was introduced more than twenty years ago as a new technique of preparing monodisperse fine spherical oxide particles (pigment powders) with controlled morphology and ranging in size from 30 - 200 nm.[1,5] In this method, an appropriate metal precursor (e.g. metal acetate, alcoholate or halogenide) is mixed with water and a multivalent, high-boiling alcohol (e.g. diethylene glycol, DEG) and heated to 180 - 240 ºC for 2 - 12 h.[1,6] Precipitation of the oxide occurs at a particular temperature and after a certain time period, resulting in colloidally stable suspensions of nanoscale particles in DEG, with a solids content of up to 20 wt%.[1.6.7] Centrifugation can be used to separate the oxide particles from the suspensions for further investigation. In some instances, the oxide particles are highly crystalline directly after their synthesis in the DEG mixture (e.g. $ZnCo_2O_4$)

but sometimes additional heating of the powder is required to maximize the crystallinity and produce the characteristic colour (e.g. $Co^{2+}Al_2O_4$). [1,6,7]

5.3.1 Role of the Chelating Agent Diethylene Glycol (i.e. Polyol)

Polyols such as DEG have many desirable properties such as a high boiling point, amphiprotic character, dissolving, complexing, reducing and protective properties.[5] These properties are utilized in the chemical reactions that occur during the polyol synthesis method, i.e. reduction of a metal cation, hydrolysis, and polymerization. Coverage of the growing particles with DEG is thought to play a major role in the resulting spherical morphology and size of the oxide, by complexing and stabilizing the surface of the growing oxide particles. This limits particle growth and non-homogeneous growth of the nuclei as well as resulting in almost non-agglomerated particles in a DEG suspension.[1,6,7]

5.3.2 Modification of Parameters

The polyol synthesis method is relatively straightforward and has also been used to synthesise a wide range of materials including sulphides, phosphates, and elemental metals.[1] Adjustment of the experimental conditions, such as the concentration of the metal precursor, amount of water added, and the temperature and time period of the reaction results in particle diameters ranging from about 30 - 200 nm.[1,7] Increasing any one of the parameters leads to larger particles, therefore it makes the polyol process unique in being able to control the diameter of particles down to nanometer size. The smaller the particle size, the more homogeneous the final product is. The choice of metal precursor determines the composition of the final product.[1]

In comparison to other methods such as the solid-state method (section 5.4), the required temperatures for the polyol method are relatively low.[6]

5.3.3 Synthesis

In this research, the polyol synthesis of nanoscale $ZnCo_2O_4$ and $Co^{2+}Al_2O_4$ colour pigments are described. The two cations have different electronegativities and hence are expected to exhibit different characteristics, although both are spinel.

Polyol synthesis for $Co^{2+}Al_2O_4$ was based on a method by Feldmann.[6] A silicone oil bath was pre-heated to 140 ºC. 50 mL diethylene glycol was added to a round-bottomed flask with a reflux condenser under stirring. Aluminium (III) acetate basic (8.0 g, 0.05 mol) was added to the DEG under stirring and placed in the hot oil bath. When the aluminium (III) acetate basic was fully dissolved, cobalt (II) acetate tetrahydrate (5.6 g, 0.02 mol) was added to the mixture and stirred until dissolved. The clear and colourless solution turned to a pinkish-purple colour upon the addition of cobalt (II) acetate. 2 mL water was added to the mixture and the temperature increased to 180 ºC. After 2 h at 180 ºC, the now purple suspension containing the $Co^{2+}Al_2O_4$ pigment was removed from the oil bath, cooled to room temperature, centrifuged and washed twice with ethanol (re-suspended in ethanol and centrifuged). The resulting pinkish-purple $Co^{2+}Al_2O_4$ powder was dried for 15 min at 80 ºC in an oven.

For $ZnCo_2O_4$, the metal precursors used were zinc (II) acetate dihydrate (1.0 g, 4.9 mM) and cobalt (II) acetate tetrahydrate (2.0 g, 8.4 mM). The clear and colourless solution turned to a purple colour upon addition of cobalt (II) acetate. The final colour of the suspension was green and the resulting $ZnCo_2O_4$ powder was lime green.[6] Unlike in the method of Feldmann[6], the solution did not become clear when the two salts were mixed. Instead, it turned from a purple colour when cobalt (II) acetate was added to a green colour as the reaction progressed.

The prepared $ZnCo_2O_4$ and $Co^{2+}Al_2O_4$ powders were annealed for various time periods at varying temperatures in order to prepare them for characterisation.

Tables 5-3 and 5-4 show the various precursors used in the polyol synthesis of $Co^{2+}Al_2O_4$ and $ZnCo_2O_4$ respectively as well as the resultant colours of powders based on annealing temperature.

Table 5-3: Precursors, annealing temperatures and resultant colours for various $CoAl_2O_4$ powders prepared by the polyol method.

Precursors: 8.0 g aluminium(III) acetate basic and 5.6 g cobalt(II) acetate tetrahydrate, diethylene glycol		
Sample	**Temperature**	**Colour**
P-180 ºC	Prepared at 180 ºC	Pink
P-600 ºC	Annealed for time ranges from 30 min to 24 h at 600 ºC	Green
P-700 ºC	Annealed for time ranges from 30 min to 24 h at 700 ºC	Green
P-800 ºC	Annealed for time ranges from 75 min to 6 h at 800 ºC	Blue
P-900 ºC	Annealed for time ranges from 75 min to 6 h at 900 ºC	Blue
P-1000 ºC	Annealed for time ranges from 5 min to 5 h at 1000 ºC • 5 min • 15 min • 75 min • 2 h • 5 h	 Dark Blue Dark Blue Blue Bright Blue Bright Blue

P = Polyol.

Table 5-4: Precursors, annealing temperatures and resultant colours for various $ZnCo_2O_4$ powders prepared by the polyol method.

Precursors: 1.0 g zinc(II) acetate dihydrate and 2.0 g cobalt(II) acetate tetrahydrate, diethylene glycol		
Sample	**Temperature**	**Colour**
ZCO-180 ºC	Prepared at 180 ºC	Green
ZCO-500 ºC	Annealed for 2 h at 500 ºC	Black
ZCO-2 h at 1000 ºC	Annealed for 2 h at 1000 ºC	Black
ZCO-24 h at1000 ºC	Annealed for 24 h at 1000 ºC	Black

ZCO = Zinc Cobalt Oxide.

5.4 Solid-State Synthesis

A conventional method of preparing oxide spinels is via solid-state reactions of mixtures of different cobalt and aluminum precursors at approximately 1000 ºC for a specified length of time. The composition and colour of the final product depends on the precursors used, the treatment temperature and time period.[2,4,8] Treatment at 800 ºC normally results in a blackish-blue compound, while treatment at 1000 - 1300 ºC results in a bright blue pigment. [2,4,8]

The main differences, and thus disadvantages, with the solid-state method in comparison to solution techniques mentioned in the sections above is that :

- In an attempt to obtain a proper mix of precursors, some form of grinding has to be used, which does not always lead to a homogeneous mix and could potentially introduce contaminants which can negatively affect the properties of the final product.[3]
- Despite grinding, the mixture still requires to be treated at high temperatures (1000 - 1400 ºC) and long time periods (up to 24 h). This normally results in non-homogeneous crystalline products with a low surface area.[3]

Therefore, solid-state synthesis is not an appropriate method for preparing nanosized oxide particles under low temperatures, for short processing times and consisting of low surface areas.

5.4.1 Procedure

The solid-state method used in this research to prepare $Co^{2+}Al_2O_4$ is based on the method of De Waal.[9] Cobalt sulphate (0.24 g) and aluminum sulphate octadecahydrate (0.60 g) were mixed in an alumina crucible and placed in a furnace at 300 ºC for three hours. The mixture was removed from the furnace and allowed to cool to room temperature before it was ground using a pestle and mortar and calcined for 24 h at 1000 ºC. The mixture was allowed to cool to room temperature before the sample was removed from the furnace and characterised.

In this research the glycine-gel, citrate-gel and polyol methods were used to prepare mixed Co-Al oxide particles in an attempt to follow the development of the 485 cm^{-1} and 519 cm^{-1} Raman peaks and to reduce the temperature of preparation and calcination times. The solid-state method was used only for the purpose of comparing characteristics of the oxide formed with those from the solution techniques. A full list of various processing times, temperatures and colours of crystalline powders from the synthesis methods mentioned above can be found in Appendix B. The resulting black, green or blue powders from the various synthesis techniques were further characterised by Raman, XRD, SEM and FTIR.

5.5 Characterisation

The development of the spinel crystalline phase from precursors as a function of calcining temperature can be observed by the analysis of their Raman, XRD, and FTIR results. The aim was to show variation of structure of cobalt aluminium oxide with temperature. In order to identify the Raman and IR bands and XRD peaks of the samples, Cobalt aluminate (spinel) [Farbmühle Kraemer, Germany], Cobalt(II)

oxide [Aldrich], and Cobalt(II, III) oxide [Aldrich], were used as reference materials. A full list of reference materials and reagents used in this research is found in Appendix A.

5.5.1 Raman Spectroscopy

Laser Raman spectra were collected at room temperature using a Dilor XY multi-channel spectrometer equipped with a liquid nitrogen-cooled CCD detector. A back-scattering (180°) micro-Raman configuration, using a confocal Olympus microscope with a 50 X objective, was used to focus the laser beam on the sample. The excitation radiation was provided by Kr^+ and Ar^+ Coherent Innova 300 lasers operating at 568.2 and 514.5 nm wavelengths respectively. The laser power was set at 5 mW, 10 mW and 100 mW at the source, depending on the oxide sample being analysed. An estimated 10 % of the laser output reached the sample under the microscope. The recording time was set between 300 s and 420 s with 2 and 8 accumulations per spectral segment depending on the sample being analysed. Spectra were recorded in the range 200 - 1700 cm^{-1} (for synthesized samples) and 200 - 1400 cm^{-1} (for commercial samples). The difference in spectral range was to account for any potential peaks due to impurities and/or unreacted precursors that may arise due to unrefined laboratory preparation methods as opposed to commercialized systems which tend to produce 'purer' products. The spectral resolution was 3 cm^{-1}. Data acquisition and processing were carried out with Labspec® software version 3.01 (Jobyn Yvon, Horiba Group).[10]

5.5.2 Infrared Spectroscopy

The spectra of the precursors and powders sintered under different conditions were obtained with a Bruker IFS 113V Fourier transform infrared spectrometer. The infrared transmittance was scanned through a KBr (Uvasol, potassium bromide, Merck) pellet for mid-infrared and a PE (polyethylene) pellet for far-

infrared, 32 times at a resolution of 2 cm^{-1} under vacuum. The pellets were prepared with approximately 2 mg of sample and 100 mg of KBr (mid-infrared) or 200 mg PE (far-IR). The averaged spectrum was ratioed with spectra from pure KBr or PE pellets run under similar conditions. Spectra were recorded in the range 4000 - 400 cm^{-1} (for mid-IR) and 400 - 50 cm^{-1} (for far-IR). The spectra were analysed with OpusNT v 2.0[11] and PeakFit[12] software.

5.5.3 X-Ray Powder Diffraction

The sintered and commercial powders were characterised by X-ray powder diffraction (XRD) to identify the resultant structural phases. The XRD analyses were performed using a PANalytical X'Pert Pro powder diffractometer with X'Celerator detector and variable divergence and receiving slits with Ni filtered Cu-Kα or Fe filtered Co-Kα radiation source (40 kV, 40 mA) from a Siemens D-501, with a graphite secondary monochromator and a scintillation counter detector. Samples were prepared for XRD analysis using a back-loading preparation method. The powdered sample was placed on a flat plastic plate, which was rotated at 30 r/min. The scans were performed at 25 ºC in 2θ steps of 0.04º, with a 2 s recording time for each step. Where accurate 2θ values were required, Si was added as internal 2θ standard. The structural phases were identified using X'Pert Highscore plus software and quantification (Rietveld method) was achieved by Autoquan/BGMN software (GE Inspection Technologies) employing Fundamental Parameter Approach.[13]

5.5.4 Scanning Electron Microscopy

Morphologies of the sintered powders were examined by Scanning Electron Microscopy (SEM). Energy dispersive spectroscopy (EDS) was applied in the electron microscope. Samples for SEM were prepared by placing the powder samples on conductive carbon tape, which was in turn fixed to an aluminium plate. The samples were coated with gold to prevent charge build-up. The samples for

EDS were coated for 30 s. A JEOL JSM 840 (JEOL, Tokyo, Japan) was used for imaging, and a JEOL JSM 5800 LV Noran Voyager 4 Image Analysis System (JEOL, Tokyo, Japan) for energy dispersive analyses.[14]

5.6 Experimental Considerations

Below are comments on the aspects of the research work carried out in the laboratory.

5.6.1 Solid-state

Reacting solid precursors directly at high temperatures is a core element in solid-state chemistry. However, to ensure proper contact of the chemical precursors with one another, i.e. increase the reaction surface area, grinding is necessary. Two types of solid-state reactions were perfomed in this research: (i) the direct reaction of solid precursors (solid-state method) and (ii) the annealing of powders produced by co-precipitation via the solution methods (polyol, citrate-gel and glycine-gel).

5.6.2 Reaction Conditions

In order to attain lower reaction temperatures, shorter reaction times, and a more homogeneous starting mixture of particles, co-precipitation of chemical species was necessary in the solution methods. Co-precipitation was initiated by evaporating the solvents used in the preparation. The polyol aided in reducing the reaction temperature as well as in facilitating a homogeneous reaction mixture. The excess polyol was removed by washing with ethanol, filtration and annealing/calcining.

5.6.3 Mass of Samples

Since reaction products for the solid-state method could not be separated from each other, the required mass of precursors was carefully determined and weighed in order to obtain the appropriate stoichiometry in the final product. It was this stoichiometry that determined whether the resultant powder was a spinel or not.

5.6.4 Synthesis Temperature

The temperature at which the reaction occurred as well as the rate at which the temperature was reached in the furnace was equally important. Based on published work, a temperature of 1000 ºC was necessary in order to obtain the desired crystal phase for most of the methods employed in this research. In most instances, the precursors were heated at the same rate as the furnace to the required temperature. After the predetermined time period, the products were removed from the furnace after it had cooled down to room temperature.

5.6.5 Processing Time

For the solid-state method, processing times of 24 h were used to ensure that the reactions had gone to completion and to ensure good crystallinity. For solution methods (polyol, citrate-gel and glycine-gel), processing times were 2 h because this was a determined time period from published work for the completion of the reaction at 1000 ºC in order to obtain the desired crystal phase.

5.6.6 Crucibles

All annealing/calcining steps were performed in alumina or ceramic crucibles which were chosen because normal/moderate heating rates were used as opposed to fast heating of samples where metallic crucibles would have been better suited.

5.6.7 Furnaces

Electrically heated muffle furnaces, consisting of an enclosed chamber, surrounded by the heating elements, were used in this study. Crucibles were placed in the middle of the furnace for consistency and to avoid the fluctuations of temperature based on location in the furnace.

5.7 References

1. C. Feldman, *Adv. Funct. Mater.,* 2003, **13**, 101-107.
2. Woo-Seok Cho, M. Kakihana, *J. Alloys Compd.,* 1999, **287**, 87-90.
3. C. Wang, S. Liu, L. Liu, X. Bai, *Mater. Chem. Phys.,* 2006, **96**, 361-370.
4. M. Zayat, D. Levy, *Chem. Mater.* 2000, **12**, 2763-2769.
5. L. Poul, S. Ammar, N. Jouini. And F. Fievet, F. Villain, *J. Sol-gel Sci. Techn.,* 2003, **26**, 261-265.
6. C. Feldmann, *Adv. Mater.,* 2001, **13**, 1301-1303.
7. C. Feldmann, Hans-Otto Jungk, *Angew. Chem. Int. Ed.,* 2001, **40**, 359-362.
8. G. Carta, M. Casarin, N. El Habra, M. Natali, G. Rossetto, C. Sada, E. Tondello, P. Zanella, *Electrochim. Acta,* 2005, **50**, 4592–4599.
9. D. de Waal, *Asian Chem. Lett.*, 2004, **8**, 57-63.
10. *Labspec,* Version 3.01, distributed by DILOR SA & Université de Reims, France, 1997.
11. *OPUS* version 3.1, distributed by Bruker Optik GmbH, Ettlingen, Germany, 2000.
12. *PeakFit,* version 4.06, distributed by AISN Software Inc., Mapleton, 1995.
13. S.Verryn, Details of the XRD procedure used at the University of Pretoria XRD laboratory, Personal Written Communication, University of Pretoria, Pretoria, 2006.
14. A.N. Hall, A.J. Botha, C. Van der Merwe, The instrumentation and sample preparation for SEM, verbal comm., University of Pretoria, Pretoria, 2006.

CHAPTER 6

Results and Discussion

6.1 Glycine-Gel Method

The glycine-gel method was chosen to specifically generate spinels of the formula $Co^{2+}Co^{3+}_xAl_{2-x}O_4$ (x = 0 - 2). This was achieved by selecting masses of precursors . based on different Co/Al ratios.[1] In section 6.2, results from alternative synthesis methods are given with the aim to further characterise and confirm findings from the results obtained from the glycine-gel method. The detailed glycine-gel synthesis procedure is given in section 5.2.1.

6.1.1 Synthesis of $Co^{2+}Co^{3+}_xAl_{2-x}O_4$ (x = 0 - 2) Spinels

Crystalline $Co^{2+}Co^{3+}_xAl_{2-x}O_4$ spinels, designated as GG, were obtained by calcination of amorphous glycine-Co-Al gels resulting from the heating stage of preparation. Calcination was performed at 1000 ºC for 2 h. Raman, FT-IR, and XRD was used to characterise the spinel crystalline phase and aid in proposing a method for its development from precursors. Since the gels were prepared and calcined using the same method, apart from the masses of precursors, only gels that would theoretically result in the crystalline powders GG-1 ($Co^{2+}Al_2O_4$), GG-4 ($Co^{2+}Co^{3+}AlO_4$) and GG-6 ($Co^{2+}Co^{3+}_2O_4$) were selected to characterise the development of their crystal phase by calcination (section 6.1.3 and 6.1.4.)

6.1.2 Raman and XRD Results for $Co^{2+}Co^{3+}_xAl_{2-x}O_4$ Spinels

Figure 6-1 shows the Raman spectra of samples prepared to theoretically give GG-1 ($Co^{2+}Al_2O_4$), GG-2 ($Co^{2+}Co^{3+}_{0.5}Al_{1.5}O_4$), GG-3 ($Co^{2+}Co^{3+}_{0.8}Al_{1.2}O_4$), GG-4 ($Co^{2+}Co^{3+}AlO_4$), GG-5 ($Co^{2+}Co^{3+}_{1.5}AlO_4$) and GG-6 ($Co^{2+}Co^{3+}_2O_4$). The Raman spectra show a variation in the structures of the various samples, although there are

close similarities between the spectra of GG-2 and GG-3 and between GG-5 and GG-6 possibly due to the similarity of their Co:Al ratios. Based on the objectives of the glycine-gel synthesis method, it can be assumed that GG-1 does not contain Co^{3+} and GG-6 does not contain Al^{3+}.

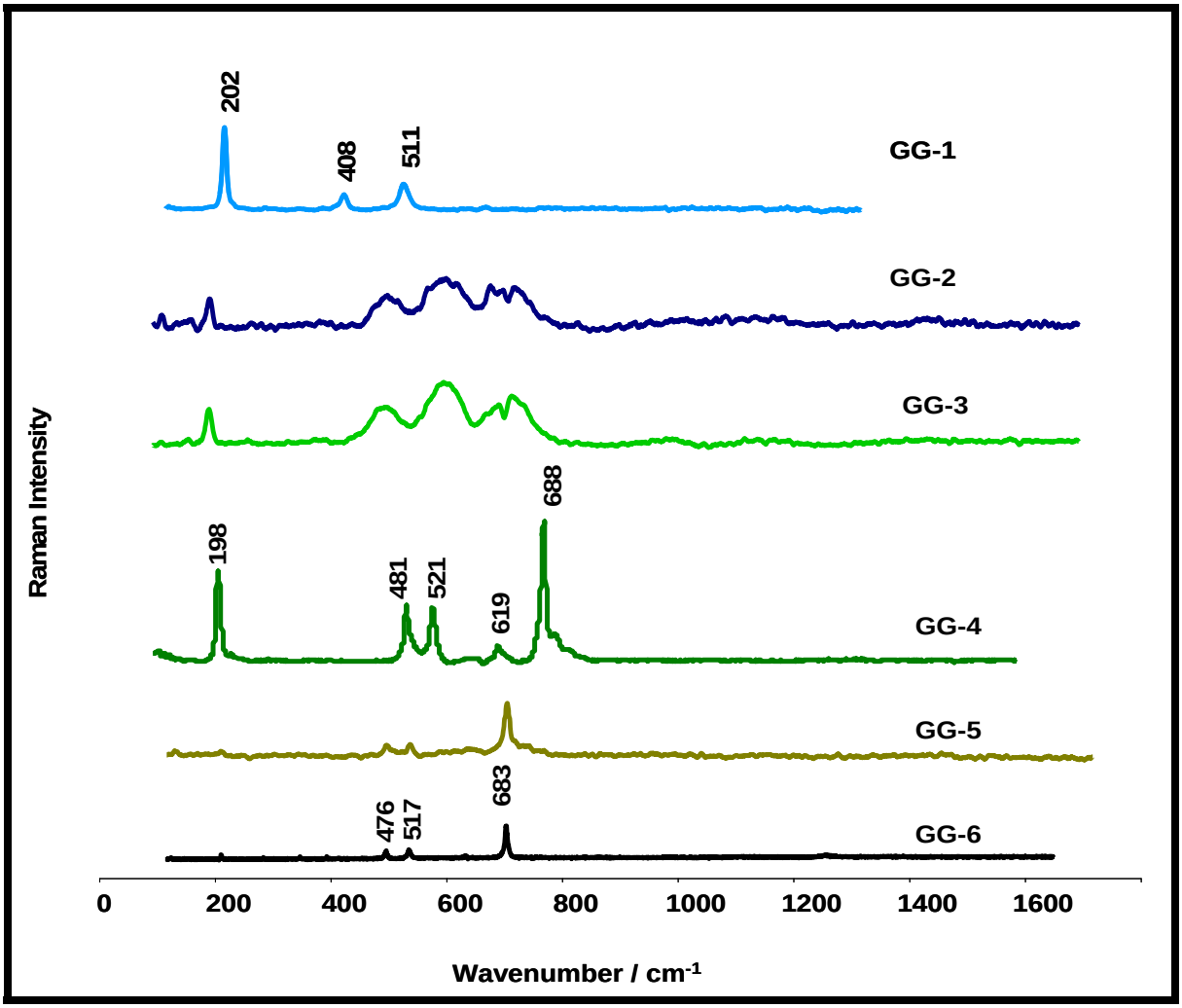

Figure 6-1: Raman spectra of samples GG-1 ($Co^{2+}Al_2O_4$), GG-2 ($Co^{2+}Co^{3+}_{0.5}Al_{1.5}O_4$), GG-3 ($Co^{2+}Co^{3+}_{0.8}Al_{1.2}O_4$), GG-4 ($Co^{2+}Co^{3+}AlO_4$), GG-5 ($Co^{2+}Co^{3+}_{1.5}AlO_4$) and GG-6 ($Co^{2+}Co^{3+}_2O_4$) prepared by the glycine-gel method (calcined for 2 h at 1000 ºC).

Table 6-1 shows the different Raman band positions and intensities for each type of sample, which can be attributed to the different Co:Al ratios. For instance, GG-1 has a

Raman band at 408 cm^{-1} which is not present in the other sample types, while GG-4 and GG-5 have strong Raman bands at 481 cm^{-1} which are not present in other samples. High Intensity Raman bands are in blue. The similarity of Raman band position and intensity between GG-2 and GG-3 as well as between GG-5 and GG-6 can be observed. Intensities are relative to each sample type and not in comparison with each other.

Table 6-1: Shifts in positions and intensities of Raman bands in cm^{-1} with changing Co:Al Ratio for samples GG-1 ($Co^{2+}Al_2O_4$), GG-2 ($Co^{2+}Co^{3+}_{0.5}Al_{1.5}O_4$), GG-3 ($Co^{2+}Co^{3+}_{0.8}Al_{1.2}O_4$), GG-4 ($Co^{2+}Co^{3+}AlO_4$), GG-5 ($Co^{2+}Co^{3+}_{1.5}AlO_4$) and GG-6 ($Co^{2+}Co^{3+}_2O_4$)..

Sample	Raman Bands									
GG-1	202vs	272w 332w 372w	408m 476w	511s	562-625w		655w			747w
GG-2	198s	271w	390w	505s		605vs	622sh	685vs	703sh	727s 777sh 833w
GG-3	197s	264w 338w 382w	400w	502s		604vs			696s	721s
GG-4	197vs	272w 330w 364w 386w	435w 481s	514w 521s	570w 582w	619m		688vs	704sh	723sh
GG-5	194w	232w 421w 453w	481s	520s	573w	598m	623w	688vs		725sh 751sh
GG-6	193m	272w 420w	476s	516s		614m		683vs		

vw (very weak), vs (very strong), w (weak), m (medium), s (strong), sh (shoulder).

Figure 6-2 shows the corresponding XRD patterns of samples GG-1 to GG-6. In contrast to the Raman spectra, the XRD patterns all show a similar spinel structure and the presence of only one phase, as determined by XRD data acquisition and analysis using X'Pert Highscore plus software (section 5.5.3) as well as by comparison with literature patterns. However, a detailed analysis of XRD patterns in section 6.1.5 show some peaks which can be used to discriminate between GG-1, GG-4 and GG-6.

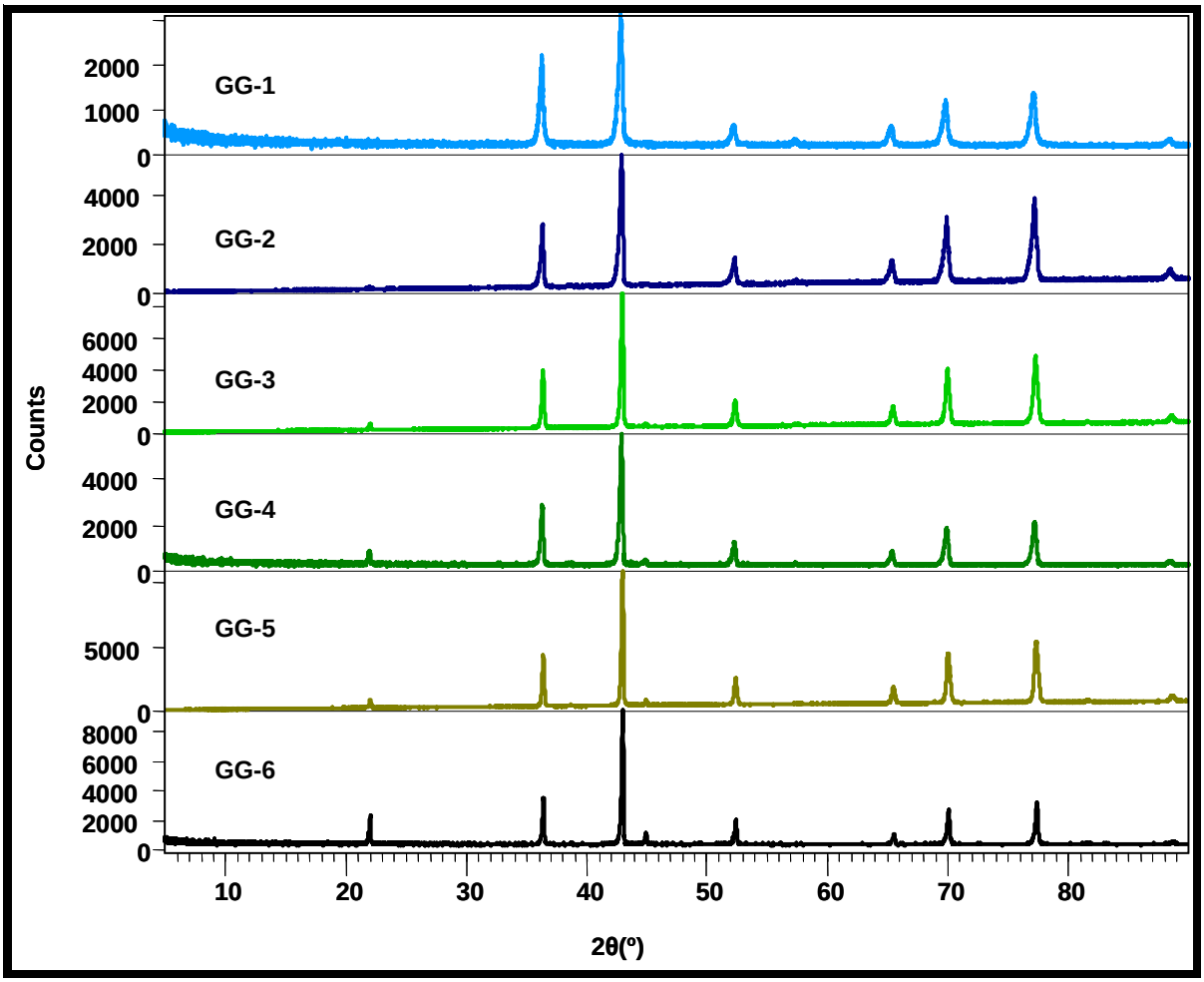

Figure 6-2: XRD patterns of samples GG-1 ($Co^{2+}Al_2O_4$), GG-2 ($Co^{2+}Co^{3+}_{0.5}Al_{1.5}O_4$), GG-3 ($Co^{2+}Co^{3+}_{0.8}Al_{1.2}O_4$), GG-4 ($Co^{2+}Co^{3+}AlO_4$), GG-5 ($Co^{2+}Co^{3+}_{1.5}AlO_4$) and GG-6 ($Co^{2+}Co^{3+}_2O_4$) prepared by the glycine-gel method (calcined for 2 h at 1000 ºC).

The samples share the same spinel cubic *(Fd3m)* crystallographic structure, as explained in section 3.3 and confirmed by analysis of data with X'Pert Highscore plus software, differing only slightly in the size of the lattice as shown in Table 6-2.[1] Also presented in Table 6-2 are the Co:Al ratios, obtained by SEM-EDX, which confirms the absence of Al in GG-6 and gives the actual Co:Al ratios for GG-1, GG-4 and GG-6 as 1:1, 8:1 and ∞ respectively. Experimental data from which these ratios were calculated is given in Appendix C.

Table 6-2: Comparison of some physical properties of samples GG-1 ($Co^{2+}Al_2O_4$), GG-2 ($Co^{2+}Co^{3+}_{0.5}Al_{1.5}O_4$), GG-3 ($Co^{2+}Co^{3+}_{0.8}Al_{1.2}O_4$), GG-4 ($Co^{2+}Co^{3+}AlO_4$), GG-5 ($Co^{2+}Co^{3+}_{1.5}AlO_4$) and GG-6 ($Co^{2+}Co^{3+}_2O_4$).

Sample	Empirical Formula	Co:Al ratio (theoretical)	Co:Al ratio (obtained)	Lattice Constant (Å) with esd (obtained)
GG-1	**$Co^{2+}Al_2O_4$ ($CoAl_2O_4$)**	**1:2**	**1:1**	**8.1114 (2)**
GG-2	$Co^{2+}Co^{3+}_{0.5}Al_{1.5}O_4$ ($Co_{1.5}\ Al_{1.5}O_4$)	1:1	-	8.1108 (63)
GG-3	$Co^{2+}Co^{3+}_{0.8}Al_{1.2}O_4$ $Co_{1.8}\ Al_{1.2}O_4$)	(1.8) : (1.2)	-	8.1019 (1)
GG-4	**$Co^{2+}Co^{3+}AlO_4$ ($Co_2\ AlO_4$)**	**2:1**	**8:1**	**8.1028 (1)**
GG-5	$Co^{2+}Co^{3+}_{1.5}AlO_4$ ($Co_{2.5}AlO_4$)	(2.5):1	-	8.0968 (10)
GG-6	**$Co^{2+}Co^{3+}_2O_4$ (Co_3O_4)**	**3:0**	**3:0**	**8.0885 (10)**

GG-1, 4 and 6 are highlighted in blue.

6.1.3 Raman Characterisation of GG-1 ($Co^{2+}Al_2O_4$), GG- 4 ($Co^{2+}Co^{3+}AlO_4$), and GG- 6 ($Co^{2+}Co^{3+}{}_2O_4$)

As mentioned in section 6.1, GG-1, GG-4 and GG-6 were selected to aid in explaining the development of the crystal phase of the spinels with the general formula $Co^{2+}Co^{3+}{}_xAl_{2-x}O_4$. GG-1 ($Co^{2+}Al_2O_4$) is referred to as the 'normal' spinel, while GG-4 ($Co^{2+}Co^{3+}AlO_4$) is the 'inverse' spinel and GG-6 ($Co^{2+}Co^{3+}{}_2O_4$) the Co_3O_4 spinel. Figure 6-3 depicts the Raman spectra of samples GG-1, GG-4 and GG-6.

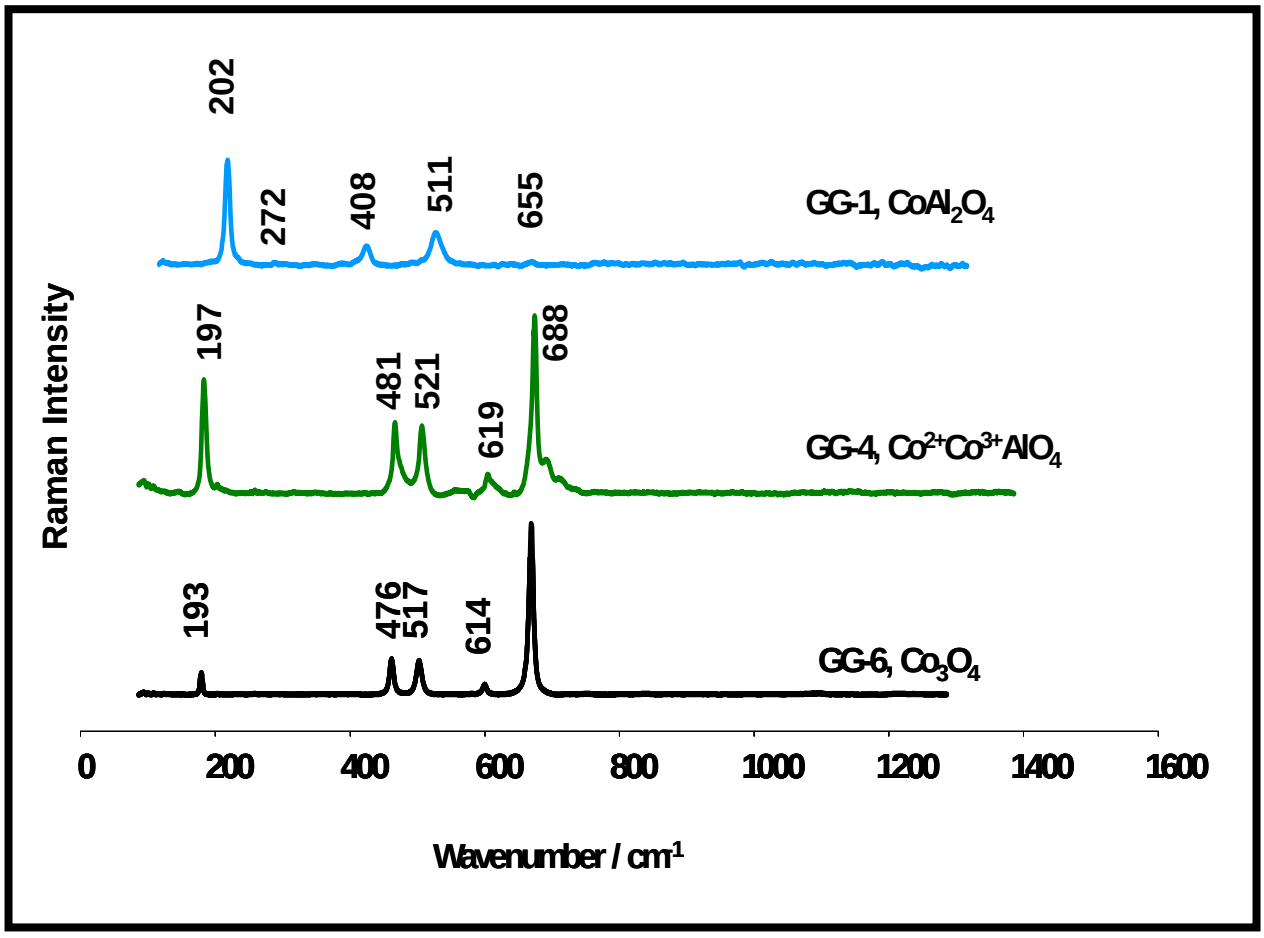

Figure 6-3: Raman spectra of samples GG-1 ($Co^{2+}Al_2O_4$), GG-4 ($Co^{2+}Co^{3+}AlO_4$), and GG-6 ($Co^{2+}Co^{3+}{}_2O_4$) prepared by the glycine-gel method (calcined for 2 h at 1000 ºC).

As predicted by group theory for spinels (section 3.4), there are five Raman active vibrational modes in the spectra for GG-1 (normal spinel) and GG-6 (Co_3O_4 spinel). For GG-4 (inverse spinel), there appears to be eight Raman active bands (five of high intensity and three of low intensity/shoulders). As mentioned in section 3.6, this could be an example of a breakdown in Raman selection rules due to various factors such as inversion. It appears that the normal spinel can be differentiated from the inverse spinel mainly by the presence of the 408 cm^{-1} band in the former. While the inverse spinel and Co_3O_4 spinel have similar spectra, there is a shift of bands to lower wavenumbers for the Co_3O_4 spinel. This is most likely due to the reduction in crystallite size of Co_3O_4 as opposed to $Co^{2+}Co^{3+}AlO_4$.[1] This is confirmed by a decrease in the lattice constant with increasing Co content, as determined by XRD analysis and presented in Table 6-2. In addition, the Co_3O_4 spinel can be differentiated from the inverse spinel by the drastically higher intensity of the 197 cm^{-1} Raman band for the latter. A comparison between Raman spectra of synthesised Co_3O_4 and commercial Co_3O_4 samples, later depicted in Fig 6-12, shows a similar intensity of the band at 197 cm^{-1}.

Using the work of Stanojevic et al.[2] on assignments for Raman active vibrational modes of $ZnCr_2O_4$ (also a spinel oxide) as a model as well as De Waal's[3] suggested assignments, Table 6-3 presents the Raman active vibrational modes for $CoAl_2O_4$, as determined from this research work.

The strong band around 511 cm^{-1} (normal spinel) is attributed to the Co-O stretching vibration, the strong band at 481 cm^{-1} (inverse spinel) is thought to be due to Al-O vibrations as are bands around 272 cm^{-1} and 408 cm^{-1} (normal spinel). The strong band around 197 cm^{-1} is attributed to Co-O bending vibrations.[3]

These vibrational modes can be confirmed by absence of Al in GG-6 and presence of Al in GG-1 and GG-4. None of the bands in GG-6 can be attributed to vibrations involving Al as no Al was present in the precursors for GG-6. Therefore similar bands in GG-4 (197, 619, and 688 cm^{-1}) and GG-1 (202 and 655 cm^{-1}) can also be attributed

to Co-O vibrations.

Table 6-3: Raman band assignments for GG-1 ($Co^{2+}Al_2O_4$), GG-4 ($Co^{2+}Co^{3+}AlO_4$), and GG-6 ($Co^{2+}Co^{3+}{}_2O_4$).

Raman Band (cm^{-1}) normal spinel	Raman Band (cm^{-1}) inverse & Co_3O_4 spinel	Symmetry Species	Assignment
202vs	197vs, 193w	F_{2g}	δ (Co-O)
272m			v $(Al\text{-}O)^3$
408m			Al-O
	476s, 481s	E_g, F_{2g}	v(Co-O), v $(Al\text{-}O)^3$
511s	517s, 521s	F_{2g}	v $(Co\text{-}O)^3$, v (Al-O)
	582m	F_{2g}	v $(Al\text{-}O)^2$
	614w, 619m	F_{2g}	v $(Co\text{-}O)^3$
655m		A_{1g}	v $(Co\text{-}O)^3$
	683vs, 688vs	A_{1g}	v $(Co\text{-}O)^3$

vw (very weak), vs (very strong), w (weak), m (medium), s (strong), sh (shoulder).

Although GG-1 and GG-4 have similar elements in common, they have different Raman bands (position and intensity), due to GG-1 only theoretically having only Co^{2+} while GG-4 theoretically contains both Co^{2+} and Co^{3+}. These would affect atomic interactions within the crystal lattice and therefore result in different spectra.

6.1.3.1 Comparison of Raman Patterns With Literature

As mentioned earlier, very little information is available in literature with regards to the characterisation of the cubic spinels ($Co^{2+}Al_2O_4$, $Co^{2+}Co^{3+}AlO_4$, and $Co^{2+}Co^{3+}{}_2O_4$) by

using Raman spectroscopy. Table 6-4 depicts the Raman bands of cobalt blue spectra obtained from various sources.[4,5,6,7]

Table 6-4: Raman bands of cobalt blue spectra from literature.

Reference	Raman bands (cm^{-1})
B. Jongsomjit et al., *J. Catal.*, 2001, **204**, 98–109.[4]	198vs, 412w, 480s, 519s, 619vs, 690vs, 753m
Raman Spectroscopic Library of Natural and Synthetic Pigments, I. M. Bell et al. http://www.chem.ucl.ac.uk/resources/raman/pigfiles/cobaltbl.html (Accessed on November 07, 2008)[5]	512vs, 203vs
D. de Waal, *J. Raman Spectrosc.*, 2004, **35**, 646-649[6]	190w, 280w, 404w, 485sh, 506vs, 560w, 647w
L. D. Kock et al., *J. Raman Spectrosc.,* 2007, **38**, 1480–1487[7a]	201vs, 337w, 408w, 509s, 617m, 767m
L. D. Kock et al., *J. Raman Spectrosc.,* 2007, **38**, 1480–1487[7b]	140m, 195w, 462sh, 480sh, 509vs, 565w

vw (very weak), vs (very strong), w (weak), m (medium), s (strong), sh (shoulder).

The Raman bands observed by Bell et al.[5] and Kock et al.[7a] are similar to that in GG-1 in Figure 6-3, in that there is no 485 cm^{-1} band which is indicative of the inverse spinel, while the Raman bands observed by Jongsomjit et al[4], De Waal[6] and Kock et al.[7b] are similar to GG-4 in Figure 6-3. This indicates the variation in Raman spectra depending on whether cobalt blue is in the normal spinel crystalline phase (GG-1) or inverse spinel crystalline phase (GG-4) and the importance of appropriately classifying the phase. Although the spectra found in Jongsomjit et al.[4] is due to the inverse spinel,

it is referred to as the normal spinel in the reference.

6.1.4 FTIR Characterisation of GG-1 ($Co^{2+}Al_2O_4$), GG-4 ($Co^{2+}Co^{3+}AlO_4$), and GG-6 ($Co^{2+}Co^{3+}{}_2O_4$)

FTIR measurements were used to further identify and characterise the calcined spinel powders as well as confirm the absence of precursors. This section looks at the mid and far IR results for the three spinels GG-1 ($Co^{2+}Al_2O_4$), GG-4 ($Co^{2+}Co^{3+}AlO_4$), and GG-6 ($Co^{2+}Co^{3+}{}_2O_4$).

6.1.4.1 Mid IR Characterisation of GG-1 ($Co^{2+}Al_2O_4$), GG-4 ($Co^{2+}Co^{3+}AlO_4$), and GG-6 ($Co^{2+}Co^{3+}{}_2O_4$)

Figure 6-4 shows the mid IR spectra for precursor gels 1, 4 and 6 and Figure 6-5 shows the mid IR spectra for the same precursor gels after calcining for 2 h at 1000 ºC i.e. GG-1, GG-4 and GG-6. By comparing the region above 700 cm^{-1} in both figures 6-4 and 6-5, it can be concluded that no precursors are present in the calcined samples i.e. none of the bands above 700 cm^{-1} in the spectra of the precursor gels appear in the spectra of the calcined samples. In addition, the normal spinel can be distinguished from the inverse spinel by the mid-IR spectra due to the three characteristic bands at 661, 554 and 502 cm^{-1}, obtained at a resolution of 2 cm^{-1} (666, 554 and 504 cm^{-1} according to Wang et al[1]) which are attributed to the normal spinel. On the other hand GG-4 and GG-6 cannot conclusively be distinguished from each other when only the high intensity bands are considered due to the similarity of their IR absorption bands (663 and 570 cm^{-1} for GG-6, 669 and 569 cm^{-1} for GG-4). However, if one considers the 508 cm^{-1} shoulder present in the GG-4 spectra (figure 6-5), then the two samples (GG-4 and GG-6) can be distinguished from one another by their mid-IR spectra. The 663 and 570 cm^{-1} absorption bands are characteristic for the $Co^{2+}Co^{3+}{}_2O_4$ spinel (668 and 572 cm^{-1} according to Wang et al.[1]).

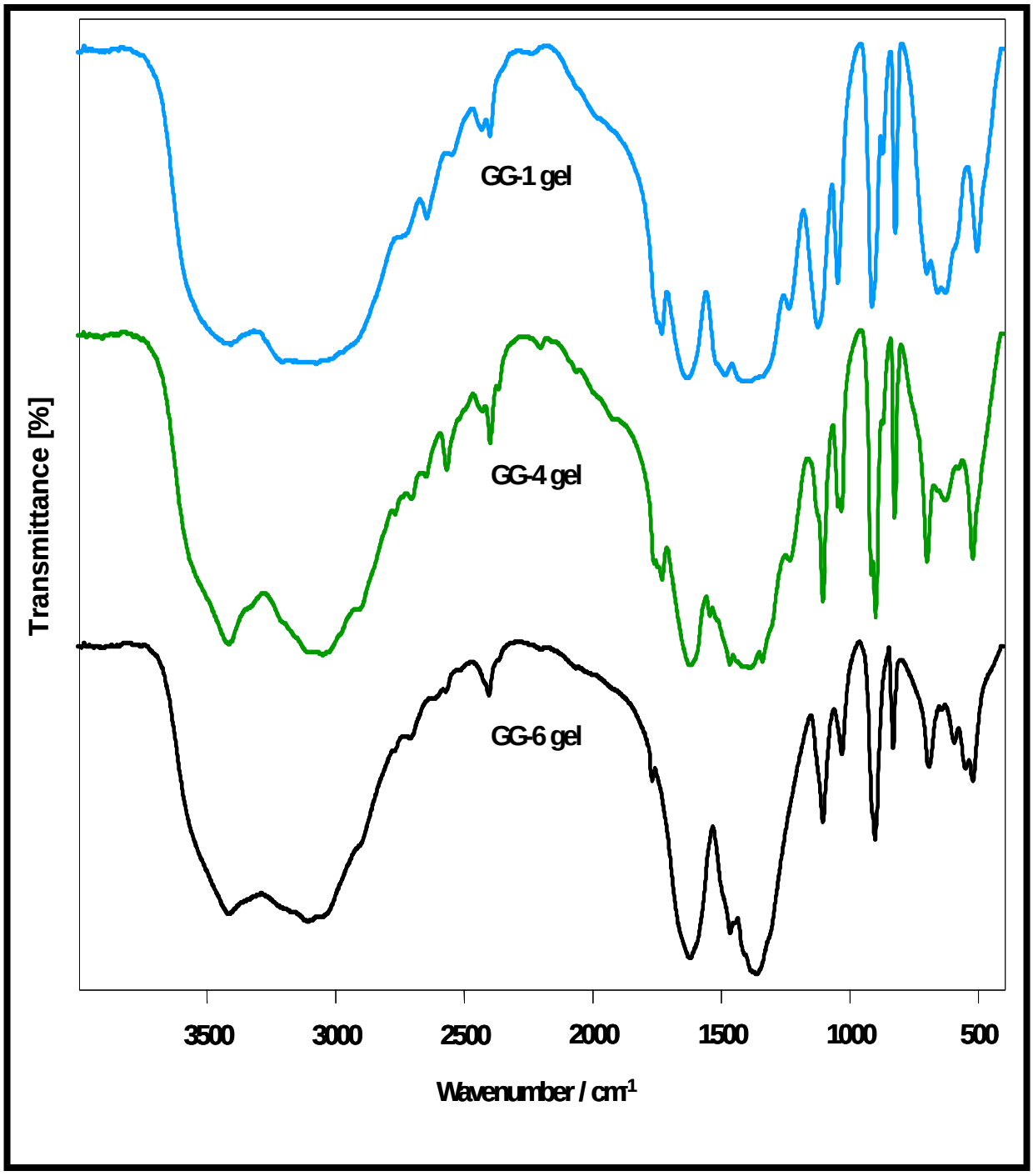

Figure 6-4: Mid-IR spectra of precursor gels for samples GG-1 ($Co^{2+}Al_2O_4$), GG-4 ($Co^{2+}Co^{3+}AlO_4$) and GG-6 ($Co^{2+}Co^{3+}{}_2O_4$).

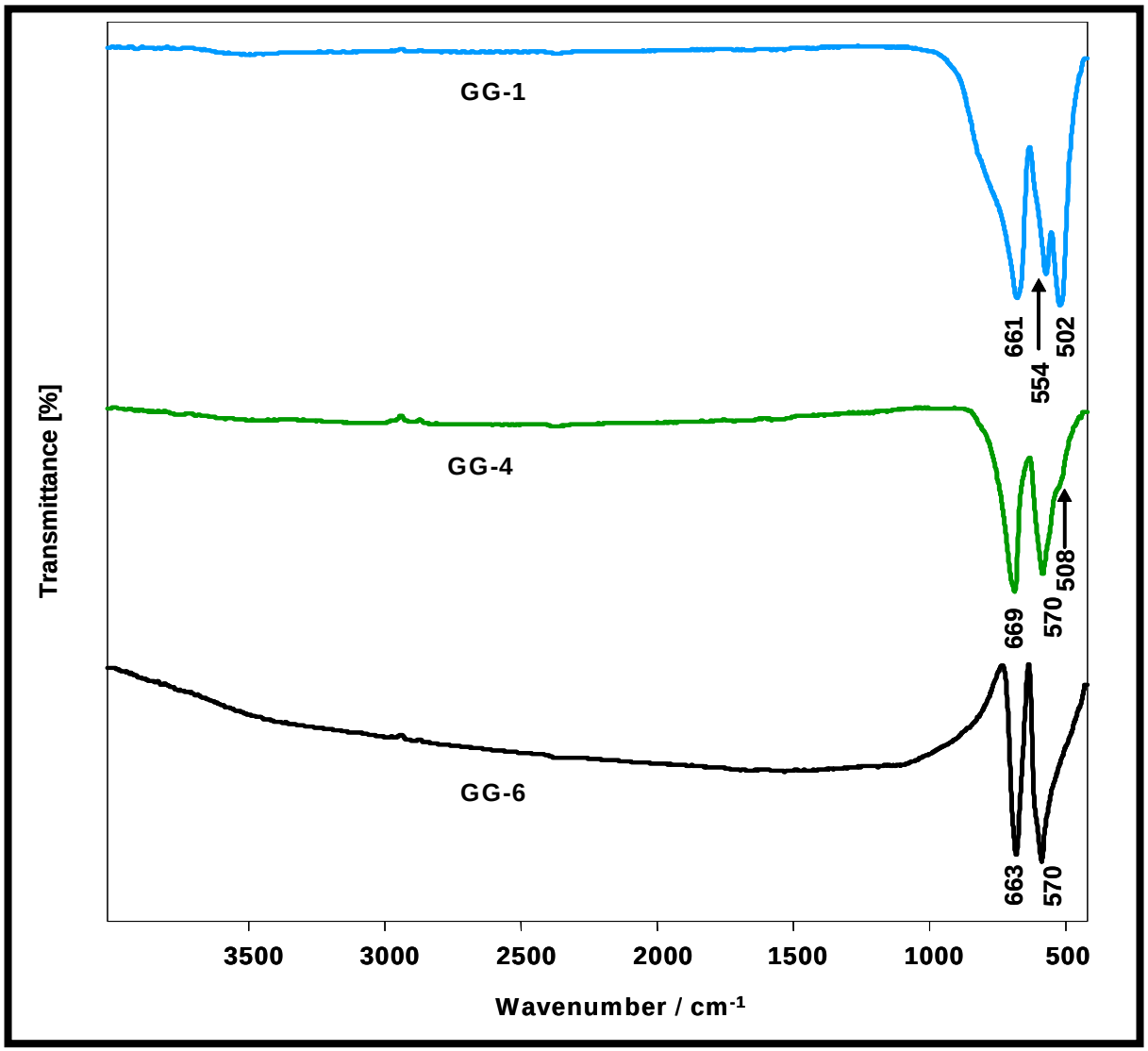

Figure 6-5: Mid-IR spectra of samples GG-1 ($Co^{2+}Al_2O_4$), GG-4 ($Co^{2+}Co^{3+}AlO_4$) and GG-6 ($Co^{2+}Co^{3+}{}_2O_4$) after calcination for 2 h at 1000 ºC, showing absence of bands due to precursor gels that are prominent in the 700 - 3500 cm^{-1} region (See Fig. 6.4).

6.1.4.2 Comparison of Mid-IR results With Literature

The bands for GG-1 ($Co^{2+}Al_2O_4$) in Figure 6-5 (502, 554 and 661 cm^{-1}) correspond with the bands in the spectra for the samples heat-treated at 1000 ºC in Wang et al.[1]

(i.e. 504, 554 and 666 cm^{-1}). These band positions are associated with normal $Co^{2+}Al_2O_4$ spinel, indicating that the sample prepared (GG-1) is the normal spinel. The bands for GG-6 (Co_3O_4) in Figure 6-5 (570 and 663 cm^{-1}) corresponds with the bands in the spectrum of the sample heat-treated at 400 °C in Wang et al[1] (572 and 668 cm^{-1}) indicating that the precursor to the normal spinel forming is Co_3O_4 (explained in 6.2.1.5).

6.1.4.3 Far IR Characterisation of GG-1 ($Co^{2+}Al_2O_4$), GG-4 ($Co^{2+}Co^{3+}AlO_4$), and GG-6 ($Co^{2+}Co^{3+}{}_2O_4$)

Figure 6-6 shows the far IR spectra of samples GG-1, GG-4 and GG-6. Once again, the normal spinel (GG-1) can be distinguished from both the inverse spinel (GG-4) and Co_3O_4 spinel (GG-6) by the IR absorption band at 232 cm^{-1}.

On the other hand, the inverse and Co_3O_4 spinels cannot be conclusively distinguished from each other, due to the similarity of their IR absorption bands in the far IR region (216 and 214 cm^{-1}, respectively). A careful analysis of both the mid-IR and far-IR spectra of GG-4 and GG-6 would be the only way to distinguish them from each other based on the slight differences in peak positions.

A summary of the mid and far-IR absorption bands for GG1, GG-4 and GG-6 are given in Table 6-5. Corresponding IR band assignments are presented in Table 6-6.

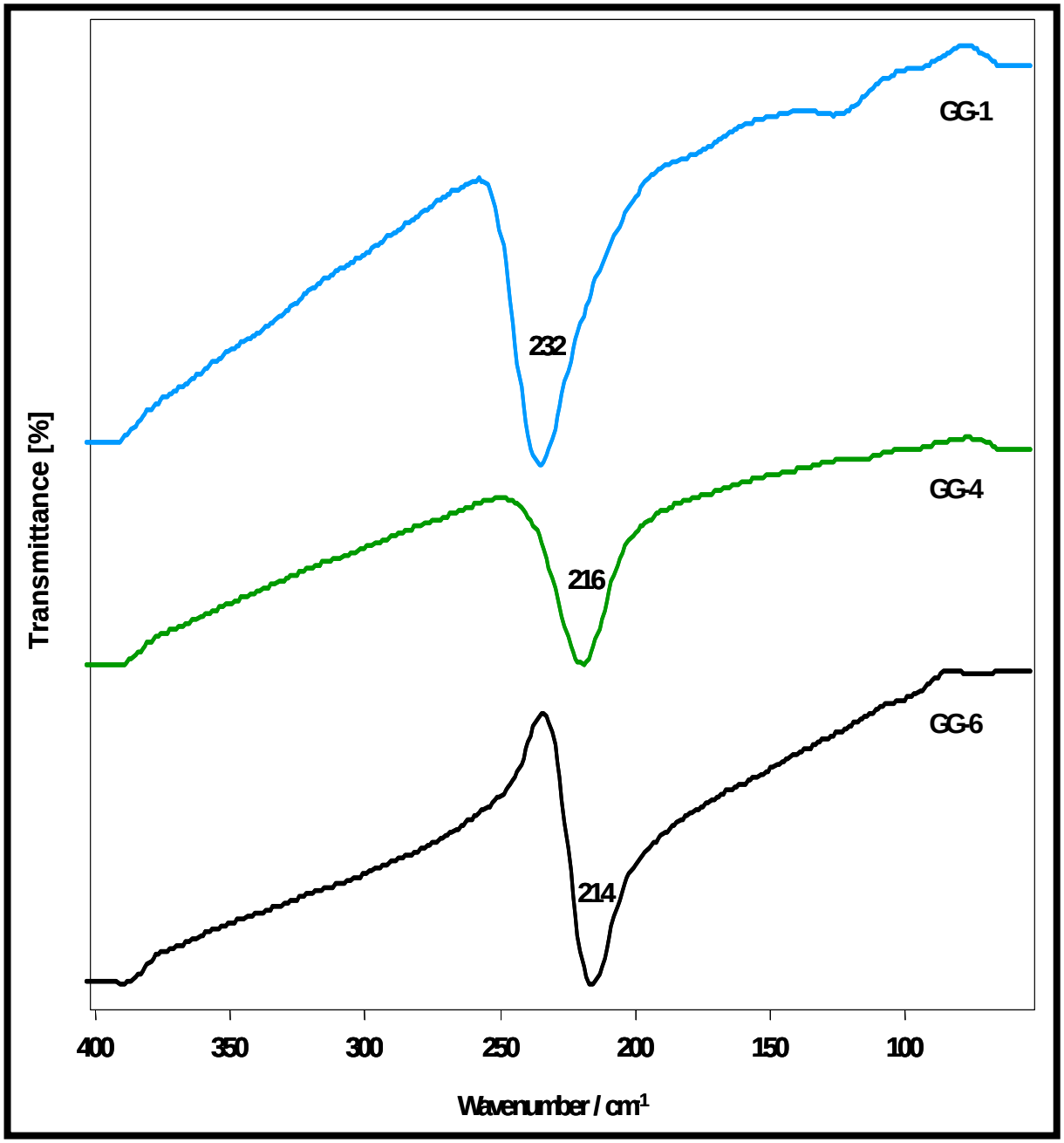

Figure 6-6: Far IR spectra of samples GG-1 ($Co^{2+}Al_2O_4$), GG-4 ($Co^{2+}Co^{3+}AlO_4$), and GG-6 ($Co^{2+}Co^{3+}{}_2O_4$) after calcination for 2 h at 1000 ºC.

Table 6-5: Mid and far-IR absorption bands for samples GG-1 ($Co^{2+}Al_2O_4$), GG-4 ($Co^{2+}Co^{3+}AlO_4$) and GG-6 ($Co^{2+}Co^{3+}{}_2O_4$).

Sample	Mid-IR absorption (cm^{-1})	Far-IR absorption (cm^{-1})
GG-1	661, 554, 502	232
GG-4	669, 569, 508sh	216
GG-6	663, 570	214

sh = shoulder.

All bands in the spectra for GG-6 (663, 570, and 214 cm^{-1}) are due to Co-O vibrations as there is no Al in GG-6. Therefore similar bands in GG-4 (669 and 570 cm^{-1}) are also due to Co-O vibrations. As mentioned in section 3.6, the IR band with the highest wavenumber is assigned to vibrational modes of the coordinated cation with the highest valency. In the case of GG-1 ($Co^{2+}Al_2{}^{3+}O_4$), this corresponds to the band at 661 cm^{-1} which is typical for octahedrally coordinated Al^{3+}. Therefore, the two high-frequency bands can be assigned to the Al-O stretching vibrations. For GG-4 ($Co^{2+}Co^{3+}Al^{3+}O_4$) and GG-6 ($Co^{2+}Co^{3+}{}_2O_4$), the presence of Co^{3+} means that the bands with the highest wavenumbers are due to Co-O.

Table 6-6: Assignments for mid and far-IR absorption bands for samples GG-1 ($Co^{2+}Al_2O_4$), GG-4 ($Co^{2+}Co^{3+}AlO_4$) and GG-6 ($Co^{2+}Co^{3+}{}_2O_4$).

IR Band (cm^{-1}) normal spinel	IR Band (cm^{-1}) inverse & Co_2O_4 spinel	Symmetry Species	Assignment
661	663, 669	F_{1u}(v1)	*v*(Co-O)[3,6]
	570		*v* Co-O[3,6]
554			Al-O[13,14,16,17]
502	508	F_{1u}(v2)	*v*(Al-O)
232		F_{1u}(v3)	δ(O-Al-O)
	214, 216	F_{1u} (v4)	*v*(Co-O)

As predicted by group theory (section 3.6), GG-1 and GG-4 exhibits the expected four IR-active vibrational modes while GG-6 exhibits only three. The latter result being possibly due to a breakdown in selection rules leading to a lower than expected number of vibrational modes.

No far-IR results for $Co^{2+}Al_2O_4$, $Co^{2+}Co^{3+}AlO_4$ and $Co^{2+}Co^{3+}{}_2O_4$ were found in literature for comparison purposes.

6.1.5 XRD Characterisation of GG-1 ($Co^{2+}Al_2O_4$), GG-4 ($Co^{2+}Co^{3+}AlO_4$), and GG-6 ($Co^{2+}Co^{3+}{}_2O_4$)

Figure 6-7 shows the XRD patterns for GG-1, GG-4 and GG-6. All 3 samples are crystalline, as indicated by sharp and intense peaks as opposed to broad and weak peaks normally associated with amorphous samples. As mentioned in section 6.1.2, they also exhibit the characteristic diffraction peaks of the cubic spinel phase and contain one phase. In order to differentiate between the spinel phases GG-1, GG-4 and GG-6, the relative intensities of peaks at lattice planes (111), (222), (331) and (531) in their diffraction patterns needs to be examined. [8]

Figure 6-8 A-D highlights the main differences in the intensities of diffraction peaks at positions 2 θ = 22.08º, 44.96º, 57.50º and 81.54º corresponding to lattice planes (111), (222), (331), and (531) respectively.

From Figures 6-8 A, B and D, it can be deduced that peaks at lattice planes (111), (222), and (531) are predominantly due to the Co_3O_4 spinel, as these peaks are of highest intensity in the Co_3O_4 spinel (GG-6). They are of a lower intensity in GG-4 (inverse spinel) and they do not appear to be present in the normal spinel (GG-1). From Figure 6-8 C, it can be concluded that the peak at lattice plane (331) is due to the normal spinel as it is of highest intensity in GG-1, is of lower intensity in the inverse spinel and does not appear to be present in the Co_3O_4 spinel.[1,8,9] It can also be assumed that the inverse spinel prepared also contains characteristics of both the

normal spinel and the Co_3O_4 spinel phase as it contains peaks that correspond to both spinel types.

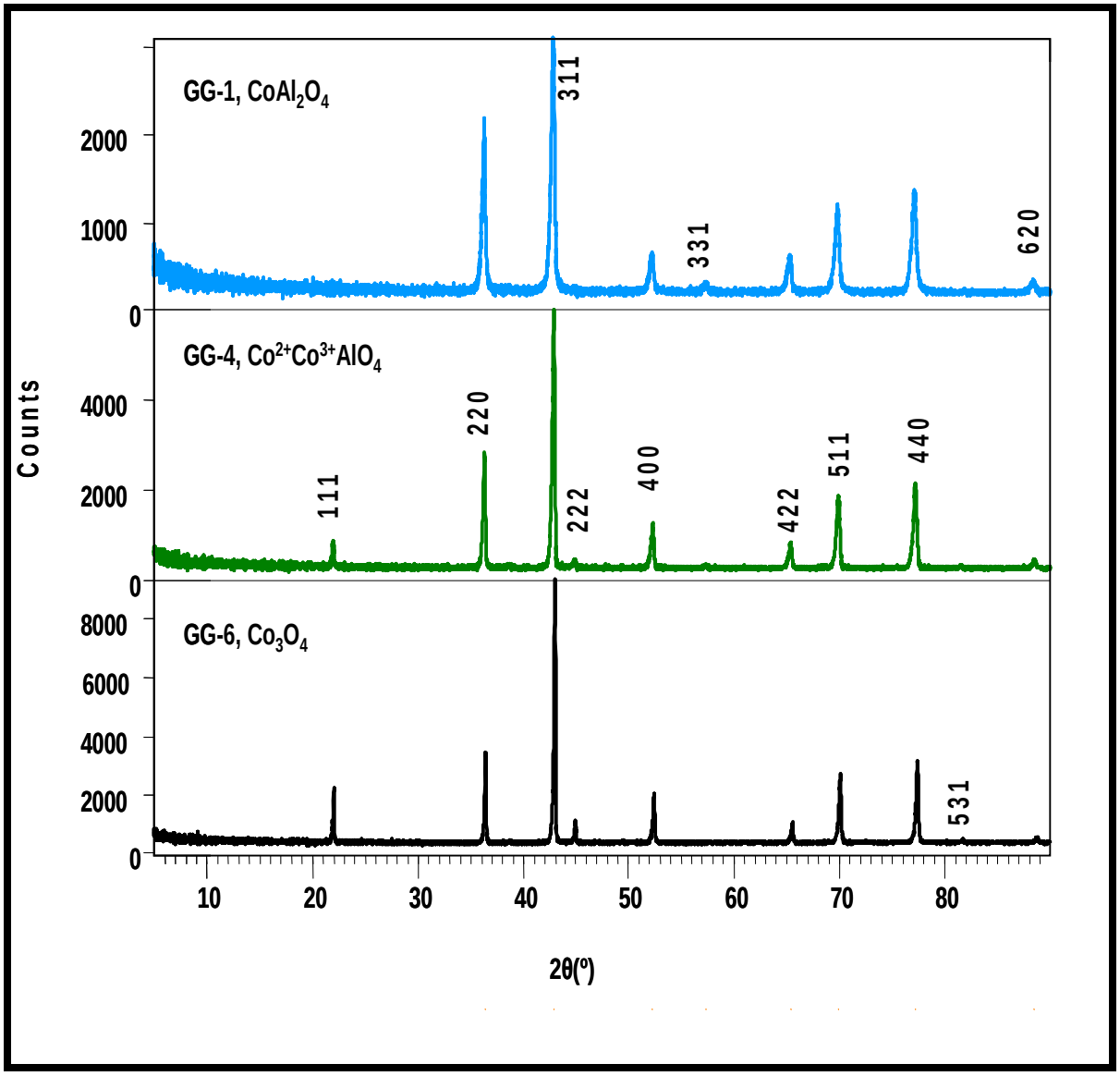

Figure 6-7: XRD patterns of samples GG-1 ($Co^{2+}Al_2O_4$), GG-4 ($Co^{2+}Co^{3+}AlO_4$), and GG-6 ($Co^{2+}Co^{3+}{}_2O_4$) prepared by the glycine-gel method (calcined for 2 h at 1000 ºC).

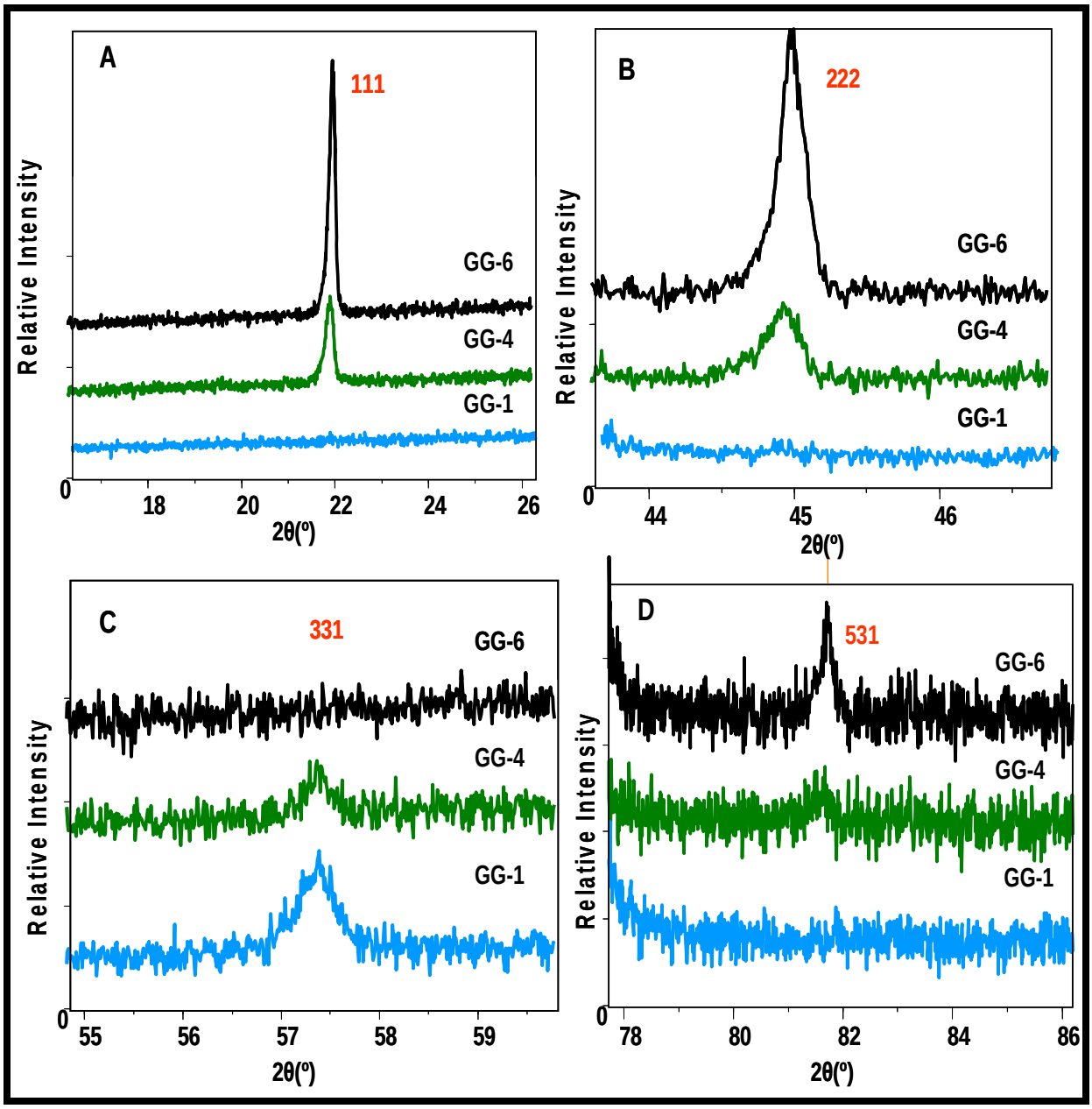

Figure 6-8 A-D: Detail of XRD patterns of GG-1 ($Co^{2+}Al_2O_4$), GG-4 ($Co^{2+}Co^{3+}AlO_4$), and GG-6 ($Co^{2+}Co^{3+}{}_2O_4$) at; (A) 2 θ = 22.081º (111), (B) 2 θ = 44.969 º (222), (C) 2 θ = 57.504 º (331) and (D) 2 θ = 81.539 º (531).

Table 6-7 provides a more detailed comparison of the lattice plane, 2 θ values and intensities for GG-1, GG-4 and GG-6. A comparison between the theoretically

calculated (Calc.) and experimentally obtained 2 θ values as well as relative intensities is also depicted. The observed differences in the XRD pattern between GG-1, GG-4 and GG-6 at lattice planes (111), (222), (331), and (531) are highlighted in yellow. The intensities of peaks at lattice planes (111) and (222) are higher in the Co_3O_4 spinel (GG-6) than in the inverse spinel (GG-4) indicating, that they are more prominent in the Co_3O_4 spinel, whereas the intensity of the peak at lattice plane (331) is higher in the normal spinel (GG-1) than in the inverse spinel (GG-4), indicating that it is more prominent in the normal spinel. The lattice constants calculated for GG-1, GG-4 and GG-6 [8.1114(2), 8.1028(1), 8.0885(10) Å respectively] compare well to the standard values of 8.104Å for $CoAl_2O_4$ (JCPDS 44-0160), 8.086 Å for Co_2AlO_4 (JCPDS 38-0814) and 8.0837 Å for Co_3O_4 (JCPDS 42-1467) as listed in the JCPDS electronic library.[1,8,9]

As observed with their Raman spectra the inverse spinel appears to have more in common with the Co_3O_4 than with the normal spinel, possibly due to the higher Co content in both the Co_3O_4 and inverse spinels. However, it would appear that the inverse spinel is an intermediary phase between the normal spinel and Co_3O_4 spinel as it also has some commonality with the normal spinel. This is further explained in Section 6.2. Other lattice planes common to all 3 spinels have not been discussed as they are not as significant in differentiating the three spinels as are lattice planes (111), (222), (331) and (531).

According to literature, crystal phases where XRD patterns have the lattice plane at (331), are considered the normal spinel ($CoAl_2O_4$) and those without the (331) diffraction plane, are either the inverse spinel (Co_2AlO_4) or Co_3O_4 spinel.[1,9,10] Comparison of the results from the XRD patterns of GG-1, GG-4 and GG-6 in Figures 6-7 and 6-8 and Table 6-7, with XRD 'library' patterns of CoO, Co_3O_4, $CoAl_2O_4$ and Co_2AlO_4 seem to support this reasoning.

Table 6-7: Comparison of relative intensities at specific lattice planes for samples GG-1 ($Co^{2+}Al_2O_4$), GG-4 ($Co^{2+}Co^{3+}AlO_4$), and GG-6 ($Co^{2+}Co^{3+}{}_2O_4$).

lattice plane	2θ(º)				Relative Intensity (%)			
hkl	Calc.	Obtained			Calc.	Obtained		
$CoAl_2O_4$	$CoAl_2O_4$	GG-1 ($Co^{2+}Al_2O_4$)	GG-4 ($Co^{2+}Co^{3+}AlO_4$)	GG-6 ($Co^{2+}Co^{3+}{}_2O_4$)	$CoAl_2O_4$	GG-1	GG-4	GG-6
111	22.08		22.02	22.05	8		9.71	20.41
220	36.39	36.31	36.34	36.45	65	65.01	45.23	30.31
			38.59				0.76	
311	42.94	42.89	42.93	43.01	100	100	100	100
222	44.97		44.96	45.01	2		3.19	7.95
				49.52				0.80
400	52.40	52.26	52.33	52.49	14	15.29	16.60	18.53
331	57.50	57.34	57.42		4	3.64	0.95	
422	65.46	65.39	65.41	65.59	13	13.69	9.26	7.40
511	69.99	69.90	69.93	70.14	27	32.88	26.17	27.31
440	77.26	77.16	77.21	77.45	33	39.93	29.58	32.16
531	81.54		81.64	81.72	1		0.56	1.28
620	88.54	88.46	88.54	88.79	4	4.01	2.50	1.93
Lattice constant (Å)	8.1040	8.1114	8.1028	8.0884				

Since Co^{3+} and Al^{3+} have a similar ionic radius, distinguishing between the diffraction patterns of $CoAl_2O_4$, Co_2AlO_4 and Co_3O_4 can be quite difficult. In addition, all three compounds share the same spinel cubic structure (space group *Fd*3*m*) with only a slight difference in the lattice size. However, as discussed above, the presence or absence of lattice planes (111), (222), (331) and (531) and their relative intensities in

the diffraction patterns, aid in differentiating between the normal, inverse and Co_3O_4 spinel.

6.1.5.1 Comparison of XRD Patterns With Literature

XRD findings from Wang et al.[1] for GG-1, GG-4 and GG-6 are a good point of comparison with findings from this research. Each precursor was treated at temperatures ranging from 150 - 1000 ºC for 2 h. In this research, the precursors were only calcined at 1000 ºC for 2 h since that was the temperature in which the respective spinel should have been completely formed.

According to Wang et al.[1], the (331) lattice plane is observed only in the XRD pattern of GG-1 when heated at and above 800 ºC and is of the highest intensity at 1000 ºC. This is in accordance with the findings from this research for the XRD pattern of GG-1 calcined for 2 h at 1000 ºC. The (111) and (222) lattice planes are observed only in GG-4 and GG-6. In both samples, the (222) lattice plane does not seem to be present at temperatures below 400 ºC, after which it increases in intensity with increasing temperature. On the other hand, the (111) lattice plane appears to be present from much lower temperatures i.e. 200 ºC. A point worth noting is that the (111) lattice plane appears in the XRD pattern of GG-1 from 250 ºC but decreases in intensity around the same temperature as the (331) lattice plane starts to appear (i.e. 800 ºC). A possible explanation for this is that since the lattice plane (111) is due to the Co_3O_4 spinel, this phase is present in GG-1 and is consumed in the formation of the $CoAl_2O_4$ spinel (explained in section 6.2.1.5), which gives rise to the (331) lattice plane. At a temperature of 1000 ºC, it can therefore be assumed that GG-1 mainly contains the $CoAl_2O_4$ spinel phase, GG-6 mainly contains the Co_3O_4 spinel phase while GG-4 contains a combination of both the Co_2AlO_4 and Co_3O_4 spinel phases.

In all three samples, the full width at half maximum (FWHM) decreases with increasing temperature, indicating an increase in crystallinity and particle size. [1,9,11,12]

Other references depicting the characteristic XRD pattern of the cubic spinel $CoAl_2O_4$ include Zayat et al.[9] and Cho et al.,[11] in which the (331) lattice plane is observed only in the XRD pattern of samples heated at and above 800 ºC and is of the highest intensity at 1000 ºC. Jongsomjit et al.[31] depicts XRD patterns of commercially purchased $Co^{2+}O$, $Co^{2+}Co^{3+}{}_2O_4$ and $Co^{2+}Al_2O_4$ spinel used as reference spectra and which also confirm the (331) lattice plane present only in the XRD pattern for $Co^{2+}Al_2O_4$.

6.1.6 Role of Co Content on the Development of $Co^{2+}Co^{3+}{}_xAl_{2-x}O_4$ Spinels

The development of crystalline $Co^{2+}Al_2O_4$, $Co^{2+}Co^{3+}AlO_4$ and $Co^{2+}Co^{3+}{}_2O_4$ from the same precursors at different ratios of Co/Al has been described above. The next section considers the role that the Co content plays on the development of the $Co^{2+}Co^{3+}{}_xAl_{2-x}O_4$ spinels.

6.1.6.1 Spinels

In this work, GG-1 ($CoAl_2O_4$), with a theoretical Co/Al ratio of 0.5, has been referred to as the 'normal' spinel while GG-4 ($Co^{2+}Co^{3+}AlO_4$) has been referred to as the 'inverse' spinel as it has a Co/Al ratio greater than 0.5. Samples calcined from precursor gel-1 to gel-5 produced the crystalline powders with chemical compositions of $Co^{2+}Al_2O_4$, $Co^{2+}Co^{3+}{}_{0.5}Al_{1.5}O_4$, $Co^{2+}Co^{3+}{}_{0.8}Al_{1.2}O_4$, $Co^{2+}Co^{3+}AlO_4$ and $Co^{2+}Co^{3+}{}_{1.5}AlO_4$, respectively. Unlike the other gels, there is no Al cation in gel-6 (Co/Al =∞) and characterisation of its powder after calcination indicated the formation of crystalline $Co^{2+}Co^{3+}{}_2O_4$, in which the Co^{2+} is in the tetrahedral sites and Co^{3+} is in the octahedral sites.[1]

6.1.6.2 Lattice Parameters

As mentioned in section 3.3, when the ratio of A/B is greater than 0.5, inversion between A and B may occur in oxide spinels with the general formula of AB_2O_4. As

observed in Table 6-7 the increase of Co content in $Co^{2+}Co^{3+}_xAl_{2-x}O_4$ (x = 0 - 2) spinels resulted in inversion which ultimately decreased the lattice constants. The lattice constants for the GG-1, GG-4 and GG-6 crystalline powders prepared in this work are 8.1114 (2), 8.1028 (1), and 8.0884 (1) Å respectively. GG-1 has the lowest Co content while GG-6 has the highest. A possible explanation for this is that when the larger cobalt ions (Co^{3+}) move to the larger octahedral sites where they fit in more easily, in comparison to the smaller tetrahedral sites where they were 'squeezed' in, which results in the relaxation of the lattice and ultimate decrease in the lattice constants.[1] An alternate explanation proposed by T. Mimani et al.,[7] is that the decrease in lattice constant with increasing Co content is due to the increasing crystal field surrounding the Co ion. This also results in the increased intensity of the characteristic blue colour of $CoAl_2O_4$ as its formation progresses.

6.1.6.3 Crystallinity

Both the Raman spectra and XRD patterns in Figures 6-1 and 6-2 depict increasing crystallinity with increasing Co content. As one moves from sample GG-1 (lowest Co content) to GG-6 (highest Co content) the Raman bands and XRD diffraction lines become narrower (i.e. lower FWHM) indicating increased crystallinity. GG-6 has the highest Co content and hence exhibits the highest degree of crystallinity. It can thus be deduced that increasing the Co content in the precursors improves the degree of powder crystallinity. It should also be noted that increased peak intensity may also be attributed to increasing interaction between incident light and larger particles.[12] It can thus be assumed that particle size also increases as the Co content increases in part due to agglomeration. This is different to lattice constant size which decreases as Co content increases (Table 6-7). As a result of their different degrees of crystallinity, the $Co^{2+}Co^{3+}_xAl_{2-x}O_4$ spinels (x = 0 – 2) exhibit different powder properties as explained in the next section.[1]

6.1.6.4 Morphology

SEM images of the calcined GG-1 ($Co^{2+}Al_2O_4$), GG-4 ($Co^{2+}Co^{3+}AlO_4$) and GG-6 ($Co^{2+}Co^{3+}{}_2O_4$) powders are shown in Figures 6-9, 6-10 and 6-11 respectively. It appears that the morphology of GG-1 (Figure 6-9) is only slightly porous while that of GG-4 and GG-6 spinel powders (Figures 6-10 and 6-11 respectively) display a highly porous structure. This is most likely because GG-4 and GG-6 contain a higher Co content which serves as a metal catalyst for breaking down the polymeric complexes thereby resulting in a more vigorous pyrolytic reaction (see section 6.1.7).[1]

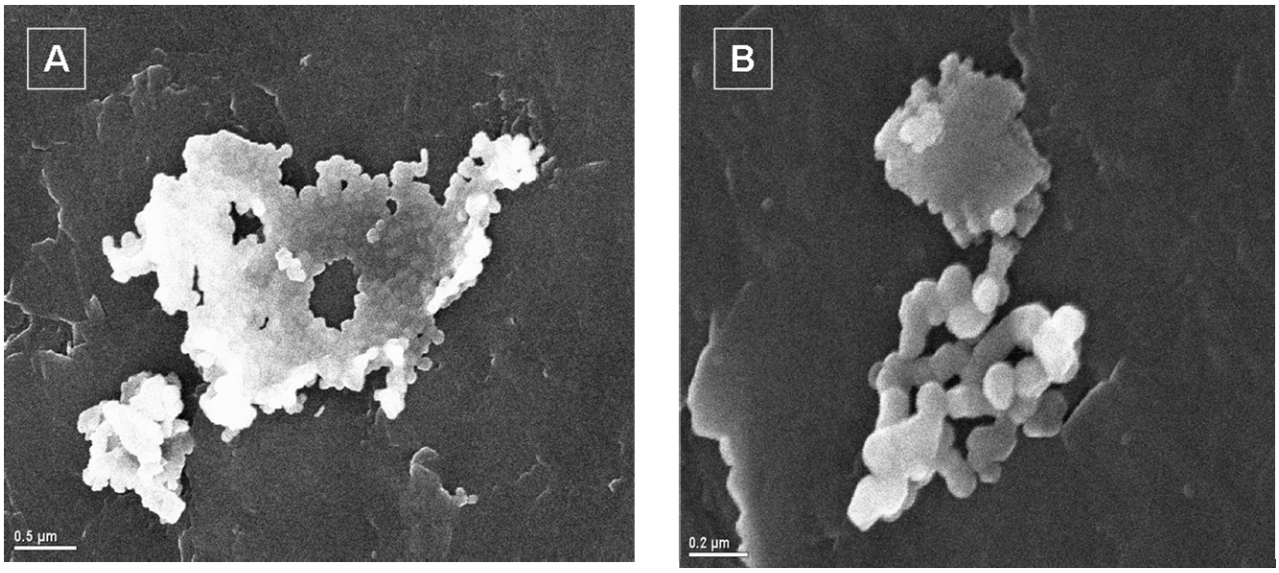

Figure 6-9: SEM of GG-1 ($Co^{2+}Al_2O_4$) showing (A) agglomerated structure and (B) irregular, hexagonal-like particles.

All three powders have particles which are highly agglomerated and irregular in shape. GG-6 powder particles are highly fused as well. According to Wang et al.,[1] powders with a higher Co content tend to be smaller in size; this is confirmed by the lattice constants in Table 6-4.

GG-1 and GG-4 powders appear to have hexagonal-shaped particles while those for GG-6 appear to be spherical and rod-like. Similar morphologies have been

documented in literature using SEM and TEM images.[1,10,13]

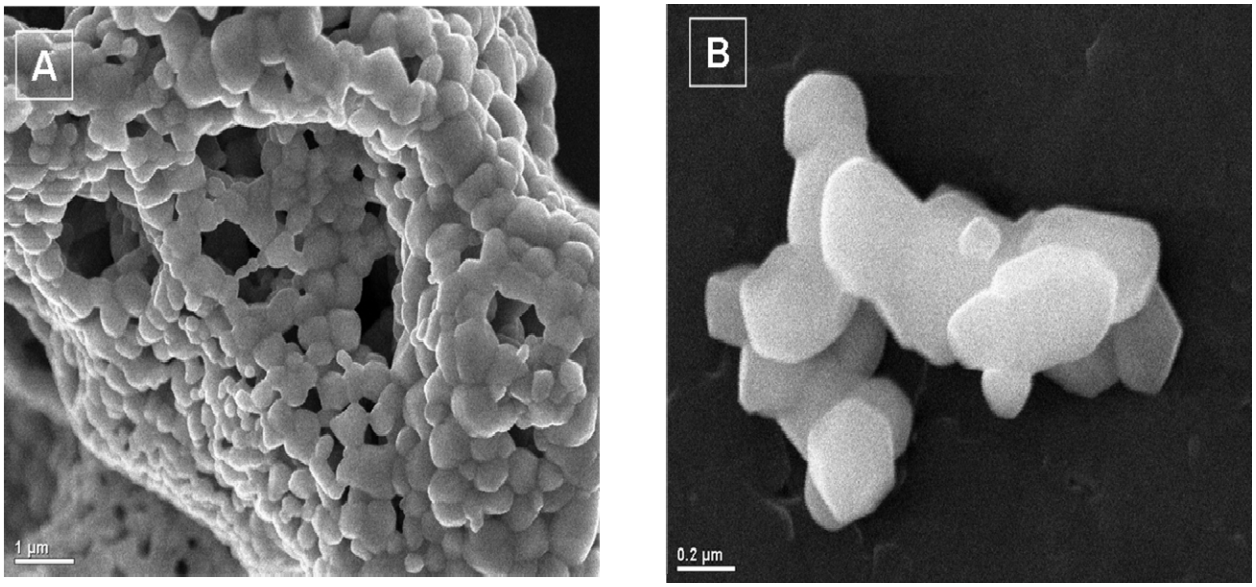

Figure 6-10: SEM of GG-4 ($Co^{2+}Co^{3+}AlO_4$) showing (A) porous, highly agglomerated structure and (B) irregular, hexagonal-like particles.

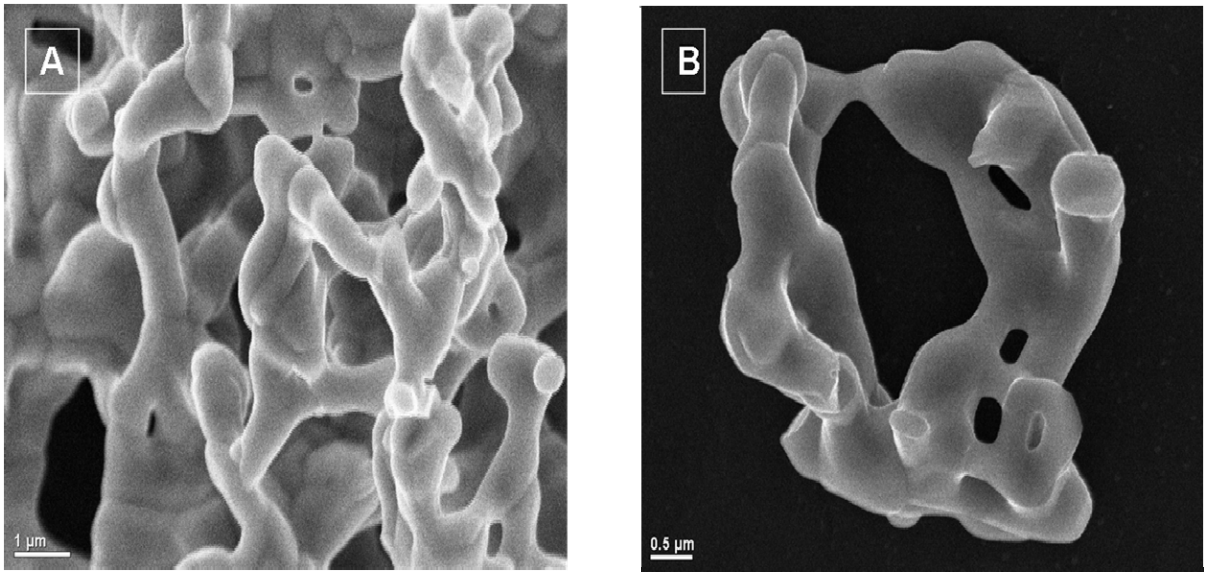

Figure 6-11: SEM of GG-6 ($Co^{2+}Co^{3+}{}_2O_4$) showing (A) porous, rod-like agglomerated structure and (B) highly fused particles.

6.1.6.5 Formation of Cobalt Oxides $Co^{2+}O$ and $Co^{2+}Co^{3+}{}_2O_4$ (GG-6)

During the refluxing stage in the preparation of the $Co^{2+}Co^{3+}{}_xAl_{2-x}O_4$ (x = 0 - 2) oxides, it is assumed that the cobalt cations and glycine (chelating agent) are homogeneously mixed within the gels, forming a complex. Upon calcination of the dried gel, cobalt acts as a catalyst for breaking the organic complexes during a pyrolytic process in which gases, such as carbon dioxide, nitrogen oxides, and water vapour are evolved.[1] Since GG-6 contains the highest amount of cobalt, the gaseous pyrolytic process is more vigorous resulting in the powder particles having a porous structure as shown in Figure 6-11.[1]

Equation 6-1 is thought to depict the formation of Co_3O_4 spinel at 1000 ºC.[1,14]

$$Co_3O_4(s) \leftrightarrow 3CoO(s) + ½O_2(g) \quad \text{..... 6-1}$$

According to the literature, Co_3O_4 is the most thermodynamically stable cobalt oxide at room temperature. The cobalt precursors used are partially oxidized above 400 ºC resulting in the stable Co_3O_4 phase. Between 700 and 1000 ºC, the Co_3O_4 spinel is reduced to CoO and oxygen gas is evolved. The exact temperature at which the reduction reaction occurs, depends on the preparation method and it is thought to lead to the formation of the normal $CoAl_2O_4$ spinel with appropriate precursors. The reverse of equation 6-1 (re-oxidation) requires the penetration of oxygen which does not occur easily when more compact or dense CoO is formed. Therefore, the CoO observed in the GG-6 (Co_3O_4) confirms this resistance to re-oxidation (Table 6-4 at 2 θ 49.52º).[1,9.10]

6.1.6.6 Raman and IR Characterisation of Cobalt Oxides $Co^{2+}O$ and $Co^{2+}Co^{3+}{}_2O_4$ (GG-6)

Figure 6-12 compares the Raman spectra of Co_3O_4 spinel synthesized during this work with Co_3O_4 spinels made commercially. A more detailed description of the

samples can be found in Appendix A. Overall, the spectra of all four samples is similar with regards to band positions and intensities. This observation takes into account the expected shift in wavenumbers due to varying particle size and synthesis method. On closer inspection the Co_3O_4 nanoparticles and Co_3O_4 pigment have very similar spectra to each other as do the Co_3O_4 microparticles and synthesized Co_3O_4 GG-6. In both instances, wavenumbers differ at most by 2 cm^{-1}. In addition, with the exception of nanoparticles, all spectra exhibit the five Raman-active bands as predicted by group theory for spinels of the general formula AB_2O_4.

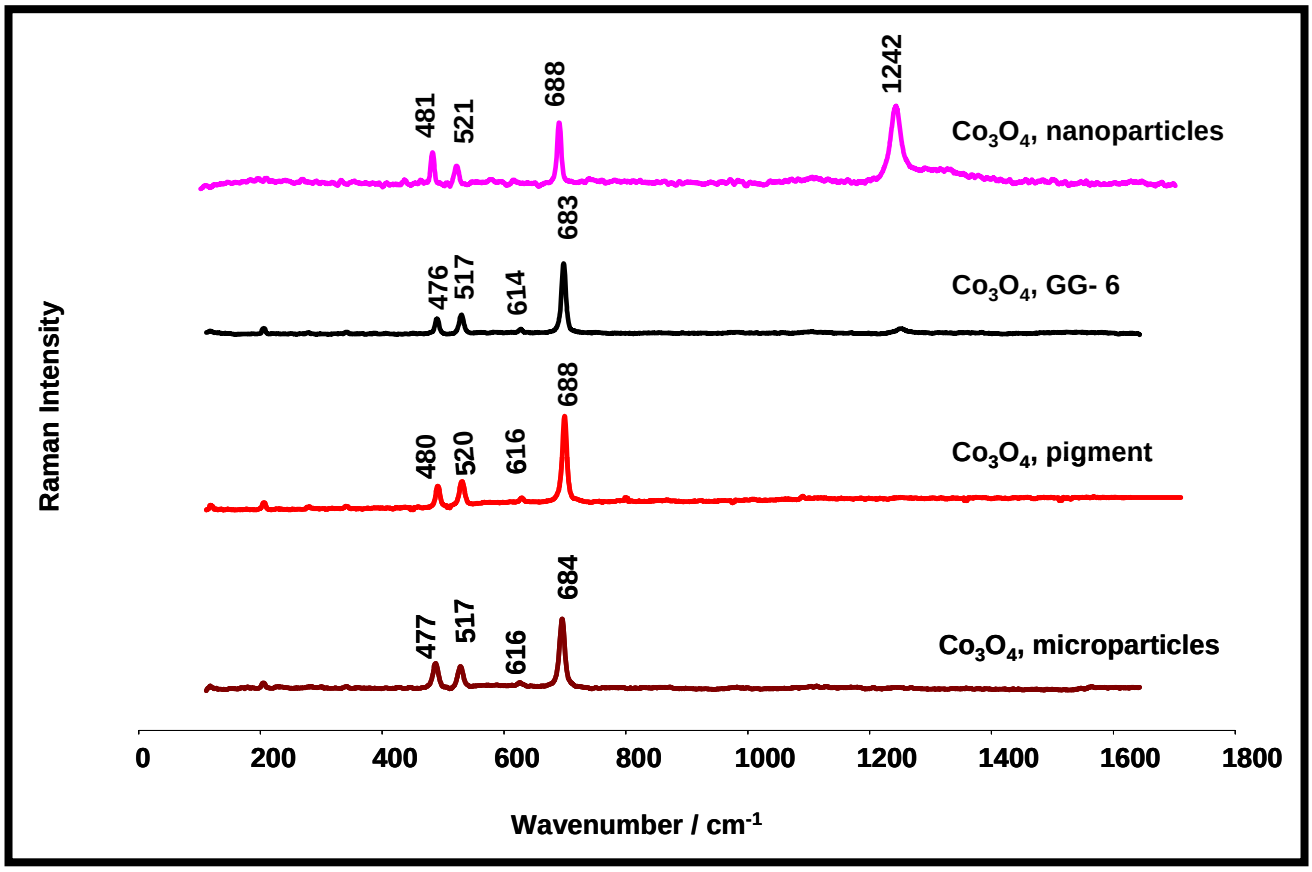

Figure 6-12: Comparison of Raman spectra of synthesised Co_3O_4 with those of commercial Co_3O_4 spinels.

In their work, Hayashi et al.,[15] discuss the size-dependence and associated shift in wavenumbers of Raman spectra. They observed that crystalline peaks broaden and

shift to lower frequencies as the grain size decreases. Therefore it can be expected that crystalline peaks narrow and shift to higher frequencies as the grain size increases.

Figure 6-13 compares the mid-IR spectra of various $Co^{2+}Co^{3+}_xAl_{2-x}O_4$ (x = 0 - 2) spinels that have been synthesized during this work with those made commercially. As with the Raman spectra, the mid-IR spectra for Co_3O_4 synthesised by the glycine-gel method (GG-6) is similar to the mid-IR spectra of the various commercial Co_3O_4. Once again, the region above 1000 cm^{-1} shows that no precursors are present in the samples.

According to the far-IR spectra shown in Figure 6-14, only GG-1 ($Co^{2+}Al_2O_4$, normal spinel) can be differentiated from the other commercial and synthesised $Co^{2+}Co^{3+}_xAl_{2-x}O_4$ (x = 0 - 2) spinels by its unique characteristic absorption band at 232 cm^{-1}. It would be difficult to distinguish the other Co_3O_4 samples (and GG-4) by their far-IR absorption bands alone.

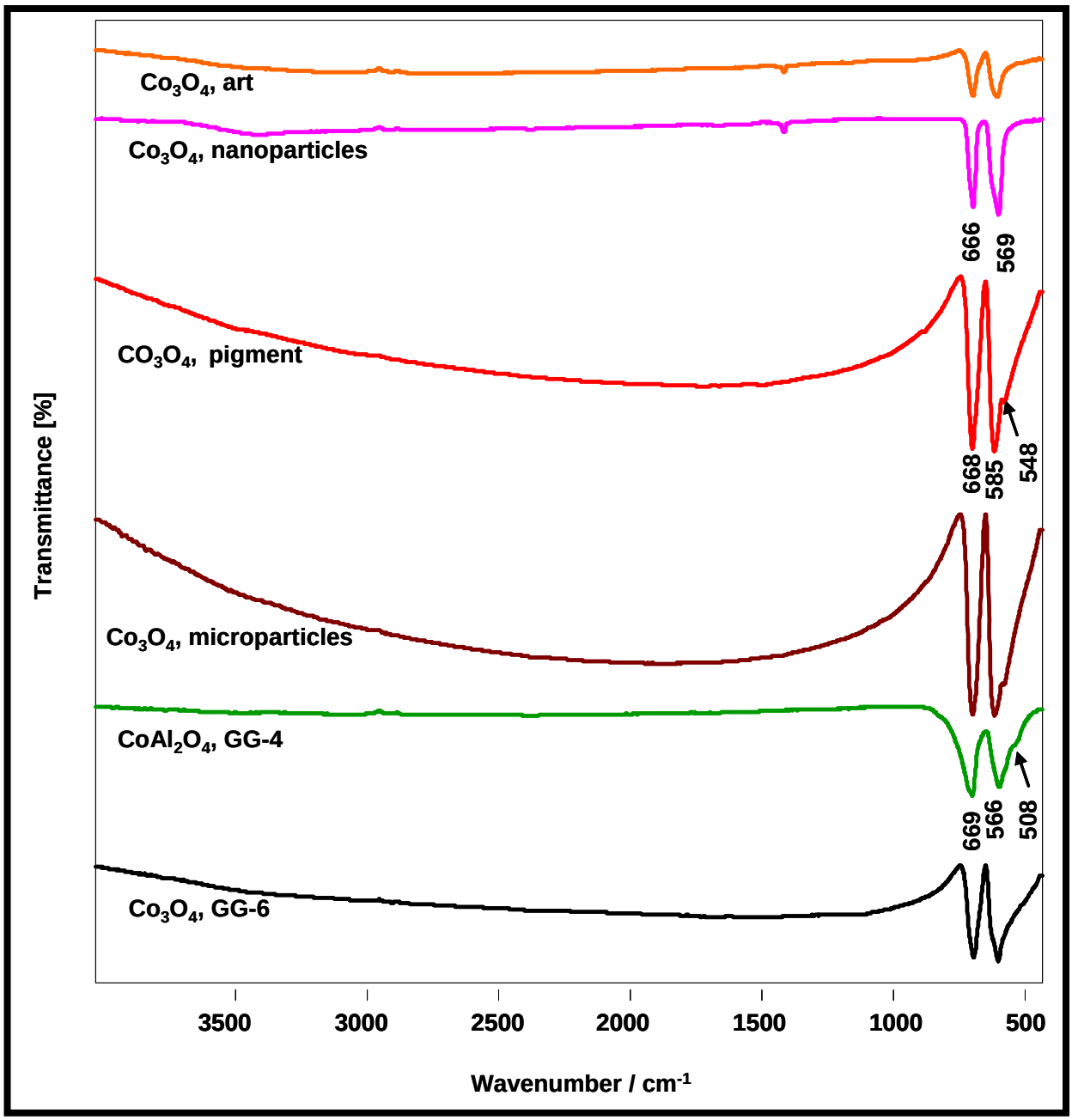

Figure 6-13: Comparison of mid-IR spectra of various synthesised and commercial $Co^{2+}Co^{3+}_{x}Al_{2-x}O_4$ (x = 0 - 2) spinels.

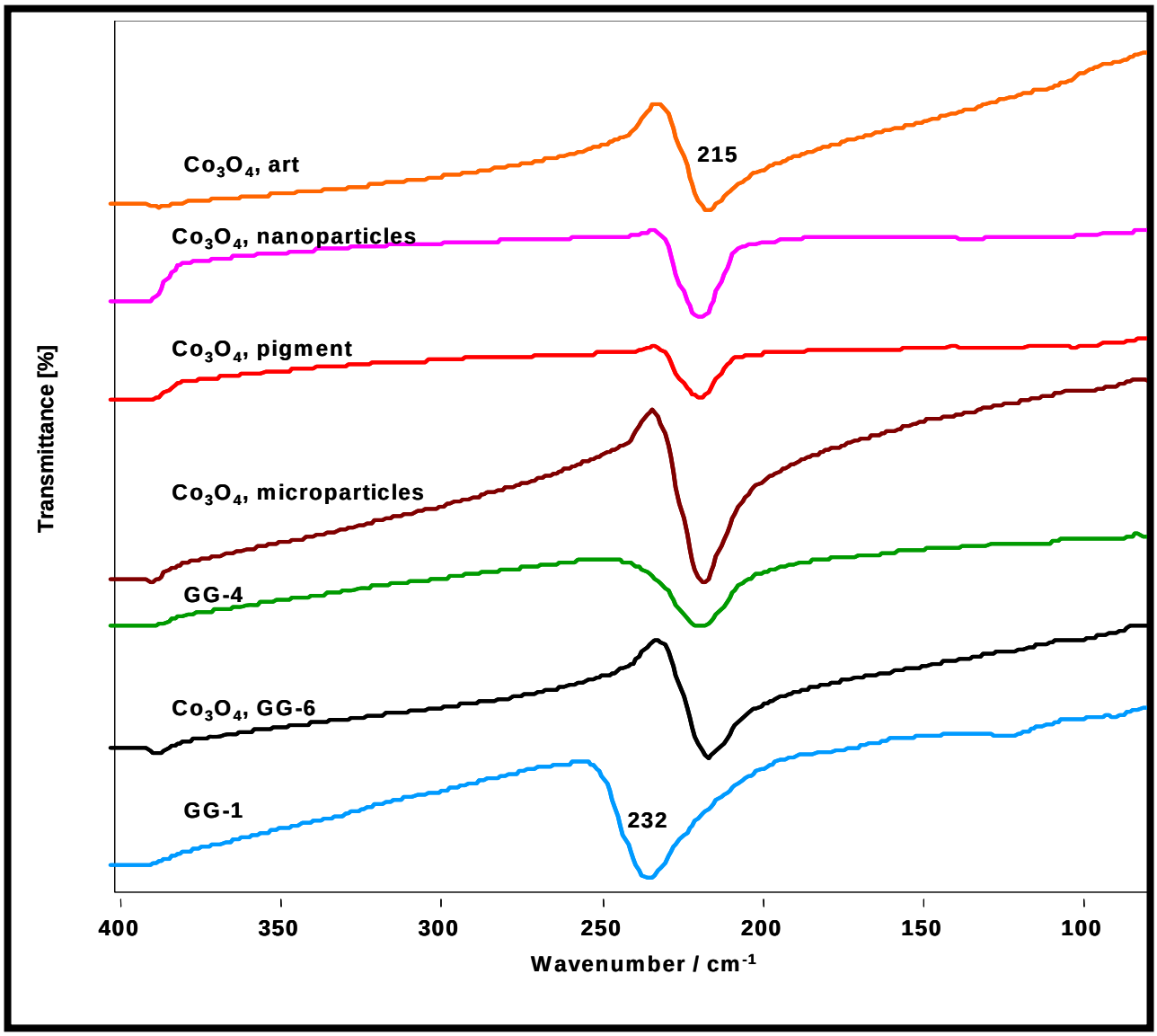

Figure 6-14: Comparison of far-IR spectra of various synthesised and commercial $Co^{2+}Co^{3+}_{x}Al_{2-x}O_4$ (x = 0 - 2) spinels.

Raman, mid and far-IR spectra of the various synthesized and commercial Co_3O_4 samples are very similar with a few minor differences indicating that the prepared GG-6 ($Co^{2+}Co^{3+2}O_4$) sample is indeed the Co_3O_4 spinel.

A summary of the Raman, mid and far-IR bands of the various $Co^{2+}Co^{3+}_{x}Al_{2-x}O_4$

(x = 0 - 2) spinels is presented in Table 6-8. Based on the Raman, mid and far-IR spectra, it appears that some Co_3O_4 powder samples share greater similarity in crystal structure with each other. In particular, Co_3O_4 (nanoparticles and art) are more similar to each other as are Co_3O_4 (pigment, microparticles and GG-6). The similarity in wavenumbers is most likely due to similarity in particle size. In addition, some exhibit the four IR-active bands predicted by group theory for spinels of the general formula AB_2O_4 (e.g. pigment) while the rest exhibit only three IR-active bands.

Table 6-8: Raman and IR bands for various $Co^{2+}Co^{3+}{}_xAl_{2-x}O_4$ spinels and $Co^{2+}O$.

Sample	Raman Bands (cm^{-1})	Mid-IR Bands (cm^{-1})	Far-IR Bands (cm^{-1})
$Co^{2+}Co^{3+}{}_2O_4$, art samples	-	1384m, 666vs, 574vs	385w, 214vs
$Co^{2+}Co^{3+}{}_2O_4$, nanoparticles (Aldrich)	435vw, 481s, 521s, 688vs, 1242vs	1384m, 666vs, 569vs	388s, 216vs
$Co^{2+}Co^{3+}{}_2O_4$, pigment (commercial)	196w, 269vw, 331vw, 480s, 520s, 616w, 688vs	668vs, 585vs, 548sh	387w, 216vs
$Co^{2+}Co^{3+}{}_2O_4$, microparticles (Aldrich)	194w, 330vw, 477s, 517s, 616w, 684vs	667vs, 584vs, 548sh	387w, 215vs
$Co^{2+}Co^{3+}AlO_4$ (GG-4)	197vs, 481s, 521s, 582m, 620m, 688vs, 705sh, 724sh	673sh, 668vs, 564vs, 508sh	386w, 216vs
$Co^{2+}Co^{3+}{}_2O_4$ (GG-6)	193w, 476s, 517s, 614w, 683vs, 1242w	662vs, 570vs, 550sh	385w, 214vs
$Co^{2+}Al_2O_4$ (GG-1)	202vs, 272w, 408m, 511s, 655w	661vs, 554s, 500vs	232vs
$Co^{2+}O$, mesh (Aldrich)	188m, 464m, 504w, 603w, 667vs	1384m, 658s, 561vs, 487vs	355w, 216vs

vw (very weak), vs (very strong), w (weak), m (medium), s (strong), sh (shoulder).

6.1.6.7 XRD Characterisation of Cobalt Oxides $Co^{2+}O$ and $Co^{2+}Co^{3+}{}_2O_4$ (GG-6)

According to Wang et al.,[1] the initial stage of the gaseous pyrolytic process of GG-6 occurs between 150 - 200 ºC during which CoO and Co_3O_4 are formed. The pyrolytic reaction is assumed to be complete at 300 ºC with the formation of a more compact structure of cobalt oxide powder. The compact structure is thought to prevent further access of oxygen, thereby making it more difficult for CoO to be converted to Co_3O_4 at temperatures below 400 ºC. However, at temperatures above 400 ºC, this conversion readily occurs. In this regard, an X-ray diffraction pattern of the CoO phase in the sample of GG-6 (Co_3O_4) heated at 1000 ºC is observed in Table 6-7 at º2θ 49.52, which does not appear in the normal and inverse spinel XRD patterns.

6.1.7 Colour of GG-1 ($Co^{2+}Al_2O_4$), GG-4 ($Co^{2+}Co^{3+}AlO_4$) and GG-6 ($Co^{2+}Co^{3+}{}_2O_4$)

Figure 6-15 shows the colour of GG-1, GG-4 and GG-6. The different colours give rise to different Raman, IR and XRD characteristics as elaborated on in the previous sections. Bright blue $Co^{2+}Al_2O_4$ (GG-1, normal spinel) is obtained by calcination of precursor gel 1 at a temperature of 1000 ºC. At the same temperature, calcination of precursor gel 4 and precursor gel 6 gave rise to black/green (GG-4) and ash black (GG-6) powders, respectively. The mid-IR vibrational bands of black/green $Co^{2+}Co^{3+}O_4$ spinel phase, calcined at 1000 ºC for 2 h appear at 570 and 663 cm^{-1} (Figure 6-13).[1]

Raman and IR characteristics for bright blue $Co^{2+}Al_2O_4$ (GG-1) are dependent on the calcination temperature (1000 ºC) and the Co/Al ratio in the precursors (Co/Al = 0.5). The colours of $Co^{2+}Co^{3+}AlO_4$ (GG-4) and $Co^{2+}Co^{3+}{}_2O_4$ (GG-6) are also dependent on the Co/Al ratio (Co/Al = 2 and ∞, respectively).[1]

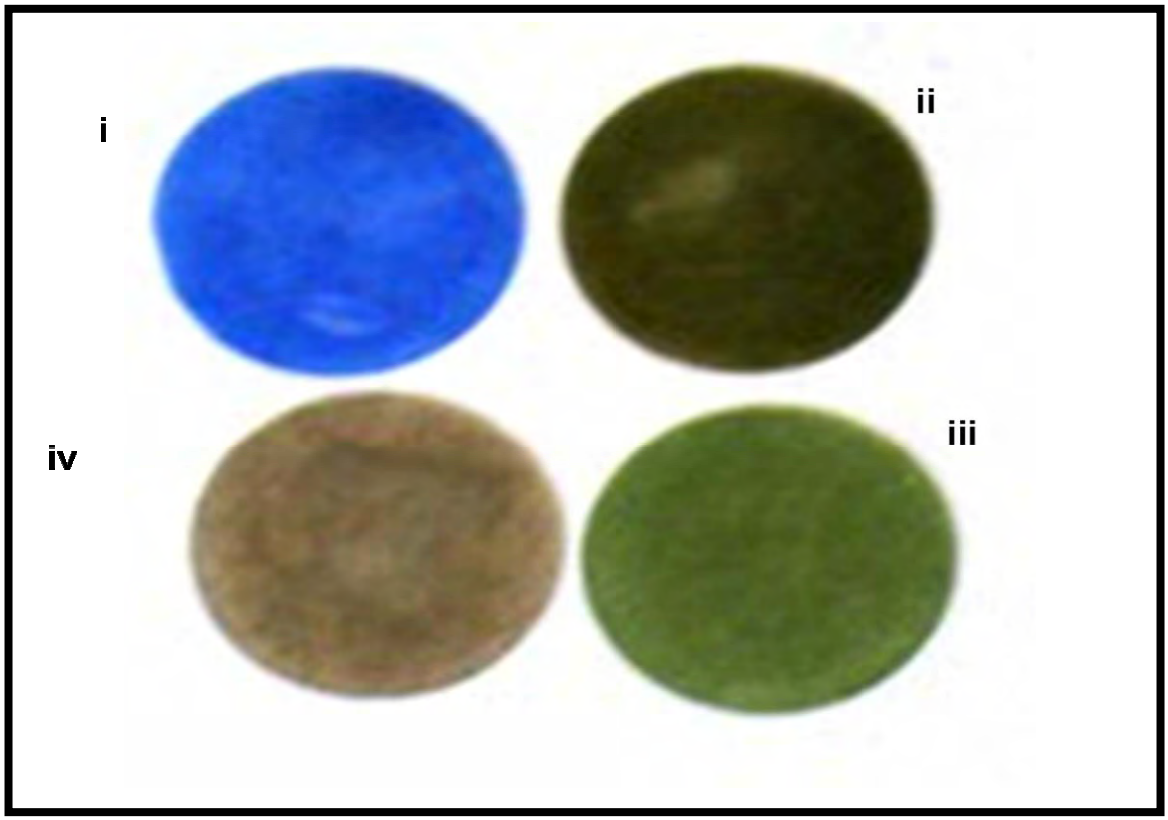

Figure 6-15: Colours of samples (i) $Co^{2+}Al_2O_4$, (ii and iii) $Co^{2+}Co^{3+}AlO_4$ and (iv) $Co^{2+}Co^{3+}{}_2O_4$ prepared by the glycine-gel method and calcined for 2 h at 1000 ºC.

In addition, as mentioned in sections 1.2 and 2.3, cobalt compounds range in colour from blue to green to pink depending upon the host lattice (idiochromatic pigments) and on both the coordination site and coordination number of the cobalt ion.[16] It can therefore be deduced that the different colours exhibited by GG-1, GG-4 and GG-6 are good examples of the role that the host lattice as well as coordination site and coordination number of the cobalt ion play in the impartation of colour. For instance GG-1 (normal spinel) contains Co^{2+} in the tetrahedral position which results in the blue colour. On the other hand, GG-4 (inverse spinel) contains Co^{2+} in the tetrahedral position, as well as Co^{3+} in the octahedral position. This results in the cobalt oxide inverse spinel ranging in colour from green to greenish black, taking into account the different colour imparting properties of both types of cobalt ions. GG-6 (cobalt oxide spinel) also contains Co^{2+} in the tetrahedral position as well as Co^{3+} in the octahedral

position but here the effect of the host lattice also plays a role in the resulting brown to black colour. The Al^{3+} is non-existent in GG-6 while it is present in both GG-1 and GG-4. In this regard, the host lattice surrounding the cobalt ion differs, depending on whether Al^{3+} is present or not.

The colour of $Co^{2+}Co^{3+}{}_2O_4$ (GG-6) compares well with the colours of commercially purchased Co_3O_4 samples as shown in Figure 6-16.

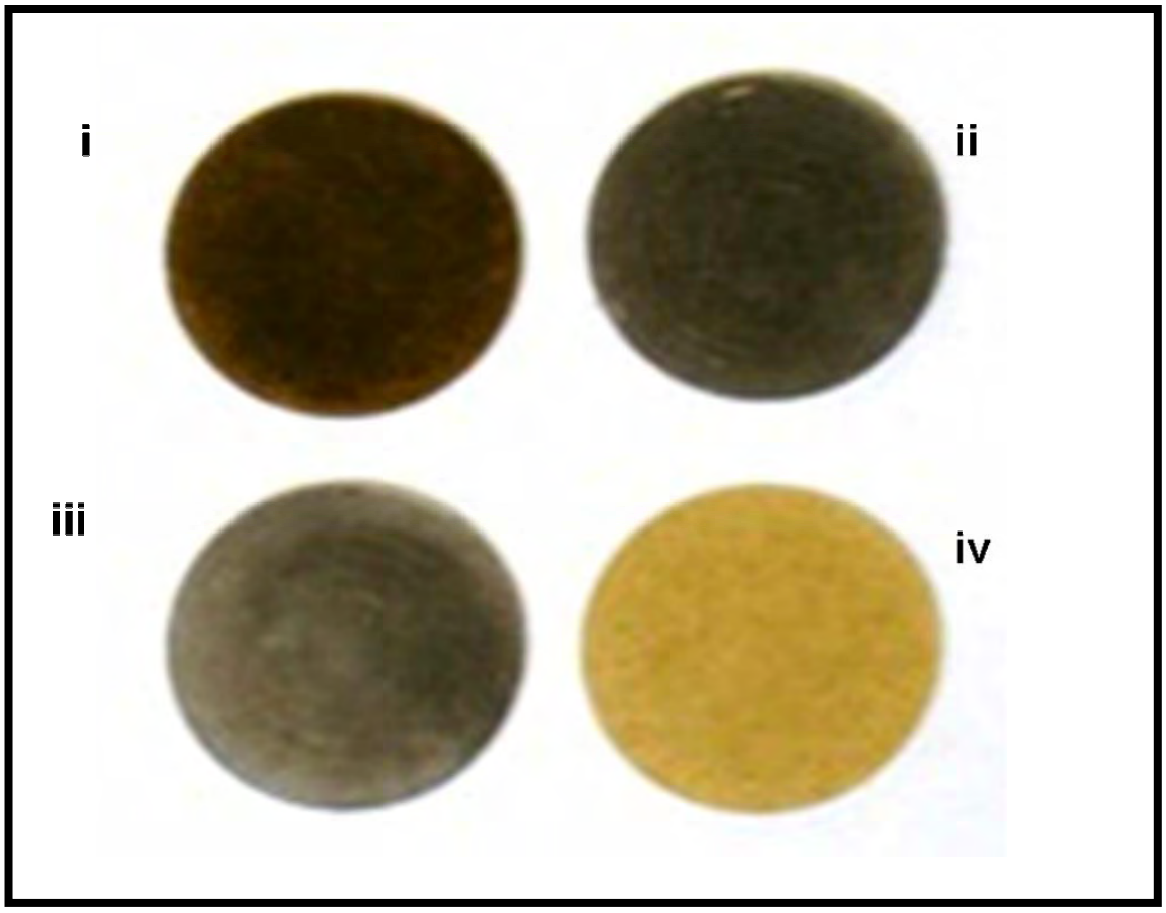

Figure 6-16: Colours of commercial cobalt oxide samples (i) Co_3O_4, nanoparticles (ii) Co_3O_4, microparticles (iii) Co_3O_4, pigment (iv) CoO mesh.

6.2 Results From Alternative Synthesis Methods

This section analyzes and compares results from alternative synthesis methods for the preparation of $Co^{2+}Al_2O_4$, as detailed in sections 5.2 - 5.4, with those from the glycine-gel method.

6.2.1 Citrate-Gel Method

The main aim of the citrate-gel method was to prepare the normal spinel oxide, $Co^{2+}Al_2O_4$. Unlike the glycine-gel method where different Co/Al ratios were used to prepare various $Co^{2+}Co^{3+}_xAl_{2-x}O_4$ (x = 0 – 2) oxides, only one Co/Al ratio was used (Co/Al = 0.5) to prepare a precursor gel, which was divided into segments that were further annealed at different temperatures in order to understand the crystallization process of $Co^{2+}Al_2O_4$, as well as to determine the temperature at which the normal spinel would form.

6.2.1.1 Raman Characterisation

Figure 6-17 shows the Raman spectra of powders obtained by heating the gel from 350 - 1000 ºC for 2 h. There is some similarity between the spectra of samples heated from 350 - 700 ºC as well as between the spectra of samples heated from 800 - 1000 ºC indicating a possible similarity in structure within the two groups. A change in crystal phase appears to occur between 700 ºC and 800 ºC based on the drastic change in Raman spectra of the powders arising from precursor gels heated at the two temperatures. The spectra of samples heated from 350 - 700 ºC also share a similarity in shape and band position to the Raman spectra obtained from the inverse spinel (GG-4, $Co^{2+}Co^{3+}AlO_4$) synthesised by the glycine-gel method (see Figures 6-1 and 6-3). The band positions of the samples heated from 800 - 1000 ºC compares well with those of the normal spinel prepared by the glycine gel method (GG-1, $Co^{2+}Al_2O_4$).

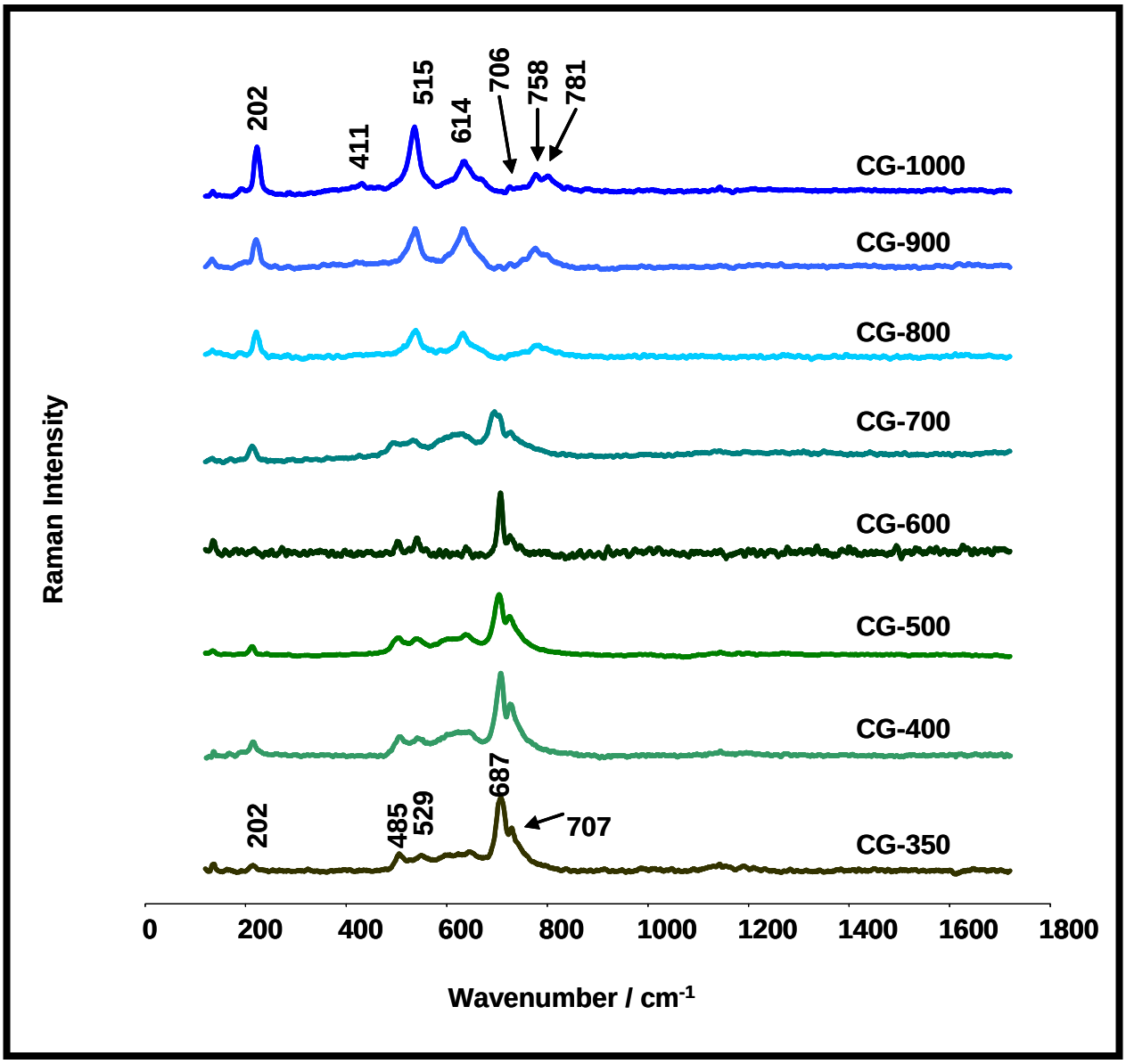

Figure 6-17: Raman spectra of samples prepared by the citrate-gel method and heated for 2 h at temperatures ranging from 350 - 1000 ºC.

Figure 6-18 focuses on the Raman spectra of powders obtained by heating the precursor gel from 700 - 1000 ºC for 2 h where the transition in crystal phases between 700 - 800 ºC can be more clearly observed. Based on the difference in

spectra between the samples heated at 700 and 800 ºC, it can be concluded that the transition temperature of the change in structure from inverse spinel to normal spinel lies between 700 and 800 ºC.

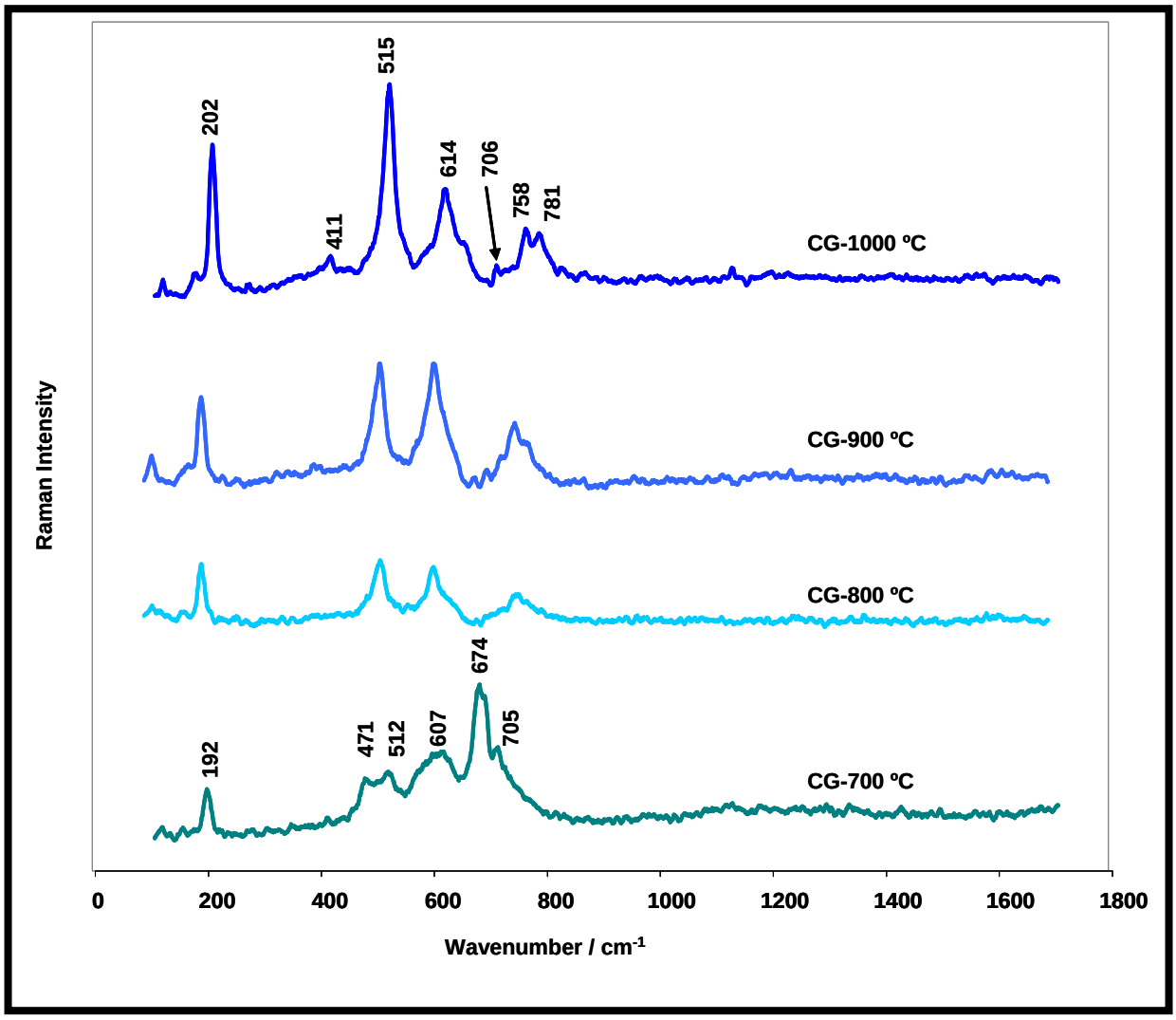

Figure 6-18: Raman spectra of samples prepared by the citrate-gel method and heated for 2 h at temperatures ranging from 700 - 1000 ºC.

Table 6-9 compares the band positions for GG-4 obtained from the glycine-gel method with band positions from samples obtained from the citrate-gel method (CG-350, 500,

and 700 ºC). There is a close similarity in Raman band position between the samples made from the different synthesis methods. Since it has already been proposed that GG-4 is the inverse spinel and is also similar in Raman, XRD and FT-IR characteristics to GG-6, it can be concluded that heating the citrate-gel at temperatures between 350 - 700 ºC produces the inverse spinel ($Co^{2+}Co^{3+}AlO_4$) and/or the $Co^{2+}Co^{3+}{}_2\,O_4$ spinel.

Table 6-9: Comparison of Raman bands for GG-4 (glycine-gel method) with those from CG-350, 500 and 700 ºC (citrate-gel method).

Sample	Raman Bands (cm^{-1})						
GG-4 (2h at 1000 ºC)	197vs	481s	521s	582m	619m	688vs	704m
CG-350 ºC (2h)	194w	485s	529s	578s 601s	623s	687vs	707s
CG-500 ºC (2h)	193m	485s	521s	582m	617s	684vs	705s
CG-700 ºC (2h)	193s	474s	513s	608s		675vs	705s

vs (very strong), w (weak), m (medium), s (strong), sh (shoulder).
Raman bands of high intensity are in blue.

Table 6-10 compares the band positions for GG-1 obtained from the glycine-gel method with band positions from samples obtained from the citrate-gel method (CG-1000 ºC) calcined for 2 h and 12 h. There is a close similarity in Raman band position between the samples made from the different synthesis methods. Since GG-1 is assumed to be the normal spinel, it can be concluded that heating the citrate-gel at 1000 ºC produces the normal spinel ($Co^{2+}Al_2O_4$).

Table 6-10: Comparison of Raman bands for GG-1 (glycine-gel method) with those from CG-1000 ºC (citrate-gel method) calcined for 2 h and 12 h.

Sample	Raman Bands (cm^{-1})							
GG-1 (2h at 1000 ºC)	202vs	272m	408m	511s		655m		
CG-1000 ºC (2h)	202vs	266w	411w	515vs	614vs		758s	781s
CG-1000 ºC (12h)	202vs		408w	511vs	608m		770m	

vs (very strong), w (weak), m (medium), s (strong), sh (shoulder).
Raman bands of high intensity are in blue.

A comparison of the Raman spectra of citrate-gel samples calcined at 1000 ºC for 2 h and 12 h is depicted in Figure 6-19. A reduction in the intensity of bands above 600 cm^{-1} and a shift of bands towards lower wavenumbers is observed with increasing period of time at 1000 ºC.

As explained in section 6.1.3 the five Raman bands predicted by group theory are present as well as additional bands which could be due to a breakdown in Raman selection rules or the presence of unwanted reaction products. See also section 3.4.

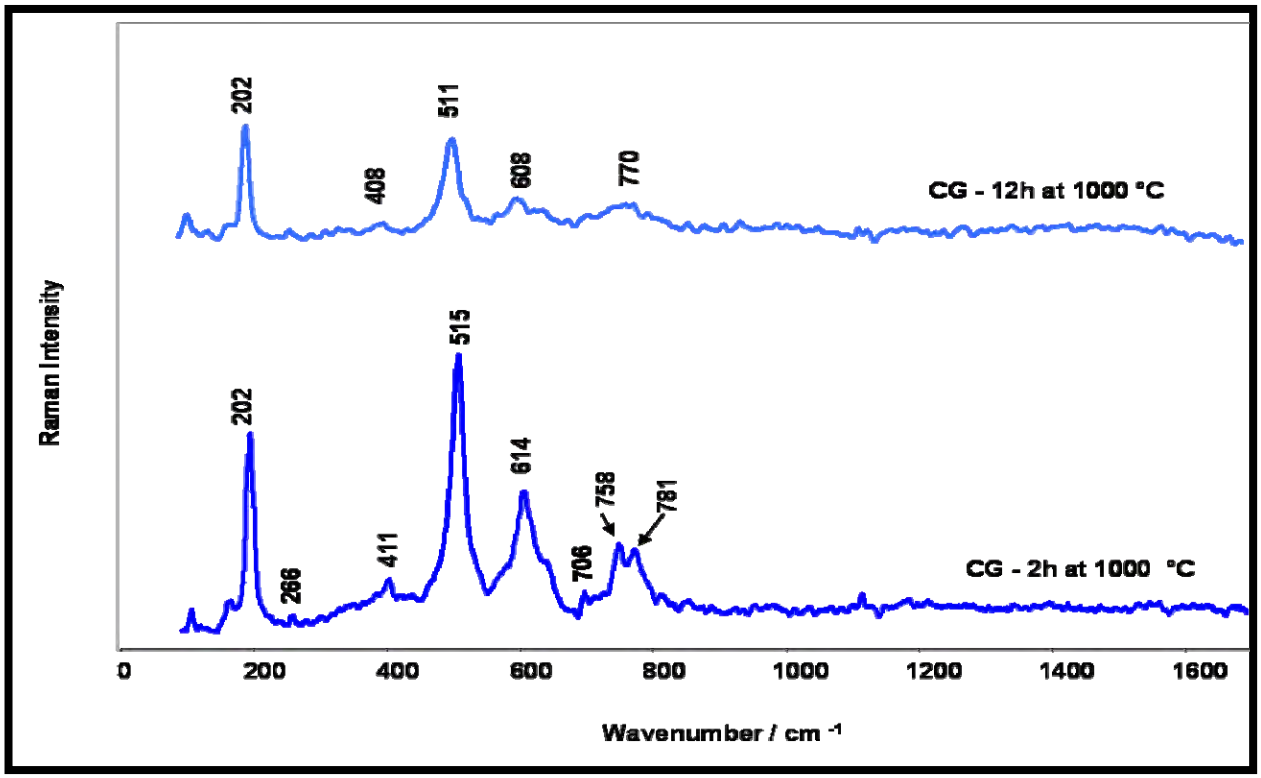

Figure 6-19: Raman spectra of citrate-gel samples heated for varying time periods at 1000 ºC.

6.2.1.2 Colour of Samples

The Raman results discussed in sections 6.2.1.1 are in agreement with the visual observation of the colouration of the samples calcined at different temperatures as shown in Figure 6-20. The sample calcined at 350 ºC is black (Figure 6-20 A), typical of $Co^{2+}Co^{3+}AlO_4$ (inverse spinel) or $Co^{2+}Co^{3+}{}_2O_4$, while that at 700 ºC is green (Figure 6-20B) which could also be due to $Co^{2+}Co^{3+}{}_2O_4$. At 800 ºC and 1000 ºC (Figure 6-20 C and D respectively) the sample is blue, indicating the formation of the normal spinel $Co^{2+}Al_2O_4$.

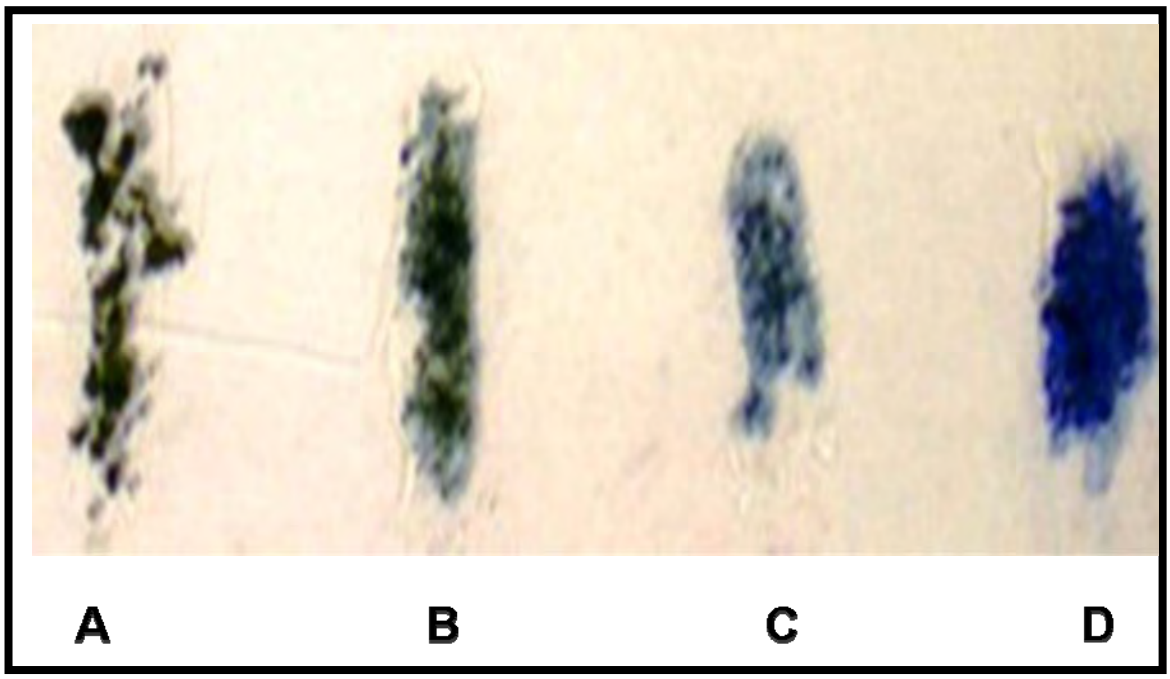

Figure 6-20: Colour of samples prepared by the citrate-gel method and heated at varying temperatures; (A) 350 ºC, (B) 700 ºC, (C) 800 ºC and (D) 1000 ºC.

6.2.1.3 XRD Characterisation – Physical Properties

XRD patterns of samples obtained by heating the citrate-gel at 350, 700 and 1000 ºC for 2 h are shown Figure 6-21. From the XRD patterns, information on the intermediate stages of the formation of the normal spinel, $Co^{2+}Al_2O_4$ can be obtained. The $Co^{2+}Co^{3+}{}_2O_4$ spinel can be observed in samples heated at 350 ºC while the normal spinel $Co^{2+}Al_2O_4$ appears only from 800 ºC (as confirmed by Raman spectra in Figure 6-22). As discussed in Section 6.1.5, the normal spinel can be distinguished from the $Co^{2+}Co^{3+}{}_2O_4$ spinel by the observation of a peak at 2 θ 57.504º (331) in the sample calcined at 1000 ºC (normal spinel).

In addition, from the XRD patterns, it can be observed that the FWHM of all peaks decreases with increasing temperature in the temperature ranges studied, which normally denotes an increased particle size and improved crystallinity.[11,12,15] The crystallinity of $Co^{2+}Al_2O_4$ therefore improved with increasing temperature and resulted

in a corresponding increase in the particle size of the powders.

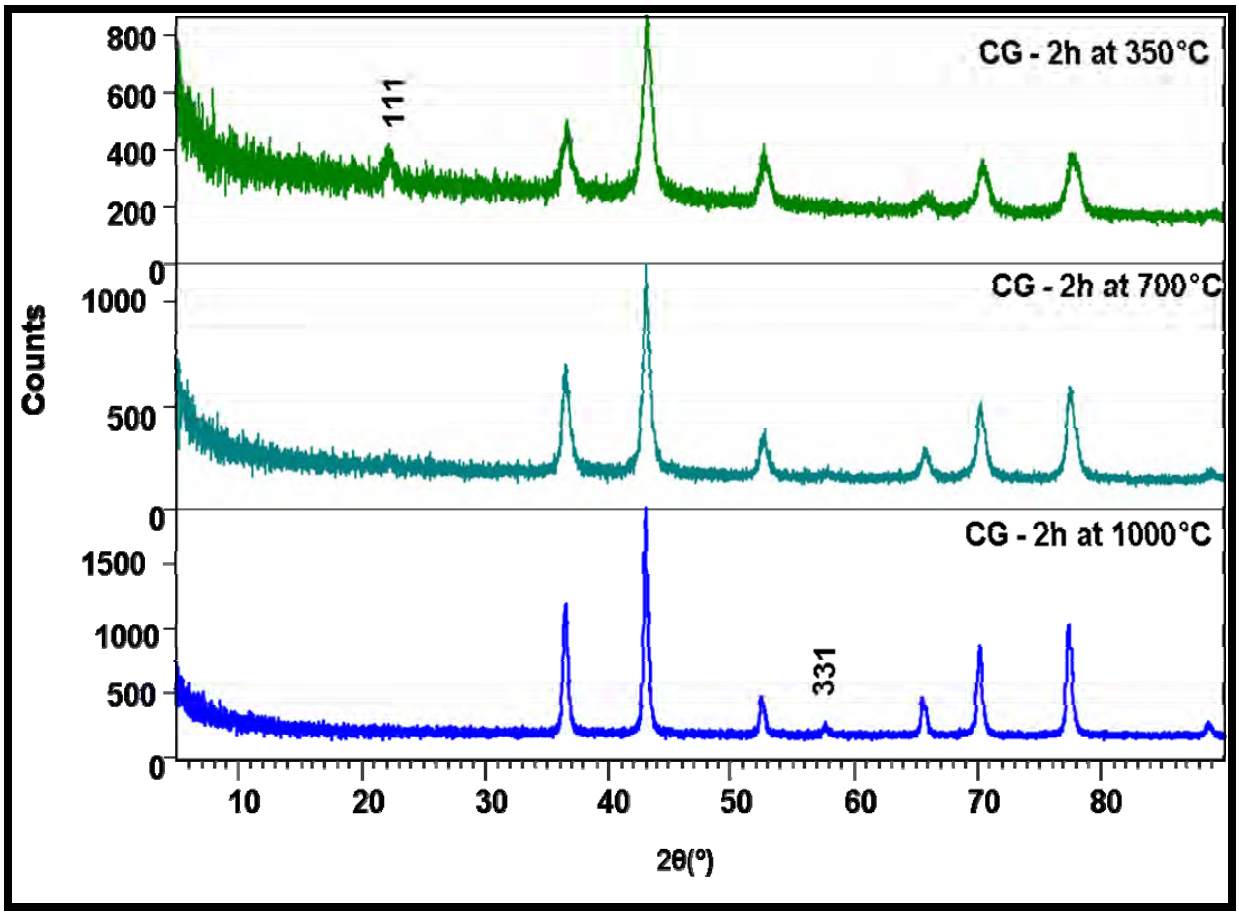

Figure 6-21: XRD patterns for samples prepared by the citrate gel method at varying temperatures.

6.2.1.4 XRD Characterisation – Lattice Planes

As observed in the diffraction patterns from the glycine-gel method (Figures 6-7 and 6-8), there are some differences in the presence and intensities of diffraction peaks at positions 2 θ 22.081º (111), and 2 θ 57.504º (331). In Figure 6-21, the lattice plane (111) can be observed in the diffraction pattern for the citrate-gel heated at 350 ºC but is hardly visible in the diffraction pattern for the citrate-gel heated at 700 ºC and does not seem to be present in the diffraction pattern for the citrate-gel heated at 1000 ºC.

In the glycine-gel method the lattice plane (111) in the diffraction pattern of GG-6 ($Co^{2+}Co^{3+}{}_2O_4$) was of a high intensity but it was of a lower intensity in GG-4 ($Co^{2+}Co^{3+}AlO_4$) and was not present in the diffraction pattern of GG-1 ($Co^{2+}Al_2O_4$). This confirms an earlier assumption that lattice plane (111) is due to the $Co^{2+}Co^{3+}{}_2O_4$ spinel, which is the stable oxide (or intermediate phase) at temperatures below 400 ºC[9] and it is consumed as the normal $CoAl_2O_4$ spinel is formed. Once again, it can be concluded that lattice plane (331) is due to the normal spinel as it is of highest intensity in CG-1000 ºC, is hardly visible in CG-700 ºC and does not appear to be present in CG-350 ºC. This further supports the notion that the presence of lattice plane (331) in XRD patterns of cobalt oxides denotes the normal spinel ($Co^{2+}Al_2O_4$) while the lack of lattice plane (331) denotes either the inverse spinel ($Co^{2+}Co^{3+}AlO_4$) or Co_3O_4 spinel (discussed in section 6.1.4).[1]

A similar trend is observed in the work of Cho et al.,[11] in that the (331) lattice plane can only be observed from 800 ºC upwards when the normal $CoAl_2O_4$ spinel is formed and accompanied by a colour change from green to blue. A narrowing of the peaks at FWHM consistent with increased crystallinity and particle size can also be observed.

6.2.1.5 Postulated Formation of $Co^{2+}Al_2O_4$

Examination of Raman and XRD spectra of cobalt oxide powders prepared by the citrate-gel method provide insight into the formation process of normal $CoAl_2O_4$ spinel. Crystalline Co_3O_4 and Al_2O_3 are thought to be formed below 700 ºC. Above 700 ºC, it appears that Co_3O_4 is reduced to CoO which then reacts with Al_2O_3 to form the normal $CoAl_2O_4$ spinel in a solid-solid interaction as depicted in equation 6-2 below. Equation 6-3 may also occur as not all Co_3O_4 is reduced to CoO.[10,14]

$$CoO(s) + Al_2O_3(s) \rightarrow CoAl_2O_4(s) \quad \text{.... 6-2}$$

$$Co_3O_4(s) + 3Al_2O_3(s) \rightarrow 3CoAl_2O_4(s) + ½O_2(g) \quad \text{.... 6-3}$$

The postulated reaction equations are supported by the difference in the Raman spectra between 700 and 800 ºC and the appearance of a diffraction line at lattice plane (331), which is considered to be due to the $CoAl_2O_4$ phase, as well as the observed colour change. A similar colour change at a similar transition temperature with the appearance of the (331) lattice plane is also observed in C. Wang et al.,[1] using the glycine-gel method.

6.2.2 Polyol Method

The polyol method was used with the aim of preparing normal $Co^{2+}Al_2O_4$ spinel with a high surface area and using a lower calcination temperature and shorter time at calcination. As with the citrate-gel method, only one Co/Al ratio was used (Co/Al = 0.5) to prepare a powder, which was divided into segments that were further heated at different temperatures and time periods in order to determine the lowest temperature at which the normal spinel phase $Co^{2+}Al_2O_4$ would form.

6.2.2.1 Raman Characterisation

Figure 6-22 shows the Raman spectra of samples prepared by the polyol method and heated at different temperatures and time periods. The narrower and more intense bands in the spectra of the sample calcined at 1000 ºC for 12 h indicates that the crystallinity of the samples increases with increasing temperature. The band positions for the sample calcined at 1000 ºC for 12 h are very similar to band positions for GG-1 ($Co^{2+}Al_2O_4$ prepared by the glycine-gel method and calcined for 2 h at 1000 ºC) and CG-1000 ºC (prepared by the citrate-gel method and calcined for 12 h at 1000 ºC). Therefore, it can be assumed that the normal spinel $Co^{2+}Al_2O_4$ is formed when the precursor powder prepared by the polyol method is heat treated at 1000 ºC for 12 h. In addition, the 507 cm^{-1} band in the sample calcined at 1000 ºC increases in intensity relative to the bands above 600 cm^{-1}, which greatly decrease in intensity. A similar trend can be observed in Figure 6-19 for samples prepared with the citrate-gel method (heated at 1000 ºC for 2 h versus that heated at 1000 ºC for 12 h).

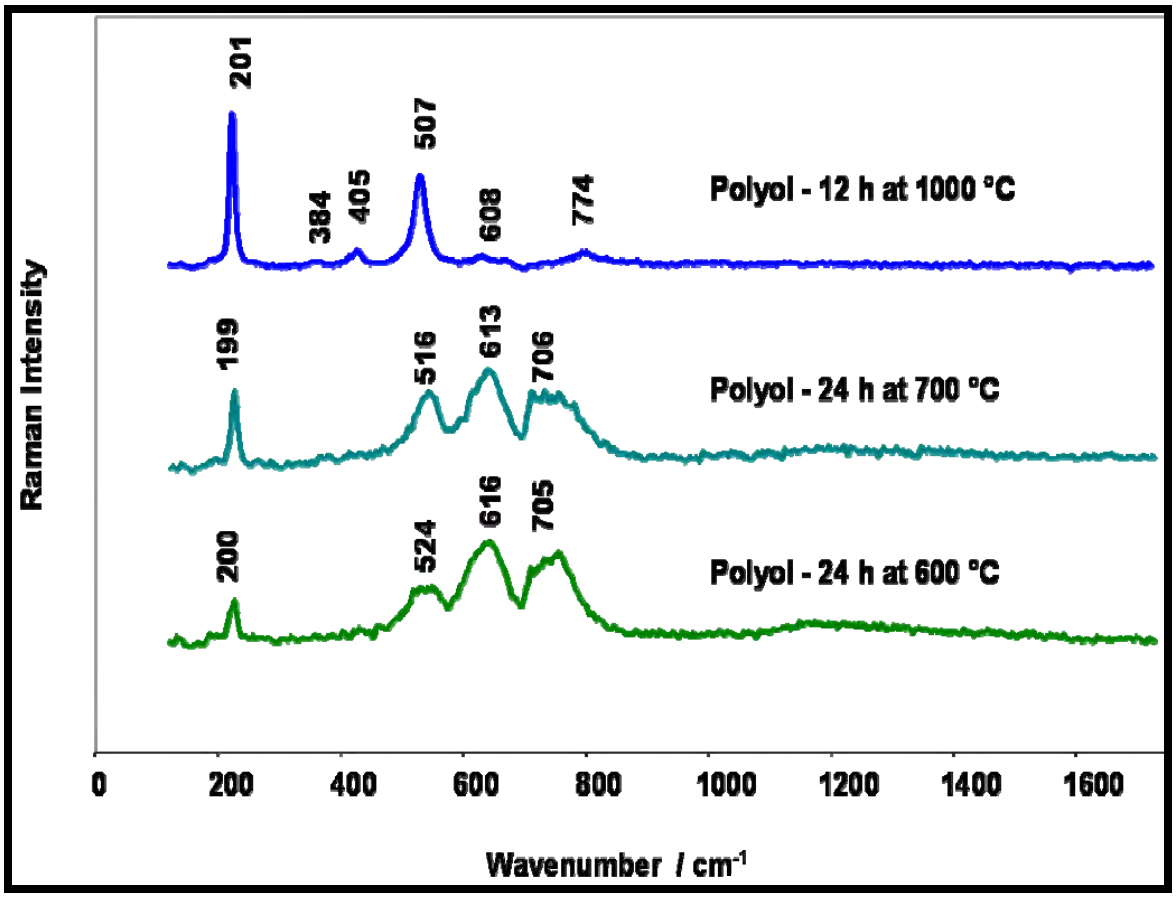

Figure 6-22: Raman spectra of samples prepared by the polyol method and heat-treated at different temperatures and for different time periods.

Figure 6-23 shows the Raman spectra of samples prepared by the polyol method and calcined at 1000 ºC for different time periods. On comparing the spectra, it can be observed that the normal $CoAl_2O_4$ spinel is formed within 5 minutes of heating the sample at 1000 ºC. The main differences include the increasing appearance of the 405 cm^{-1} band and the reduction in intensity of the bands above 600 cm^{-1} with a longer period of time at 1000 ºC. Another observation in Figure 6-23 is that the bands above 600 cm^{1} are visible in the spectra of the sample that was heated for 5 minutes but seems to disappear in the spectra of the sample that was heated for 2 h and then reappears in the spectra of the sample that was heated for 12 h. This could be due to

the change in alignment of the sample and the increase in particle size with increasing period of time at 1000 ºC.

In addition, increased annealing time led to the reduction in band width (FWHM) and increased peak intensity. A possible explanation for this is the increased interaction between incident light and larger particles formed. A qualitative relationship between particle size and band width can thus be implied. Longer times and higher temperatures result in larger average particle size which in turn results in sharper peaks.[12]

In like manner, the size dependence of Raman spectra is observed by the broadening and shifting to lower frequencies of crystalline bands as the grain size decreases. Therefore it can be expected that crystalline bands narrow and shift to higher frequencies as the grain size increases.[15]

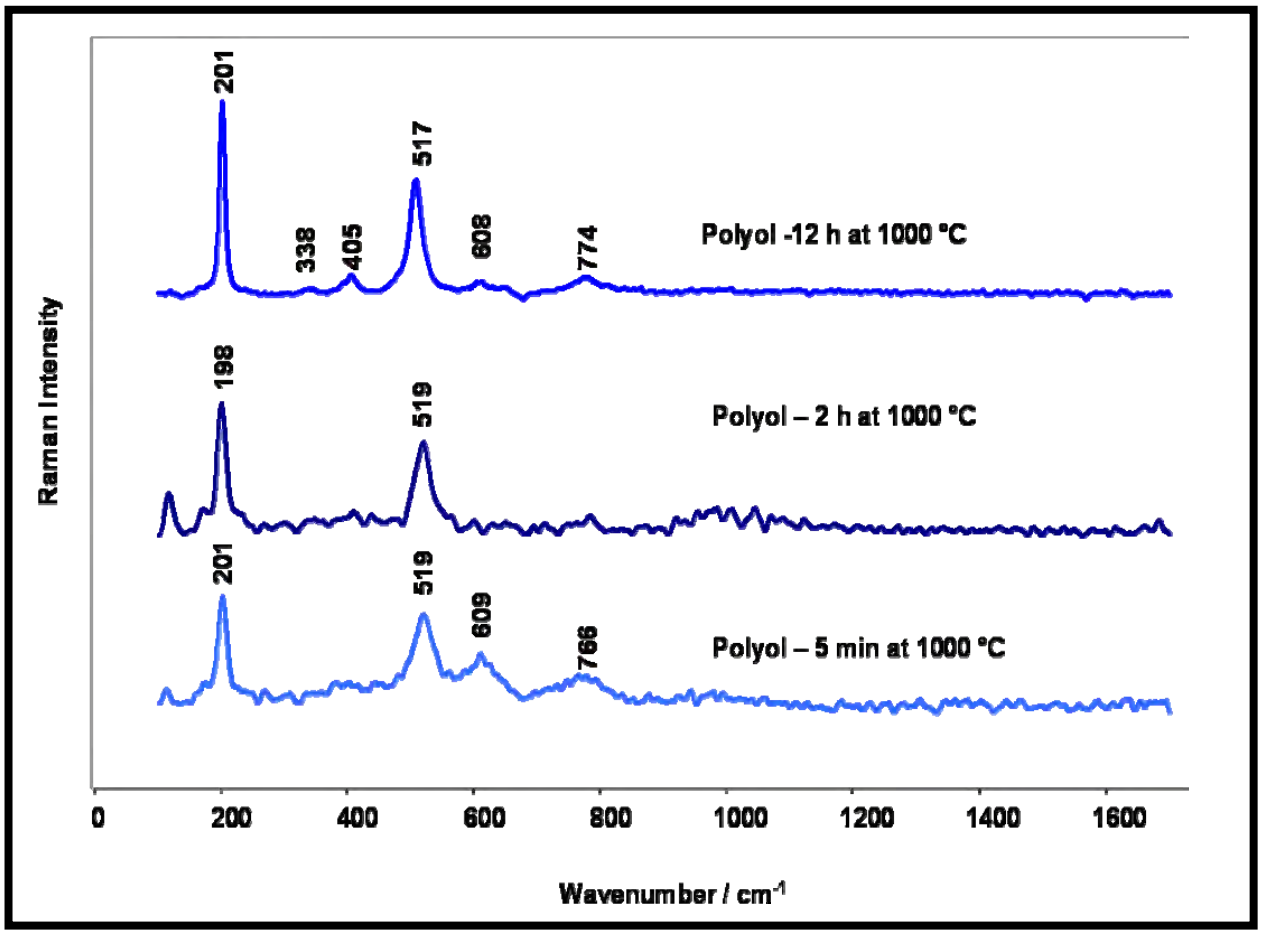

Figure 6-23: Raman spectra of samples prepared by the polyol method and calcined at 1000 ºC for different time periods.

6.2.2.2 FTIR Characterisation

Figure 6-24 shows the mid-IR spectra of samples prepared by the polyol method and heated at different times and temperatures. Only selected spectra were chosen for placement in Figure 6-24 to show the trend in spinel structure formation.

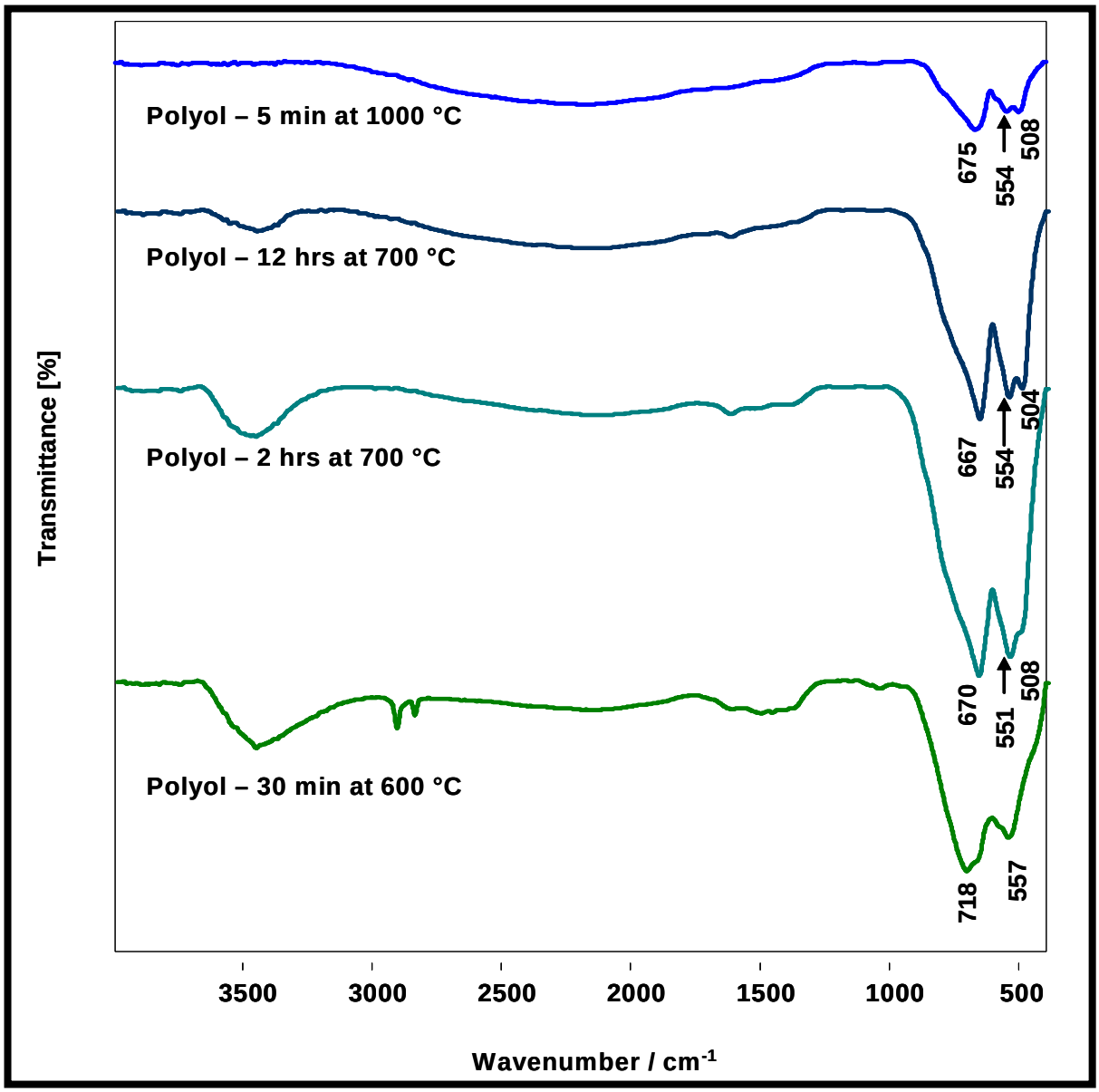

Figure 6-24: Mid-IR spectra of samples prepared by the polyol method showing variation with time and temperature.

In the spectra of the sample heated at 1000 ºC, three bands are observed around 508, 554, and 675 cm^{-1}, with a shoulder at 594 cm^{-1}, which are attributed to the vibrational bands of a normal spinel $Co^{2+}Al_2O_4$. The sample heated for 12 h at 700 ºC indicates the presence of both $CoAl_2O_4$ and Co_2AlO_4 based on the vibrational bands 667, 554

and 504 cm^{-1} (compare with Fig 6-5). The sample heated at 700 ºC for 2 h exhibited two broad bands around 551 and 670 cm^{-1}, with a shoulder at 508 cm^{-1}. These bands can be attributed to cobalt oxide as observed for commercial Co_3O_4 (Table 6-8). The sample heated at 600 ºC for 30 minutes resulted in the formation of broad $CoAl_2O_4$ bands at 557 and 718 cm^{-1} with shoulders at 596 cm^{-1} and 676 cm^{-1}, respectively. It can therefore be concluded that the Co_3O_4 spinel as well as the Co_2AlO_4 spinel are transitional phases during the formation of the normal spinel, $CoAl_2O_4$.

Across the various spectra, the band around 670 cm^{-1} becomes more intense and narrower as the temperature is raised and the bands around 551 and 504 cm^{-1} become more defined with increasing temperature and time period of calcination.

From the spectra of the sample heated for 30 minutes at 600 ºC, it can be observed that the sample is already crystalline and the spinel structure has started to form. The spectra of the sample heated at 700 ºC for 12 h shows that the spinel structure is already formed. Although the optimum temperature and time period that the normal spinel structure formed was not determined, the results indicate that the spinel structure can be obtained by heating the precursor powder at temperatures much lower than 1000 ºC and for shorter time periods as opposed to when preparing with the citrate-gel and glycine-gel methods.

Both Raman and FT-IR results, in Figures 6-23 and 6-24, seem to indicate that the normal spinel structure is fully formed when the sample is heated for 5 minutes at 1000 ºC.

Table 6-11 shows the mid-IR bands of samples prepared by the polyol method and heated at 600 ºC and 700 ºC at various time periods in comparison with bands from samples prepared by the glycine-gel method. The 511 cm^{-1} shoulder becomes more defined and shifts to the 504 cm^{-1} position as the time period at a particular temperature is increased. For instance, for the sample heated for 30 minutes at 700 ºC, the 511 cm^{-1} band is a shoulder, while for the sample heated for 12 h at

700 ºC, the band shifts to 504 cm^{-1} and is more defined.

Table 6-11: Comparison of mid-IR absorption bands for samples GG-1 ($Co^{2+}Al_2O_4$), GG-4 ($Co^{2+}Co^{3+}AlO_4$) and GG-6 ($Co^{2+}Co^{3+}{}_2O_4$) with those prepared by the polyol method.

Sample	Mid-IR absorption bands (cm^{-1})
GG-1	661, 554, 502
GG-4	669, 566, 508
GG-6	663, 570
30 minutes at 600 ºC	718vs, 676sh, 594sh, 557s
75 minutes at 600 ºC	675vs, 594sh, 555vs
3 h at 600 ºC	674vs, 553vs
7 h at 600 ºC	672vs, 552vs, 508sh
30 minutes at 700 ºC	671vs, 549s, 508sh
75 minutes at 700 ºC	671vs, 552vs, 508sh
2 h at 700 ºC	670vs, 551vs, 508sh
12 h at 700 ºC	667vs, 554s, 504s
5 minutes at 1000 ºC	675vs, 594sh, 554s, 508s

vs (very strong), m (medium), s (strong), sh (shoulder).

6.2.2.3 Colour of Samples

The Raman and FT-IR results of samples prepared by the polyol method are in agreement with the visual observation of the colouration of the samples heated at

different temperatures as shown in Figure 6-25. The normal spinel is bright blue (D) similar to that prepared by the glycine-gel method (GG-1, $Co^{2+}Al_2O_4$).

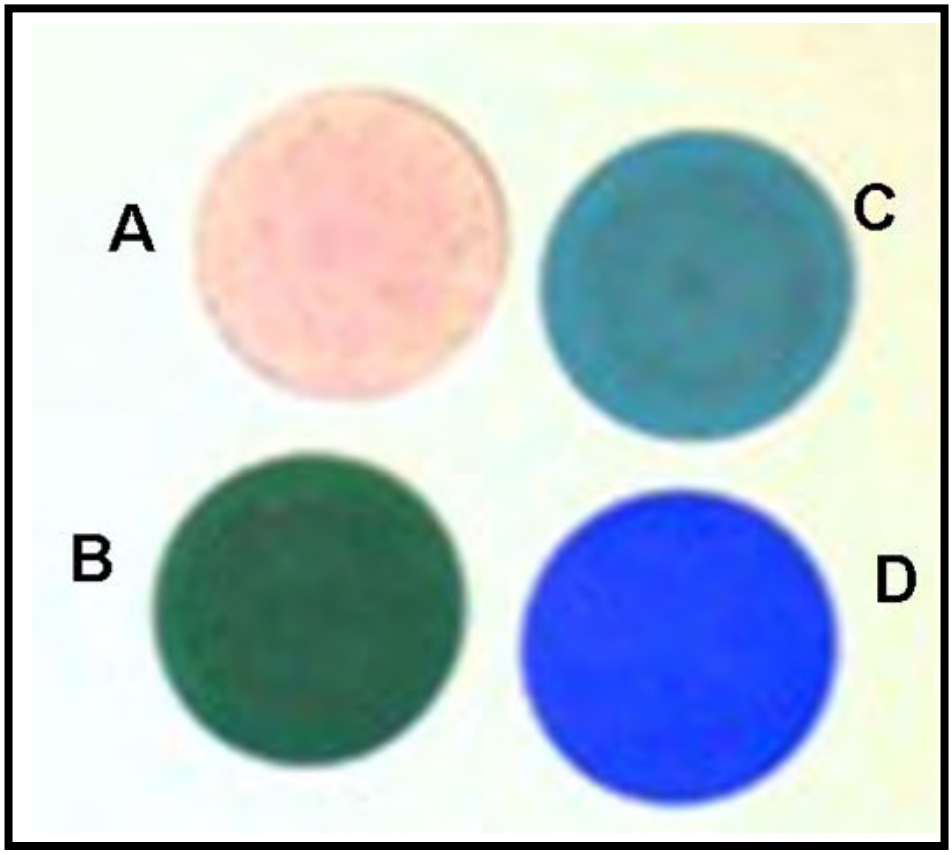

Figure 6-25: KBr pellets showing colours of samples prepared by the polyol method and heated at various temperatures and time periods; (A) precursor powder, (B) 24 h at 600 ºC, (C) 24 h at 700 ºC, (D) 2 h at 1000 ºC.

In addition, as mentioned in section 2.3 cobalt compounds range in colour from blue to green to pink, depending upon the host lattice (idiochromatic pigments) and both the coordination site and coordination number of the cobalt ion. This has been expounded upon in section 6.1.7.

Compounds in which cobalt is in the octahedral position tend to be pink to violet in colour, while those in which cobalt is in the tetrahedral position tend to be blue. The pink colour changes to blue upon annealing, as was the case in this research work, suggesting an increase in the amount of the cobalt ion occupying the tetrahedral position rather than the octahedral position as the cobalt aluminate spinel forms.

6.2.2.4 XRD Characterisation

Figure 6-26 shows the XRD patterns for samples prepared by the polyol method and heated at 600 and 700 ºC. The (331) lattice plane is barely visible in Figure 6-26 which indicates that samples heated at 600 and 700 ºC are not the normal $CoAl_2O_4$ spinel. It was mentioned in section 6.1.5 that the (331) lattice plane is indicative of the normal $CoAl_2O_4$ spinel.

The (331) lattice plane is observed in the samples prepared by the polyol method and calcined for 2 and 5 h at 1000 ºC (Figure 6-27) as well as for the sample prepared by the solid-state method (section 5.4) and calcined for 24 h at 1000 ºC. This indicates that these samples are most likely normal $CoAl_2O_4$. In both Figures 6-26 and 6-27, the powder precursor (180 ºC) appears to contain both amorphous and crystalline phases with the crystallinity and particle size increasing with increasing temperature and time period of calcination.

Raman, FTIR and XRD results seem to support the conclusion that samples prepared by the polyol method and heated at 1000 ºC have the structure of the normal spinel $CoAl_2O_4$ while those heated at lower temperatures (600 and 700 ºC) fall within the general structure of $Co^{2+}Co^{3+}_xAl_{2-x}O_4$ (x = 0 -2).

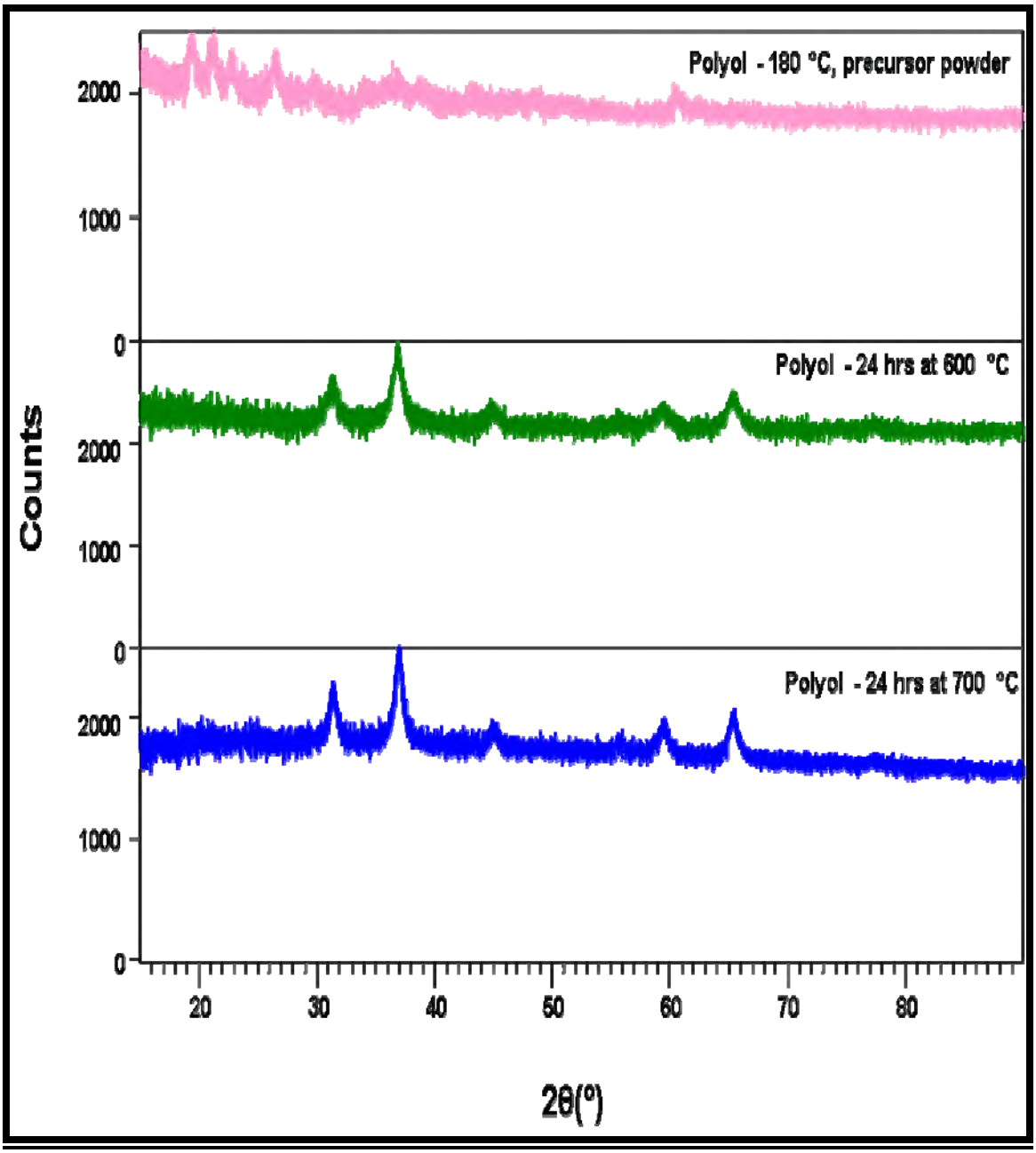

Figure 6-26: XRD patterns of samples prepared by the polyol method.

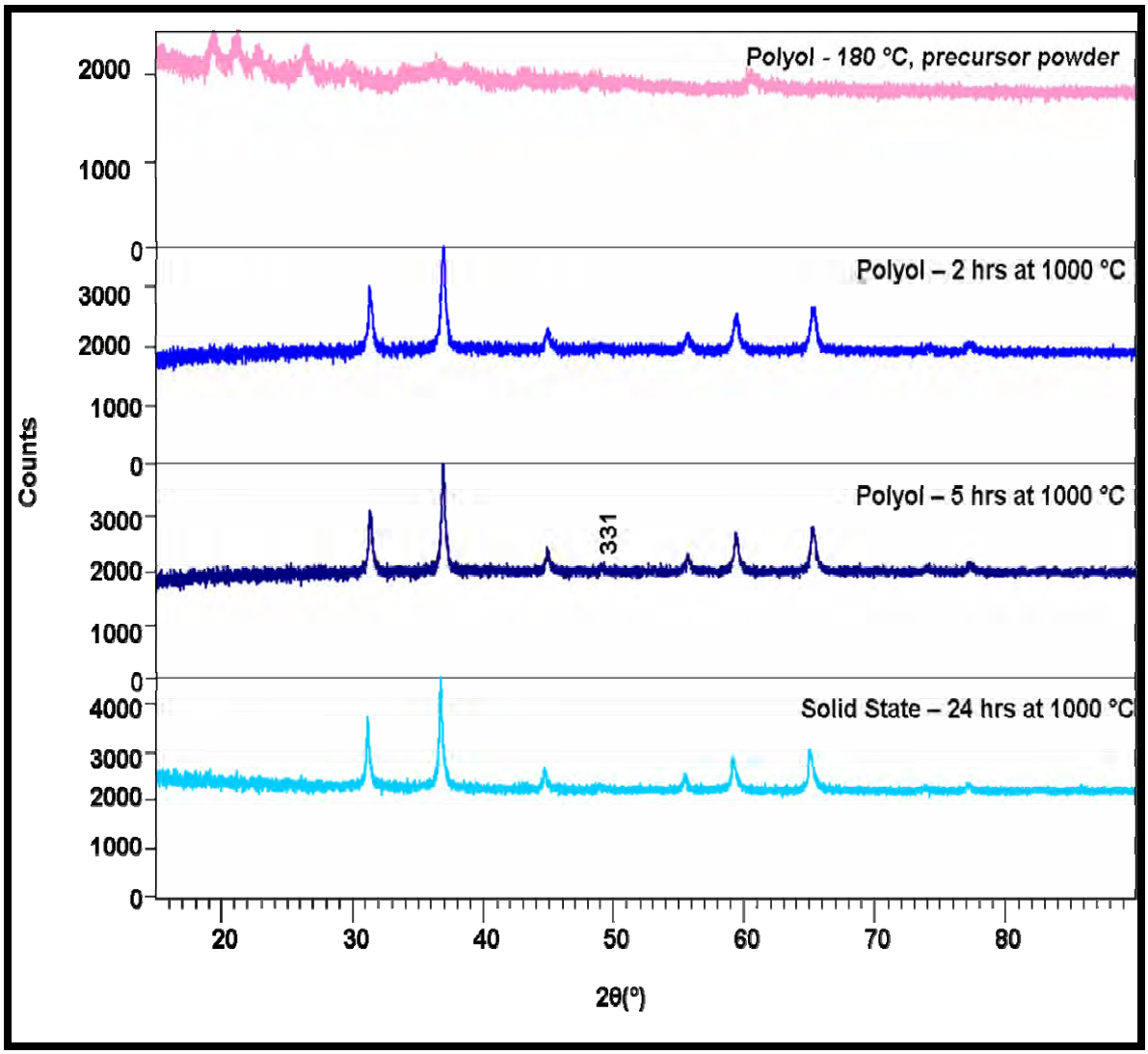

Figure 6-27: XRD patterns comparing samples prepared by the polyol and solid-state methods showing similarity in patterns.

6.2.3 Factors Affecting the Colour of Samples

The temperature and time period at which a particular sample is heated as well as the ratio of Co and Al in the precursor, especially for the $Co^{2+}Co^{3+}{}_xAl_{2-x}O_4$ samples, determines the colour of the final powder.

In the glycine-gel method, samples with a Co/Al ratio of 0.5 were blue (GG-1, $Co^{2+}Al_2O_4$), those with Co/Al ratio of 1-2 were green (GG-2, 3 and 4, $Co^{2+}Co^{3+}_{0.5}Al_{1.5}O_4$, $Co^{2+}Co^{3+}_{0.8}Al_{1.2}O_4$, $Co^{2+}Co^{3+}AlO_4$ respectively) and those with much higher Co/Al ratios were black (GG-5, $Co^{2+}Co^{3+}_{1.5}AlO_4$ and GG-6, $Co^{2+}Co^{3+}_2O_4$).[9]

With regard to the heating temperature, samples prepared by the polyol method and heated to 600 ºC exhibited a dark green colouration which progressively changed to bright blue as the temperature was increased. With the citrate-gel method, samples heated below the temperature at which the normal $CoAl_2O_4$ phase is postulated to form (i.e. 800 ºC) showed a similar dark green which is indicative of a high Co content in relation to Al content. Above 800 ºC, the samples turned a bright blue colour which is characteristic of Co^{2+} in tetrahedral coordination. In addition, the change of colour to blue tends to be observed in $CoAl_2O_4$ samples with a Co/Al ratio of 0.5 or lower.

The green colour, which is most likely due to Co^{3+} in octahedral coordination, gradually becomes bright blue as the Co content is reduced upon the reaction of CoO with Al_2O_3 to form the normal $CoAl_2O_4$ spinel (as explained in Section 6.2.1.5).[9]

Tables showing the colour of the crystalline powders prepared by the various synthesis methods can be found in Appendix B.

6.3 Comparison of Results From Different Methods of Preparation

The following section compares Raman, XRD and FT-IR results of samples prepared by the various methods detailed in chapter 5 and sections 6.1 and 6.2 with the aim of observing similarities and differences in structure related to the method of preparation.

Figure 6-28 shows samples which all exhibited the bright blue colouration of the normal spinel $CoAl_2O_4$. Samples prepared by the citrate-gel method (2 h at 1000 ºC) and solid-state method (24 h at 1000 °C) show very similar Raman spectra

characteristic of a spinel structure. This indicates that the citrate-gel method provides a shorter calcination time at 1000 ºC for preparation of normal spinel $CoAl_2O_4$.

The spectra of the sample prepared by the polyol method does not exhibit bands above 600 cm^{-1}, as compared to the spectra of samples prepared by the citrate-gel and solid-state methods. It has also been shown in Figures 6-22 and 6-23 that high intensity Raman bands above 600 cm^{-1} are associated with the initial stages of the formation of the normal spinel. The fully formed normal spinel exhibits much lower intensity Raman bands above 600 cm^{-1} with a relatively high intensity of the band between 500 and 530 cm^{-1}. As also shown in Figure 6-19, the bands above 600 cm^{-1} drastically reduce in intensity upon further heating of the citrate-gel sample at 1000 ºC for 12 h. It can be assumed that if the citrate-gel sample was heated at 1000 ºC for up to 24 h, the spectra would be more similar to that of the sample prepared by the polyol method. This indicates that the polyol method is the most suitable method for preparation of normal spinel $CoAl_2O_4$ when 1000 ºC is chosen as the calcination temperature.

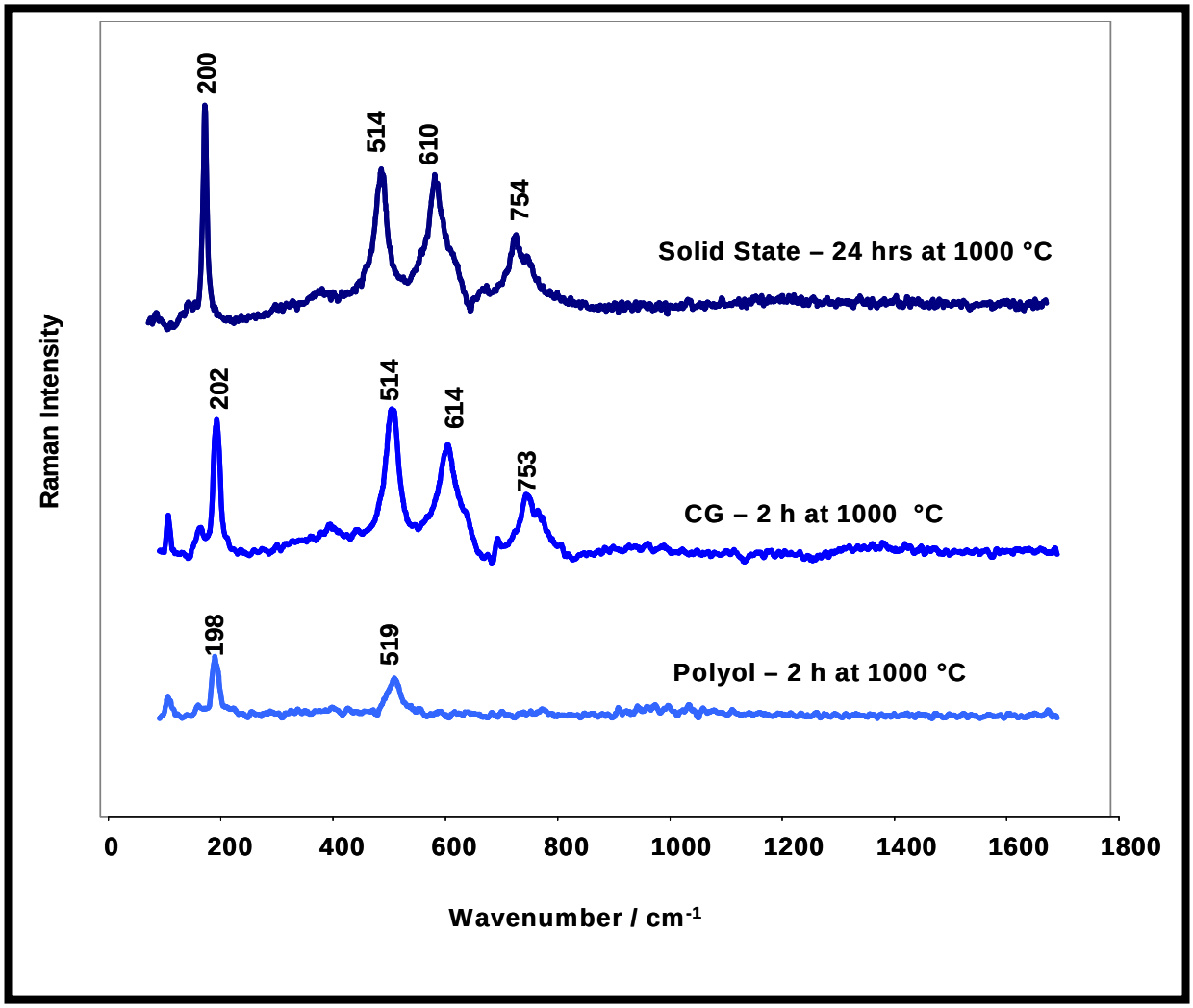

Figure 6-28: Raman spectra of $CoAl_2O_4$ samples prepared by the solid-state, citrate-gel and polyol methods showing similarities and differences in spectra.

Figure 6-29 is similar to Figure 6-28 with the exception that the glycine-gel method is included and the calcination temperatures compared are longer (12 h). Once again, Raman spectra are similar with regards to band positions and all are characteristic of a normal spinel structure. In particular, spectra of samples synthesized by the citrate-gel and polyol methods (both calcined for 12 h at 1000 ºC) show even more similarity with regards to band positions and intensity.

The spectra of the sample prepared by the glycine-gel method (GG-1, 2 h at 1000 ºC) in Figure 6-29 shows similarity with the spectra of the sample prepared by the polyol method (12 h at 1000 ºC) with respect to the relative intensity of the bands within the spectra and the presence of the band between 400 and 410 cm^{-1} and the reduction of intensity of bands above 600 cm^{-1}. However, the glycine-gel sample was calcined for 2 h at 1000 ºC as opposed to 12 h at 1000 ºC for the polyol and citrate-gel methods. It therefore competes with the polyol method spectra shown in Figure 6-28 (2 h at 1000 ºC) with regards to suitability for preparation of normal spinel $CoAl_2O_4$ when 1000 ºC is chosen as the calcination temperature.

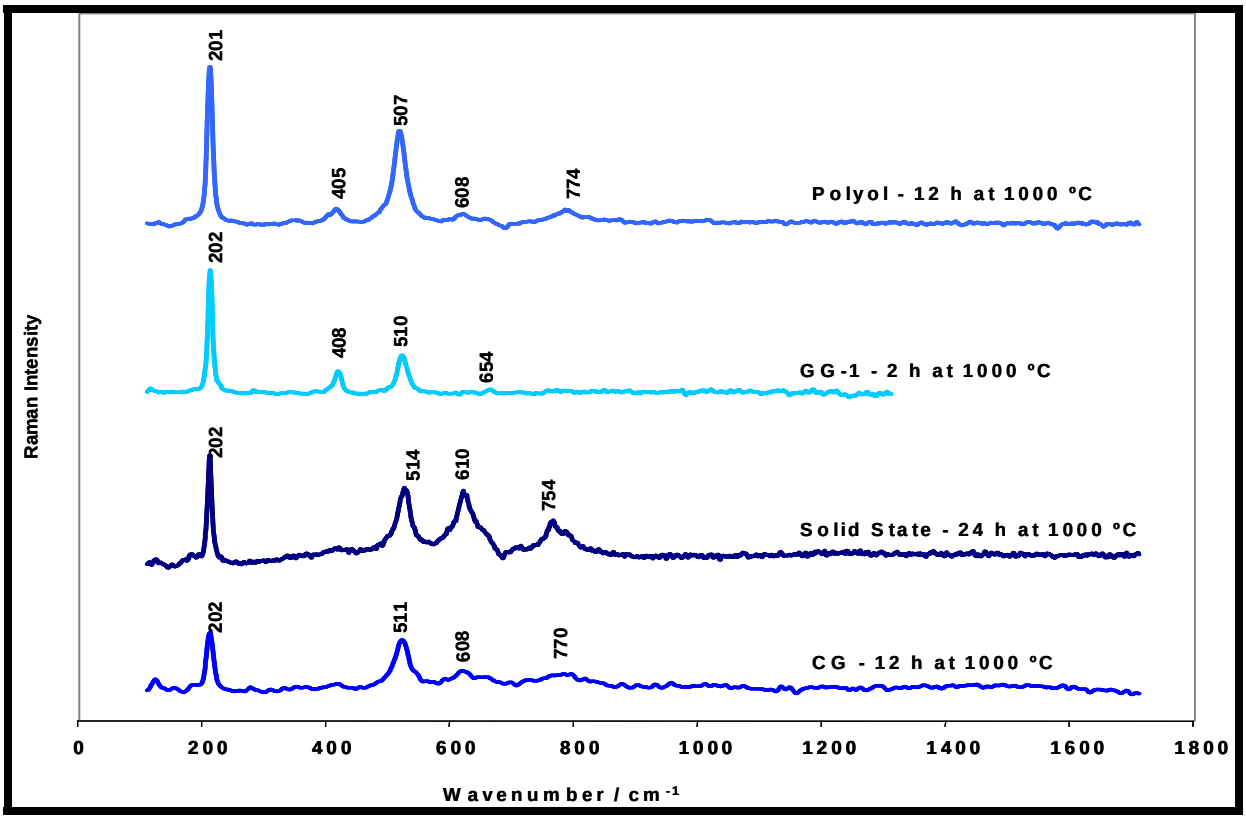

Figure 6-29: Raman spectra of $CoAl_2O_4$ prepared by the polyol, glycine-gel, solid-state, and citrate-gel methods.

Examination of the XRD patterns of the normal spinel samples prepared by various methods in Figure 6-30 shows the presence of the (331) lattice plane in all samples

analysed. This indicates that the normal spinel is the phase obtained by the various synthesis methods at the particular temperatures and processing times. The XRD patterns were found to be less discriminatory to the type of synthesis method used than Raman spectra. Due to the similarity in appearance of the XRD patterns, it is more difficult to differentiate between the various samples. On the other hand, although Raman spectra have an overall similarity with regard to band positions, the various samples can be distinguished from each other due to the notable differences, as previously discussed. Raman spectroscopy is therefore a better discriminator between different synthesis methods.

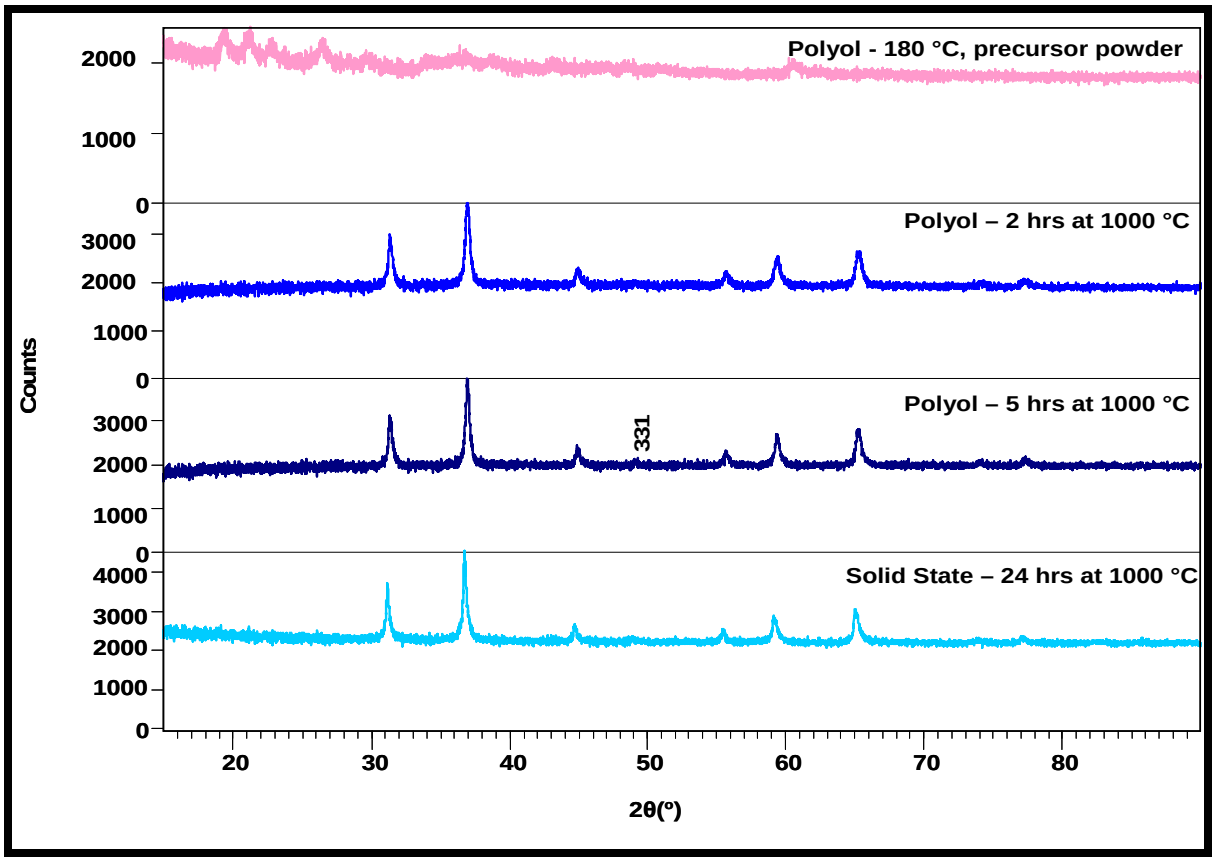

Figure 6-30: XRD patterns of normal $CoAl_2O_4$ prepared by the glycine-gel, solid-state, citrate-gel and polyol methods.

6.4 Comparison of Synthesised $Co^{2+}Co^{3+}_xAl_{2-x}O_4$ (x=0-2) Spinels With Commercially Purchased Blue Pigments

The IR spectra and XRD patterns of four blue commercial pigments purchased from an art shop were compared with those of cobalt blue synthesised by various methods, as outlined in previous sections.

Figure 6-31 shows the mid-IR spectra of commercially purchased blue pigments. Band positions and intensities differ from normal $Co^{2+}Al_2O_4$ spinel as shown earlier in Figure 6-5, indicating that the composition and crystal structure are different. The normal spinel is characterised by the bands at 661, 554 and 502 cm^{-1} (666, 554 and 504 cm^{-1} according to Wang et al.[1]), in the mid-IR region, which is not evident in the spectra of the four commercial samples depicted in Figure 6-31. However, the spectra for Degussa cobalt exhibits the 669 cm^{-1} band assigned to the Co-O vibration, as given in Table 6-6.

The far-IR spectra of the four commercially bought cobalt blue pigments are shown in Figure 6-32. While the normal $Co^{2+}Al_2O_4$ spinel is mainly characterised by a high intensity band at 232 cm^{-1} (Figure 6-6), the spectra of the commercial cobalt blue pigments are characterised by a number of bands in the far-IR region.

This once again indicates that the commercial cobalt blue pigments are different in composition and crystal structure to the synthesized cobalt blue pigments. However, the spectra of Degussa cobalt exhibits the 233 cm^{-1} band assigned to the Co-O vibration, as given in Table 6-6. It would therefore appear that Degussa cobalt contains a mixture of crystalline phases, of which one is the normal $Co^{2+}Al_2O_4$ spinel phase. This is further confirmed by XRD results shown in Table 6-12.

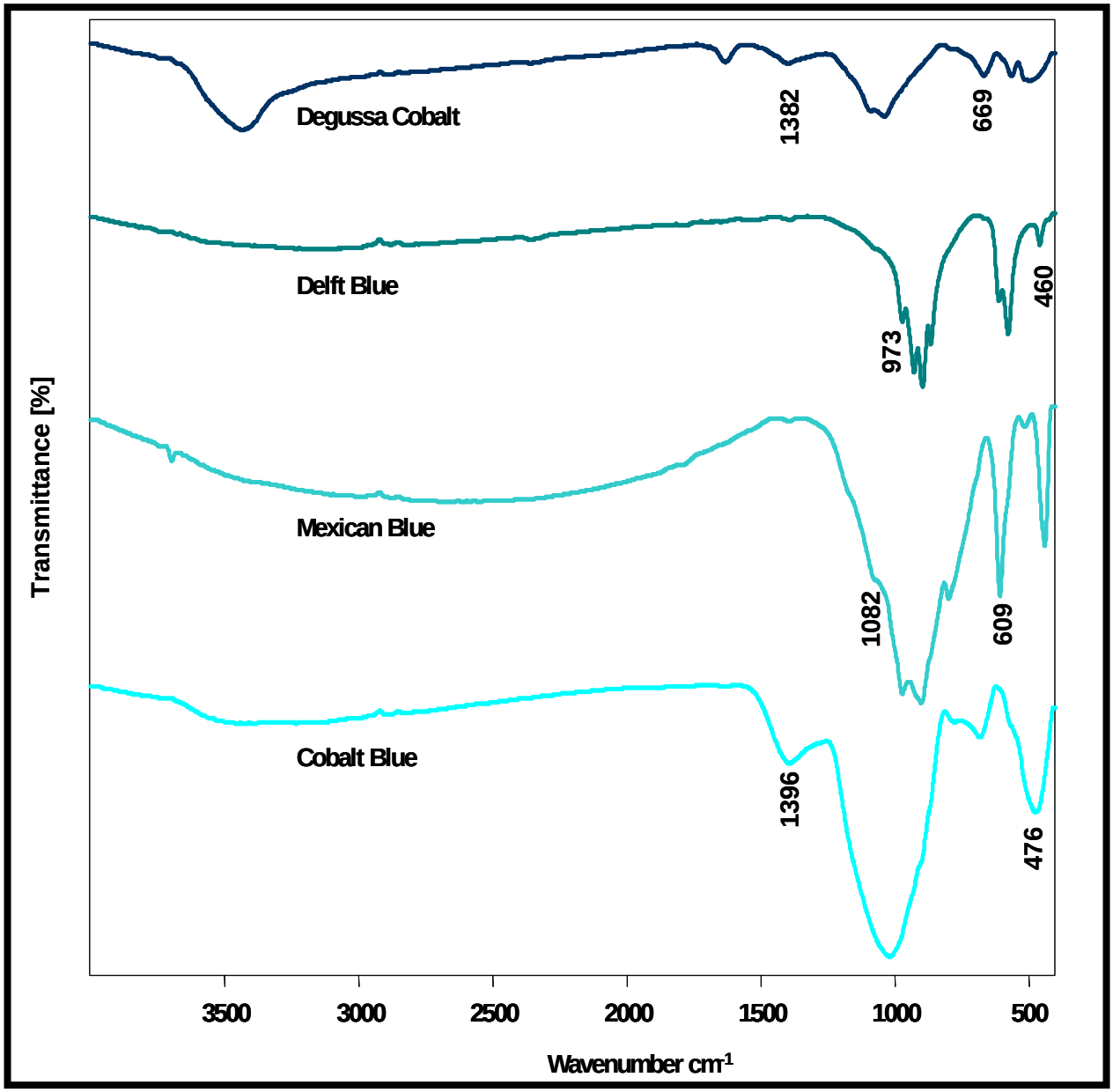

Figure 6-31: Mid-IR spectra of commercial blue pigments purchased from an art store.

Within the mid and far-IR spectra, however, Delft blue and Mexican blue have more similarity with each other, possibly due to sharing similar structures, as do Degussa cobalt and cobalt blue.

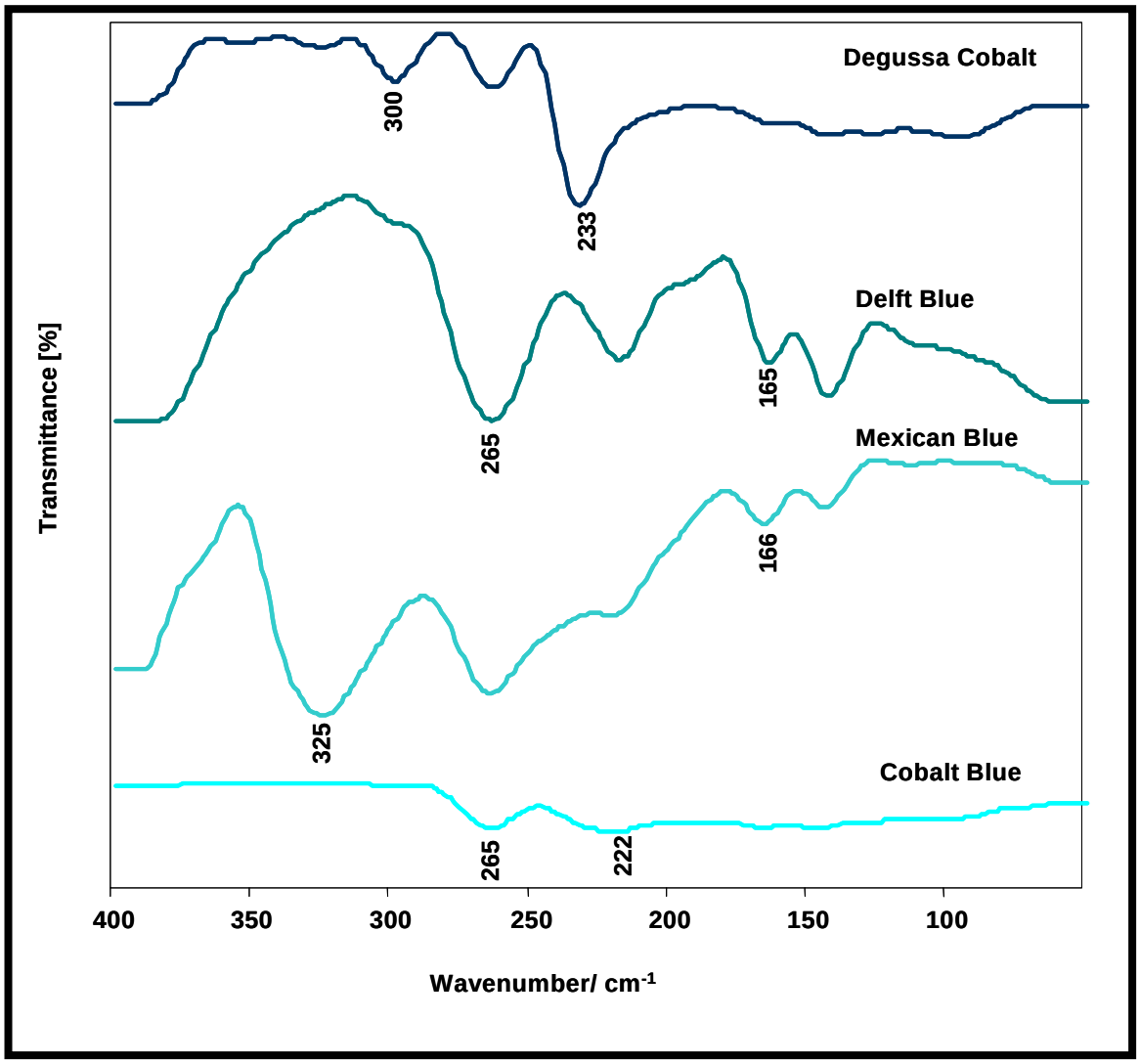

Figure 6-32: Far-IR spectra of commercial blue pigments purchased from an art store.

The XRD patterns of the commercial blue pigments are shown in Figure 6-33. The XRD patterns are different from the XRD patterns of cobalt spinels of the general formula $Co^{2+}Co^{3+}_{x}Al_{2-x}O_4$ (x = 0 - 2), as shown in Figures 6-2 and 6-7.

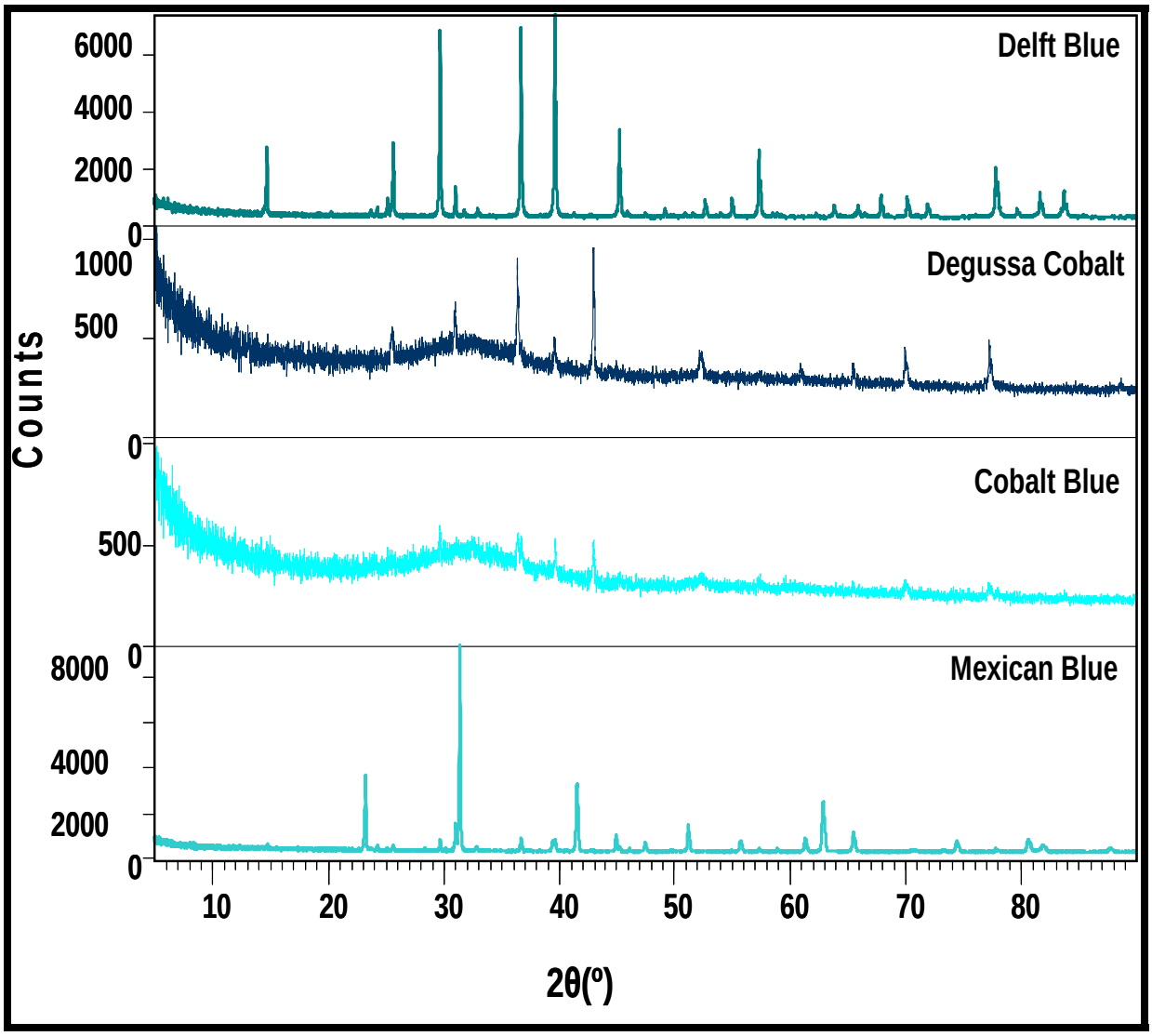

Figure 6-33: XRD patterns of commercial blue pigments.

Table 6-12 depicts the crystal phases present in the commercial blue pigments as determined by EDS and XRD. Upon comparing the XRD patterns with other patterns in the JCPDS library, the presence of more than one crystal phase (including the cubic spinel phase in cobalt blue and Degussa cobalt) and of the presence of elements other than just Co and Al can be observed in all four samples based on EDS results.

On the other hand, the synthesized cobalt blue pigments appear to comprise of only one phase, normal $CoAl_2O_4$ cubic spinel, and contain only the elements Co, Al and O (O is assumed as it is not detectable by EDS). The full list of EDS results for the synthesized cobalt blue pigments and commercial blue pigments can be found in Appendix C.

It can therefore be concluded that the commercial cobalt blue pigments comprise of more than one crystal phase and are not of a similar composition and crystal structure to the cobalt blue pigments as synthesized by various methods in this project.

Table 6-12: Crystal phases present in the commercially purchased blue pigments.

Sample	Crystal phases (XRD)	EDS results
Cobalt Blue, art	$CoAl_2O_4$ spinel; $(Zn,Co)_2SiO_4$ Willemite, cobaltiah	Al, Co, Si, K, Zn, Pb
Degussa Cobalt, art	$CoAl_2O_4$ spinel; SiO_2 Cristobalite	Al, Co, Si, Ca, Zn, Pb
Mexican Blue, art	SiO_2, quartz; $(Zn,Co)_2SiO_4$, Willemite; $Zr(SiO_4)$, zircon	Al, Co, Si, Zn, Mg, Ti, V, K, Zr
Delft Blue, art	SiO_2, quartz; $(Zn,Co)_2SiO_4$, Willemite	Al, Co, Si, Zn

6.5 Synthesis of Cobalt Green ($ZnCo_2O_4$)

Cobalt green was prepared by the polyol method, as detailed in section 5.3. Since it is also a spinel and exhibits a cubic structure with space group *Fd*3*m* (O^7_h)[17,18], the aim was to compare results with those of cobalt blue (normal spinel $CoAl_2O_4$) prepared by the various methods, as detailed in the above sections.

6.5.1 Raman Characterisation

Figure 6-34 presents the Raman spectra of cobalt green before and after annealing above the reflux temperature. During the refluxing stage of preparation, the highest temperature reached was 180 ºC. The powder sample was then heated at various temperatures and time periods in an oven. Before annealing the sample is already crystalline but as the temperature is increased from 180 to 500 ºC a narrowing and an increase in intensity of the Raman bands, as well as a shift in the bands to higher wavenumbers, can be observed. This can be attributed to an increase in particle size and improved crystallinity as mentioned in section 6.2.2.1.

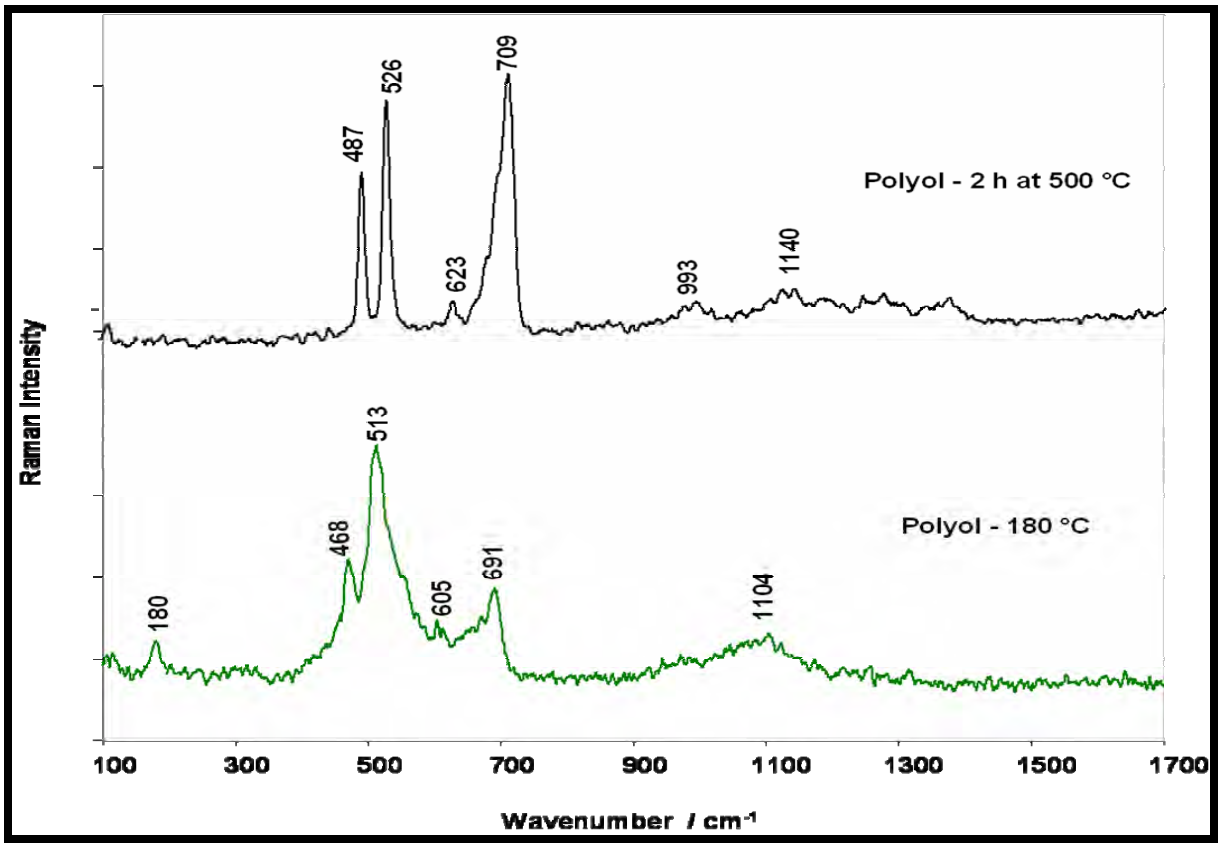

Figure 6-34: Raman spectra of cobalt green ($ZnCo_2O_4$) showing increasing crystallinity and shift of peaks to higher wavenumbers with increased temperature from 180 to 500 ºC.

In Figure 6-35, Raman spectra shows only slight changes between the sample annealed for 2 h at 500 ºC and the sample calcined for 24 h at 1000 ºC. This indicates that the crystallinity of the sample drastically increases when annealed at 500 ºC but further heating to 1000 ºC only leads to a slight increase in crystallinity.

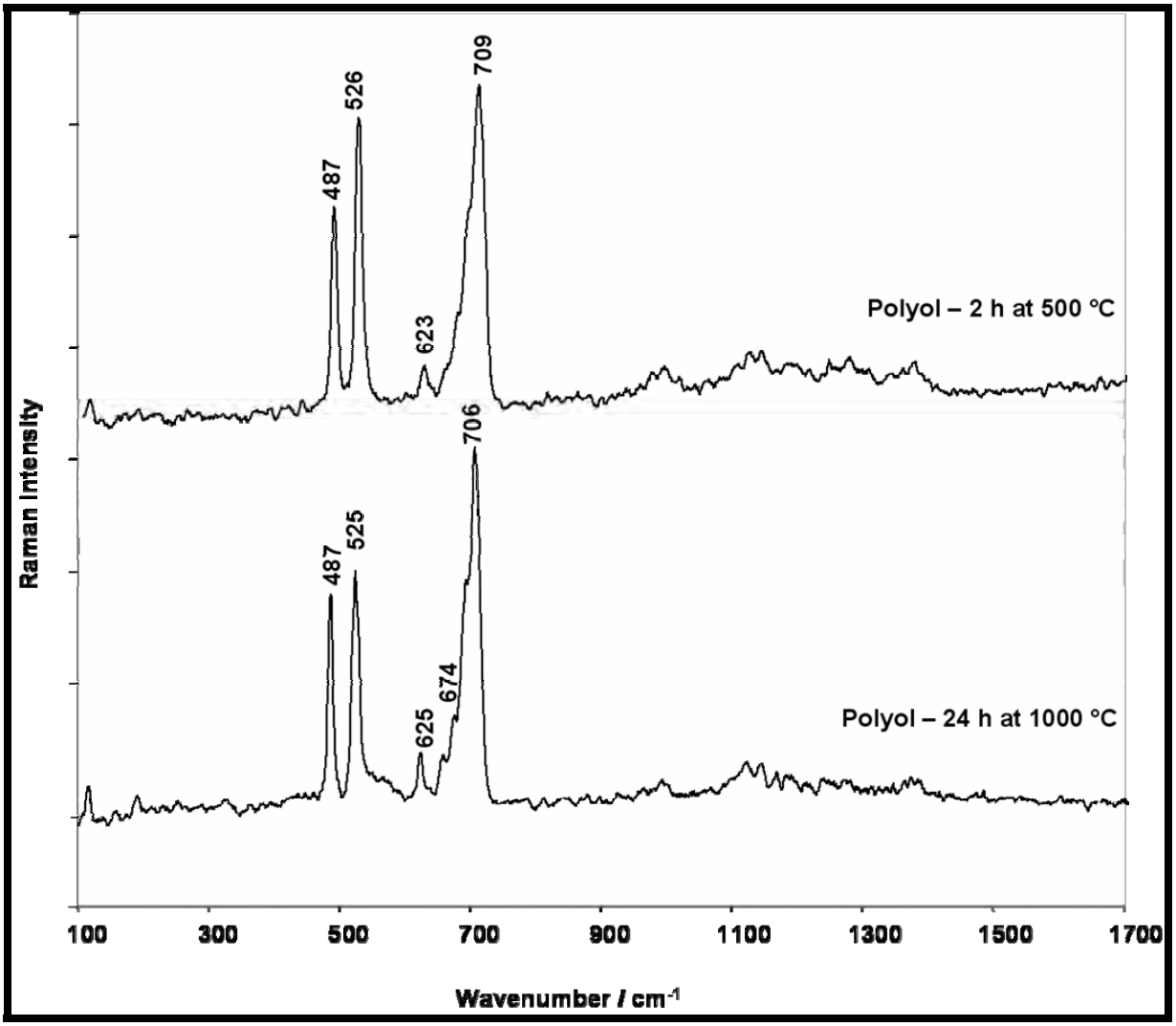

Figure 6-35: Raman spectra of cobalt green ($ZnCo_2O_4$) annealed at various temperatures showing minimal spectral change with increased temperature from 500 to 1000 ºC.

Figure 6-36 compares the Raman spectra of cobalt green ($ZnCo_2O_4$) with cobalt blue samples prepared by the glycine-gel and citrate-gel methods. The cobalt green spinel structure corresponds well with both inverse spinel structures of $Co^{2+}Co^{3+}AlO_4$ (GG-4) prepared by the glycine-gel method and of that prepared by the citrate-gel method (CG - 500 ºC).

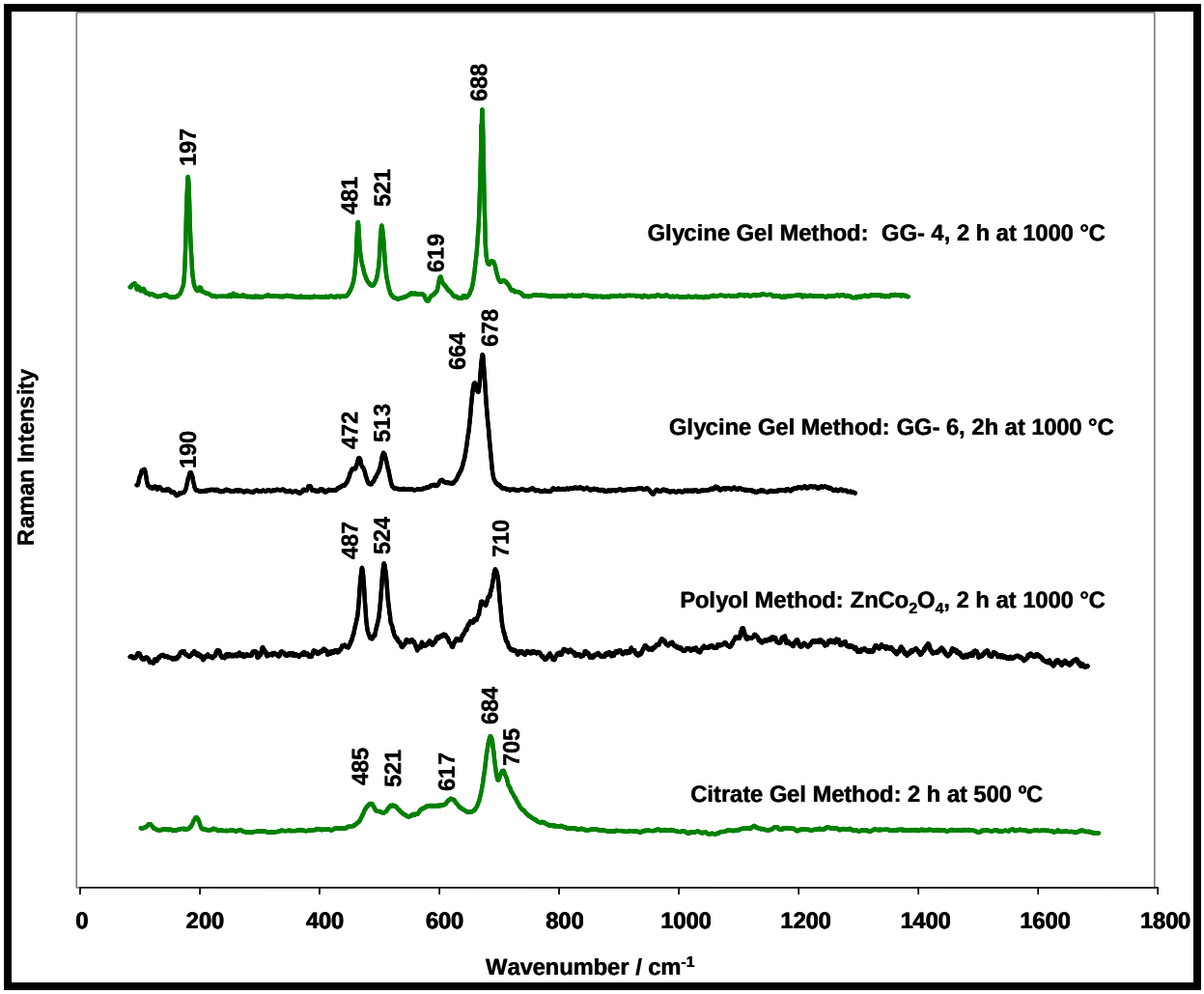

Figure 6-36: Comparison of Raman spectra of cobalt green ($ZnCo_2O_4$) prepared by the polyol method with Co_2AlO_4 (GG-4) and Co_3O_4 (GG-6) prepared by the glycine-gel method and Co_2AlO_4 prepared by the citrate-gel method (2 h at 500 ºC).

6.5.2 FTIR Characterisation

The mid-IR spectra of cobalt green in Figure 6-37 show a shift in band positions and intensity as the sample is calcined for 2 h at 1000 ºC and 24 h at 1000 ºC. As with Raman spectra, there is a more drastic observed change in mid-IR spectra when comparing the spectra of the sample before calcining (180 ºC) to that of the calcined sample (2 h at 1000 ºC) and less of an observed change between the spectra of samples calcined for 2 h at 1000 ºC and for 24 h at 1000 ºC.

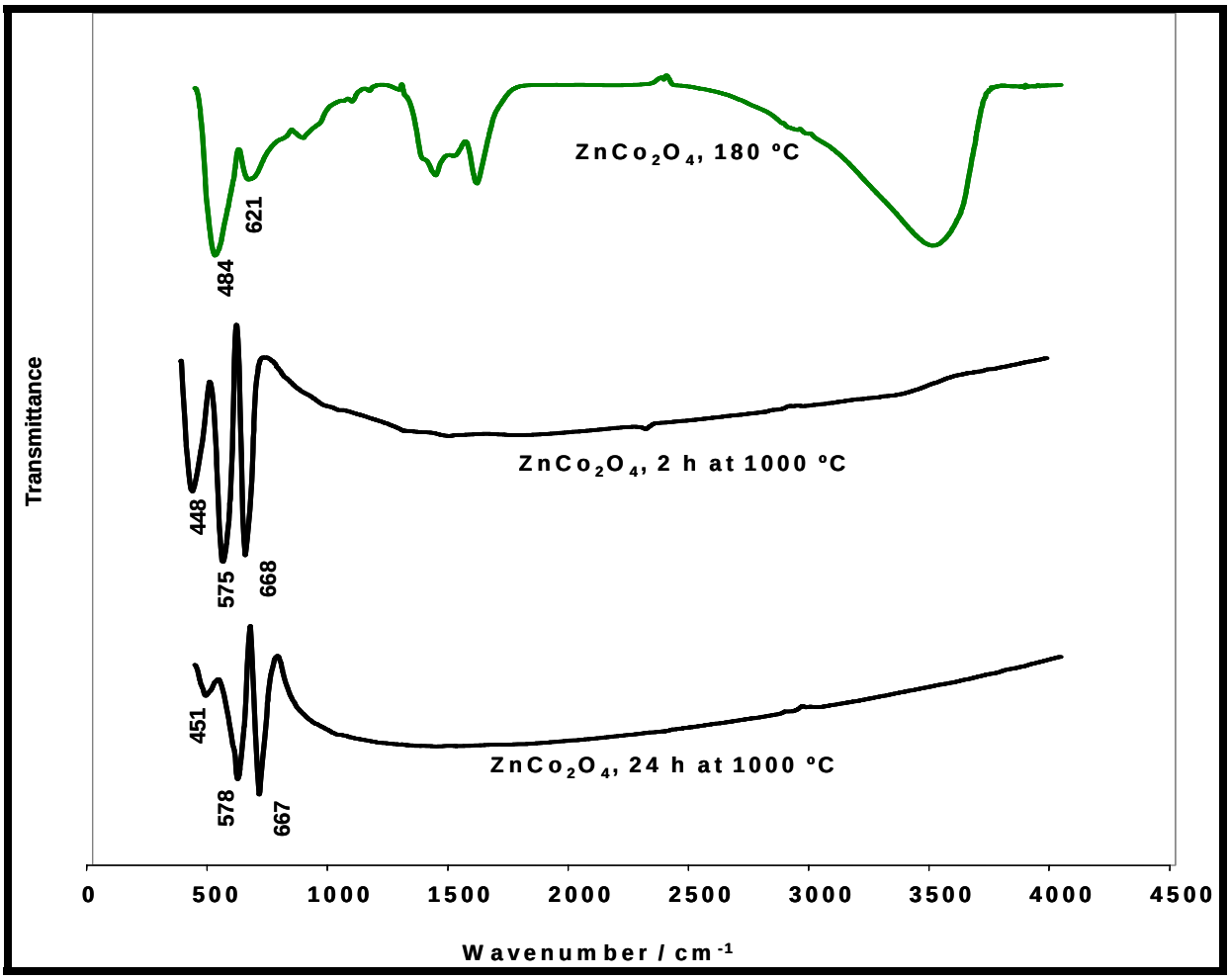

Figure 6-37: Comparison of mid-IR spectra of $ZnCo_2O_4$, prepared by the polyol method, before and after calcining at 1000 °C.

Figure 6-38 compares the mid-IR spectrum of cobalt green ($ZnCo_2O_4$) with that of cobalt blue ($CoAl_2O_4$), also synthesized by the polyol method, to show that both products have a cubic spinel structure.

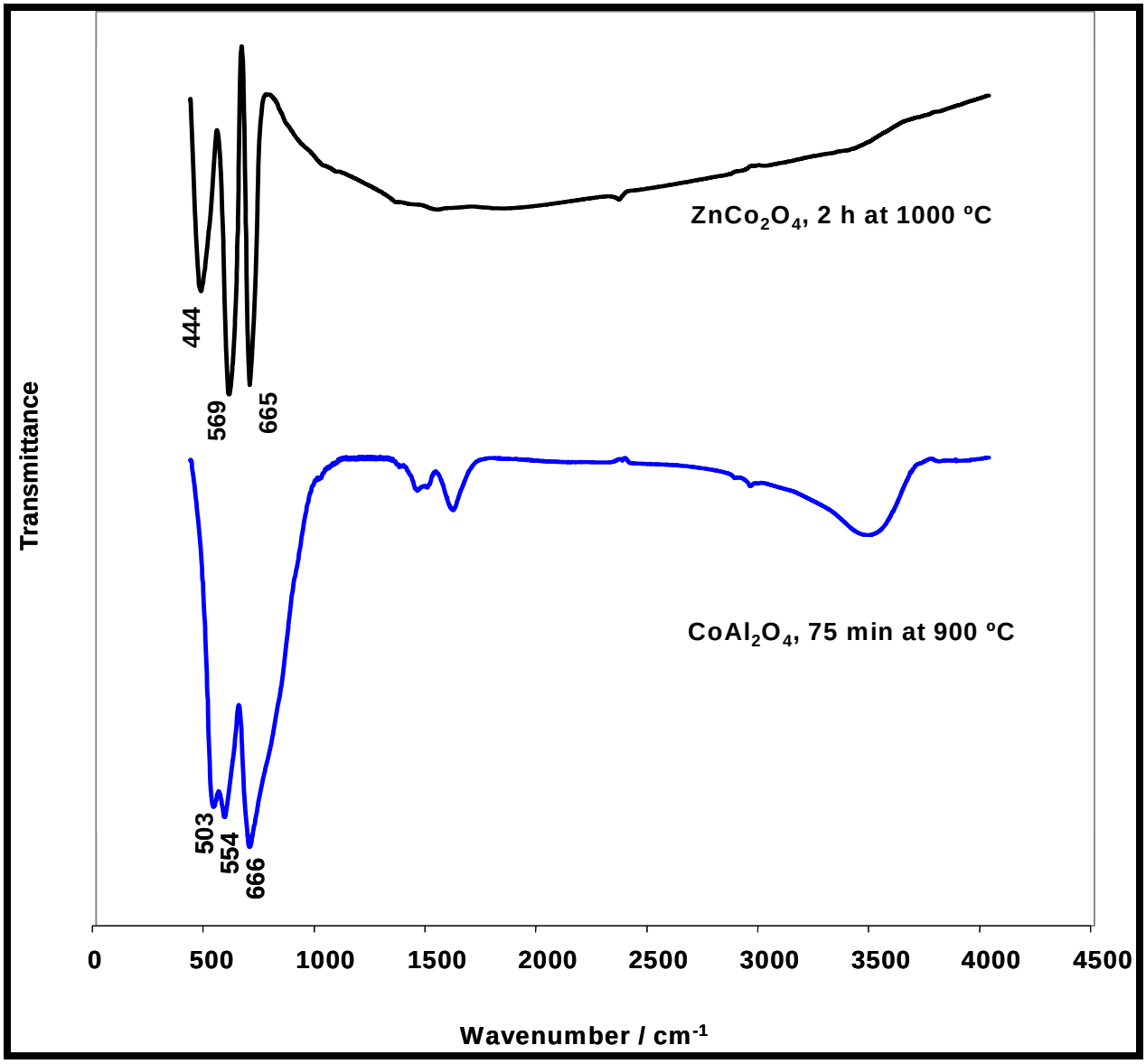

Figure 6-38: Comparison of mid-IR spectra of $ZnCo_2O_4$ and $CoAl_2O_4$ prepared by the polyol method.

6.5.3 XRD Characterisation

XRD results shown in Figure 6-39 confirm that $ZnCo_2O_4$ is already crystalline after refluxing at 180 ºC and the spinel structure is already formed by heat treatment at 500 ºC for 2 h. This differs from normal $CoAl_2O_4$ spinel prepared by the polyol method which was still mainly amorphous at 180 ºC (Figure 6-26, XRD results) and required heat treatment to at least 5 minutes at 1000 °C before the characteristic cubic spinel structure could be observed (Figure 6-23, Raman results).

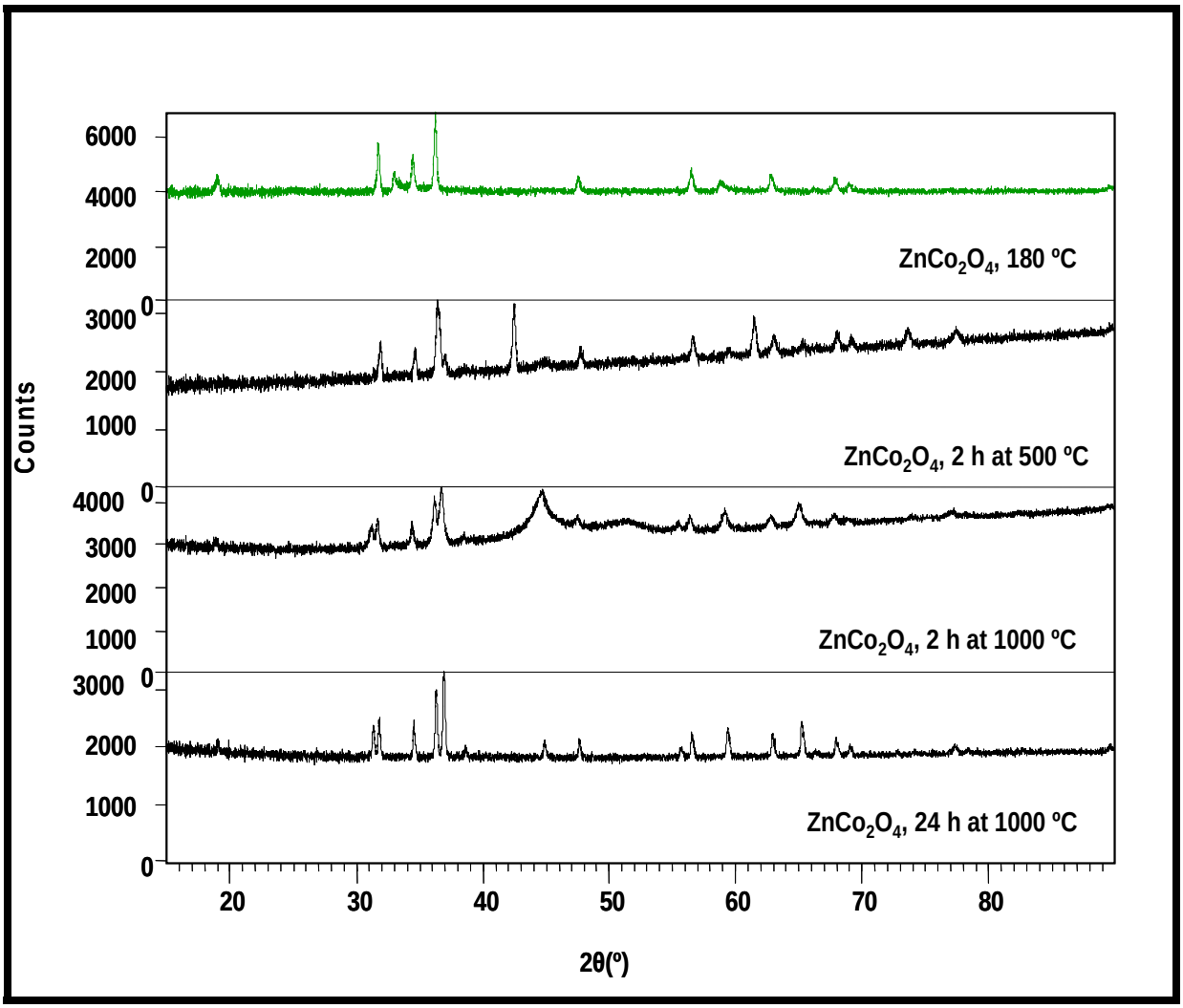

Figure 6-39: XRD patterns of $ZnCo_2O_4$ annealed at various temperatures.

6.5.4 Comparison With Literature

FT-IR and XRD results of the prepared $ZnCo_2O_4$ powder corresponds with findings in literature as reported by X. Wei et al.[17] and X. Niu et al.[18]

No comparable Raman spectra for $ZnCo_2O_4$ were found in literature. However, the Raman spectra of $ZnCo_2O_4$ (polyol - 180 ºC, Fig 6-34) were found to be similar to the Raman spectra of $ZnCr_2O_4$ in the work of Stanojevic et al.[2] In this regard, assignments for Raman- and IR-active vibrational bands for $ZnCo_2O_4$ are depicted in Tables 6-13 and 6-14, respectively. Once again, the five Raman bands are evident as predicted by group theory for spinel oxides of the formula AB_2O_4.

Although no recordings were made for $ZnCo_2O_4$ in the far-IR region, based on results for $ZnCr_2O_4$[2] and those of $CoAl_2O_4$, as discussed in section 6.1.4.2, one can postulate that a band would be present between 200 and 240 cm^{-1}, thereby confirming the four IR-active vibrational bands as predicted by group theory for spinel oxides.

Table 6-13: Raman band assignments for $ZnCo_2O_4$.

Raman (cm^{-1})	Symmetry Species	Assignment
200w	F_{2g}	δ(Zn-O)
487s	E_g	*v* (Co-O) + *v* (Zn-O)
526vs	F_{2g}	*v*(Co-O)
623w	F_{2g}	*v* (Co-O)
709vs	A_{1g}	*v* (Co-O)

vs (very strong), w (weak), m (medium), s (strong), sh (shoulder).

Table 6-14: IR band assignments for $ZnCo_2O_4$.

IR (cm^{-1})	Symmetry Species	Assignment
~200-240	F_{1u} (v4)	δ(O-Co-O)
444	F_{1u}(v3)	*v*(Zn-O)
569	F_{1u}(v2)	*v*(Co-O)
665	F_{1u}(v1)	*v* (Co-O)

6.5.5 Colour of Cobalt Green

The colours of the cobalt green samples prepared by the polyol method and calcined at various temperatures are shown in Figure 6-40. The colour changed from green to black as the temperature was increased from 180 ºC to 1000 ºC. Highly agglomerated particles were characteristic of the sample heated for 24 h at 1000 ºC and these presented themselves as specks in the KBr pellet used to show differences in colour.

A similar argument used in section 6.1.7 with regard to the colour of the samples can be used here as well. It has been shown that the final colour is affected by the ratio of A/B ions, the temperature of preparation as well as the host lattice and coordination site and number of the cobalt ion.

As discussed above, cobalt green prepared by the polyol method was also of a spinel structure. In comparison to cobalt blue (normal spinel $CoAl_2O_4$), cobalt green was crystalline at 180 ºC with crystallinity increasing when heated for 2 h at 500 ºC. Therefore, spinel $ZnCo_2O_4$ can be prepared at relatively low temperatures compared to any of the preparation methods used to prepare spinel $CoAl_2O_4$.

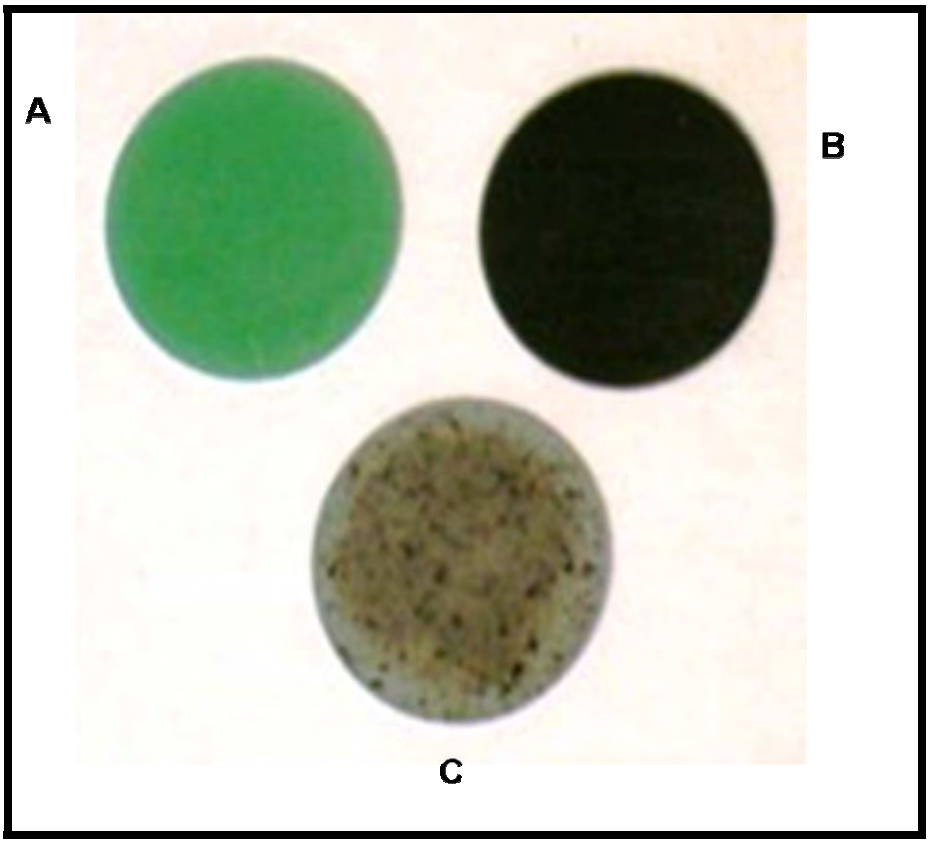

Figure 6-40: KBr pellets showing colours of various cobalt green samples prepared at different temperatures; (A) 180 ºC, (B) 2 h at 1000 ºC, (C) 24 h at 1000 ºC.

6.6 References

1. C. Wang, S. Liu, L. Liu, X. Bai, *Mater. Chem. Phys.,* 2006, **96**, 361-370.
2. Z.V. Marinković Stanojević, N. Romčević, B. Stojanović, *J. Eur. Ceram. Soc.*, 2007, **27**, 903–907.
3. D. de Waal, *Asian Chem. Lett.*, 2004, **8**, 57-63.
4. B. Jongsomjit, J. Panpranot, J. G. Goodwin, *J. Catal.,* 2001, **204**, 98-109
5. Raman Spectroscopic Library of Natural and Synthetic Pigments

Ian M. Bell, Robin J.H. Clark and Peter J. Gibbs *http://www.chem.ucl.ac.uk/resources/raman/pigfiles/cobaltbl.html (Accessed on November 07, 2008).*

6. D. de Waal, *J. Raman Spectrosc.* 2004, **35**, 646–649.
7. L. D. Kock, D. De Waal, *J. Raman Spectrosc.* 2007, **38**, 1480–1487.
8. N. Ouahdi, S. Guillemet, J.J. Demai, B. Durand, L. Er Rakho, R. Moussa, A. Samdi, *Mater. Lett.,* 2005, **59**, 334-340.
9. M. Zayat, D. Levy, *Chem. Mater.* 2000, **12**, 2763-2769.
10. G. Carta, M. Casarin, N. El Habra, M. Natali, G. Rossetto, C. Sada, E. Tondello, P. Zanella, *Electrochim. Acta,* 2005, **50**, 4592–4599.
11. Woo-Seok Cho, M. Kakihana, *J. Alloys Compd,* 1999, **287**, 87-90.
12. D. C. Paine, C. Caragianis, T. Y. Kim, and Y. Shigesatoa, T. lshahara, *Appl. Phys. Lett.,* 1993, **62**, 2842-2844.
13. L. Poul, S. Ammar, N. Jouini. And F. Fievet, F. Villain, *J. Sol-gel Sci. Techn.,* 2003, **26**, 261-265.
14. W.M. Shaheen, M.M. Selim, *Int. J. Inorg. Mater.,* 2001, **3**, 417–425.
15. S. Hayashi, M. Ito, H. Kanamori, *Solid-state Commun.,* 1982, **44**, 75-79.
16. T. Mimani, S.Ghosh, *Curr. Sci.*, 2000, **78**, 892-896.
17. X. Wei, D. Chen, W. Tang, *Mater. Chem. Phys.,* 2007, **103**, 54-58.
18. Xinshu Niu, Weiping Du, Weimin Du, *Sensor. Actuat. B-Chem,* 2004, **99**, 405–409.

CHAPTER 7

Conclusion

7.1 Summary

Crystalline spinels of the general formula $Co^{2+}Co^{3+}_{x}Al_{2-x}O_4$ (where x = 0-2) were prepared by four different methods and characterised by Raman, XRD, FT-IR, SEM and EDS techniques. The different processing times and processing temperatures based on the various methods of preparation gave crystalline products with different morphological, structural, and compositional properties including colouration and particle size. The temperature at which the blue $CoAl_2O_4$ normal spinel starts to form was determined by the type and ratio of the precursors used as well as the annealing temperature. The inverse Co_2AlO_4 spinel was identified as an intermediate as well as a final product. The colour of the crystalline powders prepared in this work was found to be closely linked to the degree of inversion and crystallinity of the powders.

7.2 Preparation Methods

While the four preparation methods used, i.e. solid-state, glycine-gel, citrate-gel, and polyol, complemented each other with regard to the characteristics of the intermediate and final products, they each also provided a unique perspective to the understanding of the development of both the normal and inverse cobalt aluminate spinels.

The more traditional solid-state method required a long processing time (24 h) and high temperature (1000 ºC) for the formation of the normal $Co^{2+}Al_2O_4$ spinel. However, the resulting spinel was highly crystalline and of the characteristic bright blue colour.

The targeted synthesis of $Co^{2+}Al_2O_4$ (normal spinel), $Co^{2+}Co^{3+}AlO_4$ (inverse spinel) and $Co^{2+}Co^{3+}{}_2O_4$ (cobalt oxide spinel) was achieved with the glycine-gel method by

carefully weighing the reagents to have specific Co/Al ratios. The various precursor gels with different Co/Al ratios were then annealed in air at the same temperature (2 h at 1000 ºC). Results indicated that increasing the Co content in the precursors improved the degree of crystallinity and produced a change in the colour of the final powders. Both the normal and inverse spinels were identified by their unique features, observed with Raman, FT-IR spectroscopy, and XRD.

Unlike the glycine-gel method, one stock of precursor gel made from reagents with only one Co/Al ratio was used for the citrate-gel method. Different portions of the gel were annealed at different temperatures (350 - 1000 ºC for 2 h), resulting in the normal, inverse and cobalt oxide spinels. The citrate-gel method allowed for a reduction of the calcination temperature of the normal spinel to between 700 and 800 ºC. The inverse spinel phase was observed as a transitional phase at temperatures below 500 ºC, while the normal spinel was observed above 800 ºC. The citrate-gel method was therefore useful in observing the structural changes that accompany the formation of the normal spinel.

Normal $CoAl_2O_4$ and $ZnCo_2O_4$ spinels were prepared with the polyol method which involved a refluxing stage and annealing the precursors in air at varying temperatures and time periods. While $ZnCo_2O_4$ was found to be crystalline directly after the refluxing stage (180 - 240 ºC), further heating of the powder material was necessary for $Co^{2+}Al_2O_4$. The temperature at which the normal $CoAl_2O_4$ spinel started forming was also found to be around 700 ºC. The polyol method was also useful in observing the structural changes involved during the formation of the normal $CoAl_2O_4$ spinel.

The glycine-gel method gave the best demonstration of the effect of stoichiometry on the colouration of the final powders. Samples with a Co/Al ratio of 0.5 were blue (GG-1), those with a Co/Al ratio >0.5 were green (GG-2, 3 and 4), and those with Co/Al ratios >2.5 were black (GG-5 and GG-6).

The polyol and citrate-gel methods best demonstrated the effect of annealing temperature on the colouration of the final powders. From the polyol method, samples heated to 600 ºC exhibited a dark green colouration, changing progressively to bright-blue as the temperature was increased to 1000 ºC. For the citrate-gel method samples heated below the temperature of formation of the blue $CoAl_2O_4$ phase (800 ºC), showed the same dark green colouration of cobalt-rich samples as in the glycine gel method. At 800 ºC, the powder turned blue which is characteristic of Co^{2+} in the tetrahedral coordination.[1] It can therefore be concluded that for $Co^{2+}Co^{3+}_xAl_{2-x}O_4$ spinels (where x = 0 - 2), a black or green colour indicates either the formation of Co_3O_4 or Co_2AlO_4 (inverse spinel), while a blue colour indicates the formation of $CoAl_2O_4$ (normal spinel).

7.3 Characterisation Methods

By observing Raman and FT-IR spectra and XRD patterns for various $Co^{2+}Co^{3+}_xAl_{2-x}O_4$ spinels (where x = 0 - 2), the structures of the intermediate and final products were found to be strongly dependent on the annealing temperature, the Co/Al ratio in the precursors and the sample preparation methods. Through Raman and FT-IR, the vibrational modes and their assignments for the spinels was determined. High frequency bands (above 600 cm^{-1}) are normally associated with vibrational stretching modes of the octahedral cations Al-O, while low frequency bands (below 300 cm^{-1}) are normally assigned to the vibrational modes of tetrahedral cations Co-O. Due to various factors including the ordering of the cations on tetrahedral and octahedral sites, a breakdown in the Raman and IR selection rules can be observed in the spectra. Although group theory predicts five Raman- and four IR-active bands for the normal and inverse spinels, the breakdown in the Raman and IR rules can be observed with the eight Raman- and only three IR-active bands for the inverse spinel.

7.3.1 Raman Spectroscopy

A variation in the crystal structures of the final products due to a change in Co/Al ratio (glycine-gel method) as well due to the annealing temperature and processing time (citrate-gel and polyol methods) can be observed in Raman spectra. Raman band positions and intensities shift and become narrower (lower FWHM) with increasing temperature and/or annealing time. Vibrational bands can also be assigned, thus aiding in pinpointing the temperature at which a particular phase forms. For instance, in the citrate-gel method, a vast change in Raman spectra is observed between samples heated at 700 ºC and those heated at 800 ºC. From this, it can be concluded that the transition temperature of the change in crystal structure from inverse spinel to normal spinel lies between 700 - 800 ºC. By further analysis of Raman spectra, normal and inverse spinel can be distinguished from each other mainly by the presence of the 408 cm^{-1} and 511 cm^{-1} bands in the normal spinel (due to Al-O and Co-O vibrations respectively) and the presence of 481 cm^{-1} and 688 cm^{-1} band in inverse spinel (due to Al-O and Co-O vibrations respectively). The inverse and Co_3O_4 spinel can be distinguished from each other mainly by the higher intensity 197 cm^{-1} band in the former (due to Co-O vibration). There also appears to be an overall shift of bands to lower wavenumbers for the Co_3O_4 spinel e.g. 481 cm^{-1} → 476 cm^{-1}.

7.3.2 FT-IR Spectroscopy

FT-IR spectra were useful in revealing the absence of precursors in the final products. In addition, mid-IR spectra could distinguish between normal ($CoAl_2O_4$) and inverse (Co_2AlO_4) spinels prepared by the glycine-gel method due to the three characteristic normal spinel bands at 661, 554 and 502 cm^{-1}. However, it was more difficult to distinguish between Co_3O_4 and inverse spinel due to the similarity of their IR absorption bands (663 and 570 cm^{-1} for Co_3O_4, 669 and 569 cm^{-1} for Co_2AlO_4). The 663 and 570 cm^{-1} absorption bands are characteristic for the Co_3O_4 spinel. The same applied for the far-IR region where normal spinel could be distinguished from both the inverse spinel and Co_3O_4 spinel by the IR absorption band at 232 cm^{-1} but the inverse

and Co_3O_4 spinels could not be distinguished from each other due to the similar IR absorption bands (216 and 214 cm^{-1} respectively).

Results from the polyol method also indicate FT-IR spectra typical for normal $CoAl_2O_4$. An increase in crystallinity and change in structure from Co_2AlO_4 and Co_3O_4 to $CoAl_2O_4$ was indicated by the shift in band positions and higher band resolution. A combination of both the normal and inverse spinel is evident at 700 ºC (667, 554 and 504 cm^{-1}) while vibrational bands sharpen and slightly shift with increased time period at a specific temperature. The typical normal spinel structure, with vibrational bands at 675, 554 and 508 cm^{-1}, is observed at 1000 ºC. These observed changes in spectra confirm the progressive reduction of the degree of inversion in the spinel structure upon annealing.

7.3.3 XRD

XRD patterns of $CoAl_2O_4$, Co_3O_4 and Co_2AlO_4, on the other hand, all show similar diffraction patterns due to their similar spinel cubic structure (*Fd3m*). Only the difference in intensities of a few critical peak positions help in differentiating between the inverse and normal spinel. For instance in the citrate-gel method it has been shown that an increase in temperature leads to a decrease in the intensity of lattice peak (111) which is assigned to the Co_3O_4 and Co_2AlO_4 spinels. For the glycine-gel method the (111), (222) and (531) lattice peaks only occur in the Co_3O_4 and Co_2AlO_4 spinels with their highest intensity in the Co_3O_4 spinel. In the citrate-gel method, the formation of $CoAl_2O_4$ (2 h at 1000 ºC) is denoted by the appearance of the lattice peak (331) which is specific to the normal spinel in which Co^{2+} ions are in tetrahedral positions, with Al^{3+} ions in octahedral ones. Distinguishing between Co_3O_4 and the inverse spinel requires extra scrutiny because they share similar diffraction patterns differing only in intensity. In the glycine-gel method, the lattice peak (331) is observed in both the normal and inverse spinels but is of higher intensity in the normal spinel.

As in Raman spectra, when annealing temperature, time and Co/Al ratio was increased, crystallinity and particle size also increased leading to peaks having a lower FWHM and higher intensity. For the glycine-gel method, narrower diffraction lines and lower unit cell parameters were observed for samples with a higher Co/Al ratio i.e. Co_2AlO_4 and Co_3O_4.

7.4 Blue Cobalt Aluminate Spinel

Comparison of Raman and FT-IR spectra and XRD patterns of blue cobalt aluminate powders (normal spinel) prepared by various methods and annealed to 1000 ºC reveals similarities with regards to band positions and intensities. The similarities, however, are more apparent within certain preparation methods and annealing times. For instance certain methods result in strong bands above 600 cm^{-1} (solid-state and citrate-gel) while others only have weak bands in the same region (polyol and glycine-gel). All, however, contain the ~200, ~408, ~510 cm^{-1} bands characteristic of normal cobalt aluminate spinel.

All XRD patterns of the samples from the different methods of preparation and calcined at 1000 ºC reveal the presence of the (331) lattice plane which indicates the normal cobalt aluminate spinel.

Comparison of Raman and FT-IR spectra and XRD patterns of the synthesized powders with those of commercially purchased samples (and from literature) confirm the synthesis of either $CoAl_2O_4$ (normal), Co_2AlO_4 (inverse), and Co_3O_4 (cobalt oxide) spinels.

Mid- and far-IR spectra of commercially purchased blue pigments (art samples) differ in band positions and intensities from the normal cobalt aluminate spinel indicating that not all blue pigments are made purely from a combination of cobalt and aluminium. This is further confirmed by EDS and XRD which shows the presence of many crystalline phases and elements in the commercially purchased blue pigments

unlike the synthesized blue pigments which comprise of only one phase, $CoAl_2O_4$ spinel, and contain only the elements Co, and Al.

7.5 Cobalt Green Spinel

Comparison of Raman, FT-IR spectra and XRD patterns reveal that the as-prepared $ZnCo_2O_4$ (cobalt green) is already crystalline at 180 ºC and the spinel structure is formed by 500 ºC. Raman and mid-IR spectra show a more drastic shift in band positions and relative intensities as the sample is heated from 180 ºC to 2 h at 1000 ºC than when it is heated from 2 h at 1000 ºC to 24 h at 1000 ºC.

The mid-IR spectrum of cobalt green ($ZnCo_2O_4$) compares well with that of cobalt blue ($CoAl_2O_4$), synthesized by the polyol method, indicating that both products have a spinel structure.

Comparison of the Raman spectra of cobalt green ($ZnCo_2O_4$) with that of cobalt aluminate samples prepared by the glycine-gel and citrate-gel methods reveals a strong similarity with both inverse spinel structures of Co_2AlO_4 (GG-4) prepared by the glycine-gel method and of that prepared by the citrate-gel method (CG-500 ºC).

The colour of cobalt green samples changed from green to black when annealed at 500 and 1000 ºC.

7.6 Final Comments and Conclusions

Ultimately, all preparation methods employed resulted in blue, crystalline cobalt aluminate ($Co^{2+}Al_2O_4$) with a normal spinel structure. However, each method provided specific insight with respect to the morphology, structure, and composition of the blue cobalt aluminate and its process of formation. For directly making any of the crystalline powders in the series $Co^{2+}Co^{3+}_xAl_{2-x}O_4$ (where x = 0-2), the glycine gel method is most suitable. In order to follow the formation of $Co^{2+}Al_2O_4$ through its

various stages, the citrate-gel and polyol methods are most suitable. In both the citrate-gel and polyol methods, the normal spinel phase starts to form between 700 and 800 ºC and the typical spinel structure is evident at 1000 ºC. For the glycine-gel and citrate-gel methods, the typical normal spinel structure is observed when the precursor gels are heated for 2 h at 1000 ºC. In all preparation methods, crystallinity improved with increased annealing temperature or processing time and well-defined crystal structures of the powders was most evident after annealing at 1000 ºC.

Therefore, based on the experimental parameters set for this work, the polyol method provided the shortest processing time (5 min at 1000 ºC) in attaining the normal spinel phase and the smallest particle size. In fact, the normal spinel phase started forming at 700 ºC. However, it is worth pointing out that the processing times and temperatures for the glycine-gel and citrate-gel methods were based on the relevant references from which they were obtained and shorter processing times were not investigated during the course of this work. The characterisation techniques used i.e. Raman, FT-IR, XRD, and SEM complemented each other with information on the crystal structure of the products. Raman and FT-IR were the best at distinguishing between the crystal structure of the three phases (normal, inverse and Co_3O_4) while FT-IR was also good at showing the 'purity' of the samples. XRD patterns of the various spinels were mostly similar to each other. For XRD and FT-IR, it was harder to distinguish between the inverse and Co_3O_4 spinel but Raman could distinguish between the three phases. The results of the prepared powders were compared with literature and from commercially bought samples to confirm their identity. Raman and Far-IR techniques were employed to a greater (and sometimes new) effect in this research project than has been previously done by any research group for the characterisation of cobalt aluminate and zinc cobalt oxide spinels.

The selection of the preparation method should be based on the desired properties of the final powder related to its applicability and whether the inverse ($Co^{2+}Co^{3+}{}_2AlO_4$), normal ($Co^{2+}Al_2O_4$) or oxide ($Co^{2+}Co^{3+}{}_2O_4$) spinels are desired. In order to get a more complete picture of the properties of the final powder, at least two characterisation

methods should be used preferably employing a combination of vibrational spectroscopy and diffraction techniques.

7.7 Suggestions for Further Work

In order to fully understand the effect of each of the preparation methods used on the structural properties of the final product, there is need to characterise the precursor powders or gels at similar temperatures and processing times across a wider spectrum so as to compare 'apples with apples'. For instance, while different temperatures were investigated for the citrate-gel method, this was not done for the glycine-gel method and a different set of temperatures was investigated for the polyol method. This can better pinpoint the optimum conditions for the production of the normal and inverse spinels based on a given set of experimental conditions.

Within each preparation method, there are further aspects to be investigated. For instance, in the polyol method, the concentration of precursors, amount of water added, the refluxing temperature, annealing temperature and processing time, could all be adjusted to produce powders of different structural properties and sizes. This would be ideal in tailor-making a mixed oxide spinel of a specific size. The properties of the various powders at different annealing temperatures and processing times could then be investigated and the optimum experimental conditions for the formation of blue cobalt aluminate or zinc cobalt oxide recommended. In addition, zinc cobalt oxide could be further characterised by far-IR and its development process tracked as per cobalt aluminate.

The ratio of Co/Al in the precursors leading to specific types of spinels was investigated for the glycine-gel method but an understanding of the effect of processing time and temperature on the precursor-gel is lacking. This can be further investigated to identify the conditions at which the specific spinel starts to form or is completely formed. All investigations were conducted for 2 h at 1000 ºC but lower

temperatures were not investigated and the products not characterised by Raman spectroscopy.

For the citrate-gel method, further characterisation by FT-IR would shed more light as to the findings of XRD and Raman techniques.

A more in-depth study of the particle size of the various powders prepared could be done in order to confirm which experimental conditions produce the smallest particle.

In addition, further investigation into the role of CoO and Al_2O_3 as intermediate products and their presence (or absence) in the final powder could shed light onto the process of formation of the normal and inverse cobalt aluminate spinels.

7.8 References

1. T. Mimani, S.Ghosh, *Curr. Sci.*, 2000, **78**, 892-896.

APPENDIX A

Chemicals Used

CHEMICAL	GRADE	MANUFACTURER	PURITY
Aluminium acetate, basic $(CH_3CO_2)AlOH$	R&D use	Aldrich	-
Aluminium nitrate $Al(NO_3)_3.9H_2O$	uniLAB	Saarchem	98%
Aluminium oxide 90 Al_2O_3	-	Merck	-
Cobaltous nitrate $Co(NO_3)_2.6H_2O$	univAR	Saarchem/Merck	98%
Cobaltous sulphate $CoSO_4.7H_2O$	univAR	Saarchem	99%
Cobaltous acetate $(CH_3COO)_2Co.4H_2O$	univAR	Saarchem	99%
Zinc oxide ZnO	uniLAB	Saarchem/Merck	99%
Zinc acetate $(CH_3COO)_2Zn.2H_2O$	univAR	Saarchem/Merck	99%
Zinc sulphate $ZnSO_4.7H_2O$	AR	Holpro Lovasz	-
Glycine H_2NCH_2COOH	AR	Associated Chemical Enterprises	99%
Citric acid $C_6H_8O_7.H_2O$	AR	Associated Chemical Enterprises	99.7%
Diethylene glycol $(CH_2.OHCH_2)_2O$	uniLAB	Saarchem/Merck	99.7%
Ethylene glycol $CH_2(OH)CH_2OH$	GPR	BDH	99%

Cobalt (II,III) oxide, nanopowder 99.8% Co_3O_4	R&D use	Aldrich	-
Cobalt (II,III) oxide, <10 micron Co_3O_4	R&D use	Aldrich	-
Cobalt (II) oxide, -325 mesh CoO	R&D use	Aldrich	-
Commercial cobalt oxide pigment	-	University of Pretoria	-
Commercial cobalt blue pigment,*45710 kobaltblau mittel deckend*[19]	-	*Farbmühle Kraemer,* Germany[19]	-
Cobalt oxilate, cobalt carbonate, cobalt blue, delft blue, Mexican blue, cobalt oxide, degussa cobalt	Art samples	The Clay Pot	-

Calcinations were carried out in a muffle furnace in air at varying temperatures and processing times.

APPENDIX B

Colour of powder samples prepared by various methods

A. Polyol Method

Sample	Time (h)	Temperature ºC	Colour
$CoAl_2O_4$ Precursor	3	140-180	Pink
$CoAl_2O_4$	0.50	600	Green
	1.15	600	Green
	3	600	Green
	7	600	Green
	24	600	Green
$CoAl_2O_4$	0.50	700	Green
	1.15	700	Green
	2	700	Green
	12	700	Blue-Green
	24	700	Blue-Green
$CoAl_2O_4$	1.15	800	Blue
	3	800	Blue
	4	800	Blue
	6	800	Blue
$CoAl_2O_4$	1.15	900	Blue
	2	900	Blue
	3	900	Blue
	6	900	Blue

$CoAl_2O_4$	5mins	1000	Dark blue
	15mins	1000	Dark blue
	1.15	1000	Blue
	2	1000	Bright blue
	5	1000	Bright blue
$ZnCo_2O_4$ Precursor	4	140-180	Lime green
$ZnCo_2O_4$	2	500	Black
	2	1000	Black
	24	1000	Black

B. Citrate-gel Method

Sample	**Time (h)**	**Temperature ºC**	**Colour**
$CoAl_2O_4$ Precursor	8	250	Brown
$CoAl_2O_4$	2	350	Black/green
	2	400	Green
	2	500	Green
	2	600	Greenish-black
	2	700	Blue-green/ green
	2	800	Blue
	2	900	Blue
	2	1000	Blue

C. Glycine-gel Method

Sample	Time (h)	Temperature ºC	Colour
Precursor	8	1000	Brown
1	2	1000	Dull blue
2	2	1000	Brighter green
3	2	1000	Duller green
4	2	1000	Duller green/ black
5	2	1000	Greenish-black
6	2	1000	Ash Black

D. Solid-state Method

Sample	Time (h)	Temperature ºC	Colour
SS-1,2,3	24	1000	Bright Blue

APPENDIX C

EDS Results for Cobalt Blue and Cobalt Green

Cobalt Blue

Sample	Atom %	Weight %
$Co^{2+}Al_2O_4$ (GG-1)		
Al	50.13	31.52
Co	49.87	68.48
Al:Co	**1:1**	**1:(2.2)**
$Co^{2+}Co^{3+}AlO_4$ (GG-4)		
Al	10.87	5.29
Co	89.13	94.71
Al:Co	**1:(8.2)**	**1:18**
$Co^{2+}Co^{3+}{}_2O_4$ (GG-6)		
Al	0.11	0.05
Co	99.89	99.95
Al:Co	∞	∞
Cobalt Blue (Art)		
Al	2.59	0.99
Co	10.24	8.59
Si	56.15	22.45
K	2.12	1.18
Zn	8.36	7.78
Pb	19.89	58.65
Al:Co	**1:4**	**1:(8.7)**
Degussa Cobalt (Art)		
Al	9.2	2.71
Co	2.83	1.82

Si	44.12	13.55
Ca	2.64	1.16
Zn	8.12	5.81
Pb	33.09	74.96
Al:Co	**(3.2):1**	**(1.5):1**
$CoAl_2O_4$ (Citrate gel)		
Al	64.27	45.37
Co	34.97	53.92
Si	0.27	0.20
Ca	0.48	0.51
Al:Co	**2:1**	**1:(1.2)**

Cobalt Green

Sample	**Atom %**	**Weight %**
$ZnCo_2O_4$ (180°C)		
Co	59.77	57.25
Zn	40.23	42.75
Zn:Co	**1:(1.5)**	**1:(1.3)**
$ZnCo_2O_4$ (2h/1000°C)		
Co	56.41	53.84
Zn	43.59	46.16
Zn:Co	**1:(1.3)**	**1:(1.7)**
$ZnCo_2O_4$ (24h/1000°C)		
Co	68.60	66.32
Zn	31.40	33.68
Zn:Co	**1:(2.2)**	**1:2**